R. & M. No. 3686

R. & M. No. 3686

MINISTRY OF DEFENCE (PROCUREMENT EXECUTIVE)

AERONAUTICAL RESEARCH COUNCIL

REPORTS AND MEMORANDA

Theoretical Assessment of the General Stability and Gust Response Characteristics of STOL Aircraft

By W. J. G. PINSKER

Aerodynamics/Flight Dept., RAE, Bedford

LONDON: HER MAJESTY'S STATIONERY OFFICE

1971

PRICE £2·92 NET

Theoretical Assessment of the General Stability and Gust Response Characteristics of STOL Aircraft

By W. J. G. PINSKER
Aerodynamics/Flight Dept., RAE, Bedford

Reports and Memoranda No. 3686*
February, 1971

Summary

Results are presented of theoretical studies into the likely stability and gust response characteristics of four distinct classes of STOL aircraft, namely those using low wing loading and high $C_{L_{max}}$ alone, partly jet-borne configurations, aircraft using jet-flap-type wing-lift augmentation, and designs exploiting propeller slipstream. The areas considered are gust sensitivity, cross-wind control, dynamic response to gusts, speed stability, stability in flight under attitude constraint and dynamic longitudinal and lateral stability with fixed controls.

LIST OF CONTENTS

* Replaces RAE Tech. Report 71028—A.R.C. 32 844.

1. *Introduction.*

One of the limitations of the present day airliner is its dependence on large airfields. This has prevented the location of airports at the true origins of traffic demand near city centres and made it economically impossible to serve population centres of only modest size. To exploit the potential market excluded by these limitations a new class of aircraft is required. These must be able to operate from substantially smaller airports and do so with the regularity and safety of competing surface transport. This is the stimulus to the current interest in STOL and VTOL. The merits of these two alternative solutions are at present hotly contested and much of the argument appears to be at least as much emotive as it is technically informed. One of the difficulties is that although a quite substantial body of practical experience is available on VTOL aircraft—much of it due to the development of the Harrier VTOL fighter—no comparable technical background helps us to assess STOL. This situation is further bedevilled by lack of precise definition of what is meant by STOL and by the multitude of the possible design approaches towards STOL. It should be noted that tentative airworthiness requirements now begin to emerge[1,2], to set at least design targets, but these do not of course define the flying characteristics such aircraft will possess.

The present report is an attempt to assist in this discussion by studying—as far as this is possible by theoretical reasoning—the general handling characteristics one may expect STOL aircraft to have in low speed flight and how these may be affected by the various alternative lifting mechanisms that could be employed in a practical design. The aim is to present a broad picture and for this reason general trends are presented rather than specific answers derived for any particular hypothetical designs. The areas selected for analysis are those in which STOL aircraft are generally expected to show deficiencies, such as response to gusts, control in cross-winds and stability. Both stability in the generally accepted sense and flight under partial constraint by the pilot are considered. Under this latter heading particular attention is drawn to flight under pitch attitude constraint which is perhaps the most important control mode and one in which STOL aircraft may be less satisfactory than conventional designs.

The work reported here is essentially an elaboration of the relatively superficial assessment of Ref. 3, improving it in depth as well as in scope. Aerodynamically the most significant aspect distinguishing STOL aircraft from conventional designs are the extreme demands for lift and hence the mechanism adopted for its realisation. Most of the analysis will be based on the properties of appropriate aerodynamic models defining these lifting characteristics. First we must therefore identify the principal classes of STOL design according to the high lift mechanism used and these are:

(a) 'Conventional' STOL aircraft, where speed is lowered by a combination of reduced wing loading and ultra-powerful mechanical flaps.

(b) Wing lift supplemented by direct vertical thrust*.

(c) Jet flap or augmentor flap, in which circulation is increased by air supplied from the engines.

(d) Slipstream vehicles, where a major part of the wing is immersed in a powerful propeller slipstream.

After defining the general aerodynamic properties of these various alternative STOL techniques we shall consider the consequent gust response, stability and control characteristics. First we shall study basic gust sensitivity, considering in turn, vertical, horizontal and lateral gusts. Next, cross-wind control will be considered and this is followed by an attempt to predict dynamic gust response, using Jones' self-similar discrete gust model. In Section 4, two particular cases of flight under partial pilot constraint will be studied, first the well-known problem of speed stability when the flight path is constrained and secondly aircraft stability resulting from tight control of pitch attitude. This particular mode has not received much attention in the past, as the remaining longitudinal motion is usually highly damped. However, in the STOL regime, as will be shown, pitch attitude constraint may leave the aircraft with a relatively short period phugoid-like mode with perhaps less than adequate damping.

---

* This technique is seen by many as a first stage towards full VTOL, differing only in the amount of vertical thrust. This suggests similarity in the handling characteristics of this type of STOL with those of VTOL aircraft during transition. However, the designer of an economic STOL aircraft will strive to extract maximum lift from forward speed and provide more wing C_L than makes sense in a VTOL aircraft. This may significantly affect handling and not too much resemblance should be expected.

In the final sections, the conventional rigid body modes of the STOL aircraft are analysed showing a strong tendency towards instability of the phugoid and of the dutch roll as speed is reduced. Root locus analysis is employed to obtain a more generalised answer.

2. *Simplified Aerodynamic Models of the Principal Types of STOL Aircraft.*

2.1. *General remarks.*

In the Introduction we have identified four main class of possible STOL machines with respect to their lifting mechanism. We shall refer to these from now on briefly as

(a) 'Conventional' STOL.
(b) Partly jet borne.
(c) Augmented flap.
(d) Slipstream.

It should be noted that 'conventional STOL' is used here to describe STOL aircraft not utilizing powered lift whereas 'conventional aircraft' refers to typical current subsonic jets of the VC 10 or Boeing 707 variety. Frequently we shall also refer to the augmented flap and the slipstream designs together as aircraft using power augmented wing lift.

On most STOL designs the total lift is made up of two components, one associated with engine augmentation, and the other related to the airfoil lift supporting a conventional aircraft. In an idealised case, to which the partly jet-borne aircraft approximates, it is easy to separate these two components: assuming that in the STOL regime incidence and flap angle are held constant, the wing lift or 'aerodynamic' part of the lift is proportional to the square of speed, the balance of lift force being made up by 'powered' lift. This relationship is illustrated in Fig. 1. V_{00} is defined as that speed at which, in this aerodynamic configuration, the aircraft is just able to sustain itself without power assistance to lift. Above V_{00}, incidence (or an equivalent flap angle) must of course be reduced to maintain trim; below V_{00} lift must be increasingly augmented by vertical thrust until a minimum operational speed $V_{\min}$ is reached when all available power less any allowances for manoeuvring etc. is used.

When power is used more indirectly to increase airfoil lift the separation between 'aerodynamic' lift and powered lift is less clear cut and we have to define more carefully what is meant by 'aerodynamic' lift and 'non-aerodynamic' lift.

We are concerned here with stability and gust response and in this context we are interested in two aspects. Firstly, we will want to know how lift varies when speed changes at constant power and incidence and secondly how it changes with incidence at constant speed. We shall show that within the usual limitation of small perturbation theory it is always possible to divide the total lift for any trimmed datum condition V_0 into two components,

$$\Sigma L = L_A + L_E \tag{1}$$

such that near the trimmed conditions the 'aerodynamic' lift L_A varies as $(V_0+\Delta V)^2$ in response to small increments ΔV in speed and the 'powered lift' L_E is in the same sense insensitive to speed variations. It will also be possible to define a lift slope appropriate to each datum speed V_0. This general concept is illustrated in Fig. 2.

Although the suffix E used to denote L_E, the 'non-aerodynamic' component of lift, suggests an engine contribution, only in the case of a design using distinct lift engines can this be uniquely attributed to the engine. Generally, and especially when power is used to increase airfoil (jet flap and slipstream aircraft) L_E is not necessarily or exactly that portion of the total lift which is generated by the engine.

In order to be able to perform stability and response analysis in the STOL speed range $V_0 \leqslant V_{00}$, we shall require an estimate of the way in which the ratio $L_A/\Sigma L$, which we shall refer to as F_A, varies with trimmed speed V_0 and also how the effective lift slope varies in this regime. Above V_{00}, no power augmentation is required and all lift can be assumed to be 'aerodynamic'. Hence the ratio of aerodynamic to total lift is then $L_A/\Sigma L = 1$ and the lift slope a_{00} is that of the basic wing. In Fig. 1 the ratio of 'aerodynamic' lift to total lift is depicted as following a V^2 law up to V_{00}, but this particular relationship is only valid for

aircraft using distinctly separate lift engines and not necessarily for such schemes as jet flap and slipstream designs for which appropriate data will be established in the analysis to follow.

We shall now consider in detail these lifting properties for the various STOL types defined earlier.

2.2. *'Conventional' configurations.*

If STOL performance is achieved by simply lowering wing loading and increasing the effectiveness of mechanical flaps, we have in the present context a 'conventional' STOL aircraft in which all lift is 'aerodynamic ($\Sigma L = L_A$) and the nondimensional lift slope is sensibly constant at all speeds.

2.3. *Designs using direct vertical thrust.*

Relations are still relatively simple with aircraft in which wing lift and powered lift are physically separated, as in the lift engine layout. If one ignores possible effects of the engine flow on the aerodynamics of the airframe then the 'aerodynamic' lift L_A would follow precisely the square law illustrated in Fig. 1, and change of airspeed by ΔV from a given trimmed speed V_0 would result in a lift (or normal acceleration) change

$$\Delta n = \left\{ \left(\frac{V_0 + \Delta V}{V_0} \right)^2 - 1 \right\} \left(\frac{V_0}{V_{00}} \right)^2. \tag{2}$$

In Ref. 4 Williams and Wood show that, in practice, a jet leaving the engine nozzles near to a lifting surface results in sometimes substantial lift losses. These losses are relatively insensitive to incidence but vary markedly with speed or more precisely with the ratio of aircraft speed V to jet efflux velocity V_j. A few examples of the many results presented in Ref. 4 are shown in Fig. 3. We note that the magnitude and even the sign of the jet interference effect depends on details of the configuration and it is impossible to derive meaningful simple generalizations. The absolute magnitude of the loss in lift or in effective lift thrust is a performance matter and does not concern us here. For stability and response we are mainly interested in the rate of change of this effect with airspeed. It will help in the interpretation of Fig. 3 and also of Fig. 4 where corresponding pitching moment data are shown if we note that within the STOL range typical values of V/V_j are 0·1–0·2 for jets and between 0·2–0·5 for fans.

We observe from Fig. 3 that, with centrally-mounted engines, lift loss increases with increasing airspeed and this effect will of course counteract the basic increase with V^2 in aerodynamic lift. This phenomenon will for example, reduce the response of such aircraft to horizontal gusts. This trend is reversed as indicated in Fig. 3 for the fans in wing pods.

One will observe that installations leading to large losses in effective lift will be undesirable for performance reasons and this is even more important for STOL aircraft, where the potential losses may be particularly large.

In Fig. 4 corresponding pitching moment data are shown. We note that in all cases considered there will be an increase in nose-up pitching moment with increasing airspeed. This will tend to stabilise the phugoid (*see* Section 5.1) and amplify the normal acceleration response to fore and aft gusts.

2.4. *Power augmented wing lift.*

If power is used to alter the flow past the lifting surfaces of the aircraft, rather than directly to give vertical lift, the aerodynamic situation clearly becomes more involved and we can no longer distinguish readily between airfoil and powered lift. It is to be able to make a meaningful distinction that we had earlier introduced the concept of 'aerodynamic' lift, defining it as that portion of the total lift, which varies according to V^2 when speed changes by a small increment from a given datum value V_0, assuming incidence and power setting remain constant. For the two principal types of engine-augmented airfoil lift system, i.e. classes (b) and (c) defined in section 2.1, the appropriate answers have been derived in Appendix I (jet flap) and Appendix II (slipstream effect). With these methods of lift augmentation the effective lift slope also varies as power is used and this phenomenon is also investigated.

The treatment of the jet flap is based on a theoretical model derived by J. Williams *et al.*, in Ref. 5, and reproduced in Fig. 5. This graph applies to the case where blowing extends over the full span. The results of the analysis of Appendix I are given in Fig. 8. As speed is reduced below V_{00} and blowing is introduced to maintain lift, the proportion of 'aerodynamic' lift to total lift is seen to decrease in a fashion not too dissimilar to the V^2 law observed for the partly jet-borne configuration but at the same time the effective lift slope increases quite rapidly.

A similarly generalised result has been derived in Appendix II for the slipstream aircraft illustrated in Fig. 9 with the answers plotted in Fig. 11. Again the general trends resemble those found for the jet flap type lift augmentor. The analysis suggests, however, that when the propeller axis incidence $\alpha_p = 0$, the so-called aerodynamic lift contribution becomes negative for $V < 0{\cdot}4V_{00}$, implying that in this regime, increasing airspeed will result in reduced lift at constant engine power. This is due to the fact that there the slipstream effect dominates over the natural trend for lift to increase with airspeed. However, this result is physically unrealistic since it is caused by the assumption $T \propto 1/V$ which at very low speed is no longer valid also, this occurs at speeds below those of practical interest for STOL and need not concern us further. The curves given in Fig. 11 do not pass through 1 at $V/V_{00} = 1$, as distinct from the other cases considered. This reflects the fact that with this layout it is not possible for the lift augmentation mechanism to be switched off when it is no longer required. It should be noted that here $(\partial C_L/\partial\alpha)_{V_{00}}$ refers to the hypothetical case in which the slipstream effect is assumed absent and not to the actual lift or lift slope obtaining at V_{00}. With both types of lift augmentors considered here there would of course also be changes in pitching moment, but they are too complex to yield to generalised treatment and are therefore ignored.

3. *Response to Gusts and Cross-Wind.*

Low speed aircraft are generally expected to be less tolerant to atmospheric disturbances and STOL aircraft are often viewed with apprehension in this context. Unfortunately, an attempt at an objective assessment of this problem is immediately faced with the lack of a universally recognised criterion, by which one might judge gust sensitivity of this or any other class of aircraft. What we shall do here is to present the results of various alternative methods of estimation.

The most frequently quoted parameter is what we shall refer to as gust sensitivity, i.e. the instantaneous acceleration experienced by the aircraft meeting a step gust. Such parameters can be defined in relation to gust components in all three spatial directions. We shall then consider response to simultaneous longitudinal and vertical gusts. If aircraft dynamics are ignored, such simple measures of gust response, although clearly relevant, can only give a partial answer. We shall therefore also carry out some dynamic response calculations. It must be noted that this process also meets with difficulties and that the answers to such analysis will always be influenced by the chosen method and cannot claim unique validity.

3.1. *Sensitivity to Vertical Gusts.*

The response of an aircraft to a vertical gust w_g is governed by the fact that it produces an increment in incidence

$$\Delta\alpha = \frac{w_g}{V}. \tag{3}$$

It is of course well known that as airspeed reduces, vertical gusts require the aircraft to have an appropriately larger incidence margin to protect it against stalling or other incidence-dependent handling hazards.

The initial angular pitching acceleration in response to a vertical gust is given by

$$\frac{\dot{q}}{w_g} = V\frac{\rho}{2}\frac{g}{W/S}\frac{1}{k_y^2}m_w \tag{4}$$

and therefore assuming longitudinal stability m_w remains constant, response is proportional to airspeed, becoming less with lower speed.

Both these relationships (equations (3) and (4)) are essentially independent of the lifting mechanism employed and therefore apply to all classes of STOL aircraft. In Fig. 12 they are represented graphically, defining relative changes in relation to V_{00}. It should be noted in this context too that dynamic control power varies with the square of airspeed, so that at the lower speed it may become insufficient to counter a given gust. However, this problem is eased in many STOL designs when aerodynamic control is augmented by reaction control.

Another frequently quoted gust response parameter is the normal acceleration

$$\frac{\Delta n}{w_g} = \frac{\rho}{2} V \frac{\partial C_L/\partial \alpha}{W/S} \tag{5}$$

which varies as $\dot{q}$ does with V. Normal acceleration response is of course primarily the concern of the structural designer and in this respect one is mainly interested in high speed flight. Nevertheless, in the generally more turbulent air met during the approach and take-off, Δn is a measure of discomfort and is at least relevent to passenger acceptance. If equation (5) is applied to STOL aircraft, we must consider that in the low speed regime according to section 2, $\partial C_L/\partial \alpha$ may itself be a function of V. Using the results derived there for the various types of possible STOL aircraft considered, equation (5) has been evaluated with the result shown in Fig. 13. To give the analysis more generality, the answer obtained for a given speed and aircraft in terms of $\Delta n/w_g$ has been divided by the response of the same aircraft at V_{00}, the lowest conventional flying speed*. In this way general trends in the STOL regime are depicted. There is one exception. The curve shown dotted and labelled 'reduced W/S' indicates the change in response with approach speed, if this is lowered by progressively reducing wing loading. So whereas the data given for the other aircraft types show what happens to a given aircraft throughout the speed range including that beyond V_{00} the result indicated for aircraft achieving STOL by reducing W/S is only valid at the design point defining approach speed and its response at other speeds must be obtained by drawing a linear radial line through this point as indicated in Fig. 14.

The important conclusion from Fig. 13 is that only for aircraft not using power-augmented airfoil lift can one expect the normal proportional reduction in gust sensitivity from reduced airspeed, as this is counteracted by increased lift slope and in the case of the jet flap aircraft, response actually increases at the lower speed. Of course, if in addition to using high lift systems, wing loading is reduced to achieve the desired speed reduction, this will have an unfavourable effect as is evident from the trend shown in Fig. 13 for reduced W/S. An appropriate allowance has to be made according to equation (5) for the combined effects.

3.2. *Sensitivity to Horizontal Gusts.*

A horizontal gust or more precisely a gust in the direction of flight, u_g, leaves aircraft incidence unchanged and unless the aircraft has exceptional aerodynamic properties there will be no significant pitching acceleration. The change in effective speed will, however, affect lift and hence normal acceleration. Considering that only that portion of lift defined earlier as 'aerodynamic' lift will respond, we get

$$\Delta n = 2 \frac{u_g}{V} F_A . \tag{6}$$

This phenomenon becomes more severe at low speed, so that one may expect it to predominate over vertical gust response if a sufficiently low speed is used. This tendency is further strengthened in flight near the ground, where vertical turbulence is more strongly attenuated than horizontal turbulence. We shall return to this topic in Section 3.3.

---

* The reader is reminded that in the case of the slipstream aircraft the results are referred to the hypothetical condition of the aircraft flying at V_{00} with the slipstream effect assumed absent.

faster than those corresponding to these C_L values, overall gust sensitivity increases as vertical gusts become more powerful but at lower speeds again the aircraft could become more disturbed as fore and aft gust have then more effect. At the conditions of minimum sensitivity both components of turbulence make equal contributions. It is interesting to note that current aircraft are in fact operating in the approach near this response optimum, a fortunate coincidence. It also follows that when considering longitudinal behaviour in turbulence during landing and take off fore and aft gusts must be given as much weight as vertical gusts. The trend in gust sensitivity with wing loading goes of course in the expected sense.

If an aircraft uses partial jet lift below V_{00}, the ratio of 'aerodynamic' lift $F_A = (V/V_{00})^2$ and equation (10) reads

$$\frac{\Delta n_{u+w}}{u_g} = V\sqrt{\left(\frac{w_g}{u_g}\right)^2\left(\frac{\rho}{2}\frac{a}{W/S}\right)^2+\left(\frac{2}{V_{00}^2}\right)^2}. \tag{11}$$

Hence gust sensitivity increases linearly with V up to V_{00}, above this speed equation (10) applies and so does Fig. 16. An example for such an aircraft is illustrated in Fig. 17 and it is obvious that in the STOL regime such an aircraft is significantly less sensitive to gusts than a conventional design.

To obtain a rough estimate of the corresponding response of STOL aircraft with power augmented wing lift we write approximately

$$F_\alpha = \frac{V_{00}}{V}; \quad F_A = \left(\frac{V}{V_{00}}\right)^2$$

(Fig. 31 which summarizes the lifting characteristics of the main STOL classes, illustrates how far these analytical relationships differ from the correct form of these functions). With this:

$$\frac{\Delta n_{u+w}}{|u_g|} = \sqrt{\left(\frac{w_g}{u_g}\right)^2\left(\frac{\rho}{2}\frac{V_{00}^a}{W/S}\right)^2+\left(2\frac{V}{V_{00}^2}\right)^2}. \tag{12}$$

This represents at $V \leqslant V_{00}$ the trend illustrated in Fig. 18, again indicating less sensitivity than conventional aircraft, and more than partial jet-borne designs operating at the same speed.

3.4. *Sensitivity to Lateral Gusts.*
Lateral gusts generate sideslip

$$\beta = \frac{v_g}{V}. \tag{13}$$

As the effect of vertical gusts on incidence, that of lateral gusts on sideslip becomes more powerful at lower speeds. Although it is unlikely that turbulence could be severe enough to cause the fin to stall, we must expect STOL aircraft frequently to be subject to fairly large sideslip angles and consequently to operate in an area where the associated aerodynamic yawing and rolling moments are significantly nonlinear. This must be allowed for in detailed stability analysis.

A measure of sensitivity equivalent to normal acceleration increment with the longitudinal motion may be the angular acceleration in yaw and roll, which is given by the expressions

$$\begin{aligned}\frac{\dot{r}}{v_g} &= \frac{\rho}{2}\frac{b}{W/S}\frac{n_v}{k_z^2}V \\ \frac{\dot{p}}{v_g} &= \frac{\rho}{2}\frac{b}{W/S}\frac{l_v}{k_x^2}V\end{aligned} \tag{14}$$

when k_z and k_x are the inertia radii in the two freedoms. Being proportional to V, these parameters are reduced in the STOL speed range and are unlikely to cause any difficulty. As in the pitch freedom we observe, however, that control power diminishes with the square of airspeed so that increased demands will have to be met by the designer to maintain gust effects and control reactions in balance.

3.5. *Control in Cross-Wind.*

The more demanding lateral control requirement will most probably arise in cross-wind conditions during landing and take-off.

Although cross-wind control is a much-discussed problem area and has been receiving attention for a long period, it would be pretentious to claim that we fully appreciate all the factors that play a part in limiting the capability of an aircraft in this respect. The usual procedure is to consider one or both of the two possible alternative techniques, namely the 'crabbed' approach followed by kicking-off drift or the steady sideslipping method, and calculate the maximum cross-wind in which the demands for control in these manoeuvres can be satisfied with the available control power. Some margin of control power (typically 1/3) is allowed for manoeuvres and gusts. This design procedure has the merit of leading to unique numerical results but it is less certain that by satisfying these simply defined demands one can be sure that all aspects of the problem are then covered. Nevertheless, since during the last deace or so, single runway airfields have created the need for routine operation in strong cross-winds, this method appears to have worked quite well and ensured an acceptable safety record. It is interesting to observe that the cross-wind angles typically acceptable to the modern aircraft are about 12 degrees, say 30 knots cross-wind for an aircraft approaching at 145 knots etc. We see from Fig. 19 how this angle, which can be seen either as a crab angle or as a sideslip angle depending on the chosen technique, varies with airspeed and cross-wind velocity.

To cope with presently accepted cross-winds of the order of 30 knots a STOL aircraft approaching at 80 knots would experience 22 degrees cross-wind angle. This is vastly outside present operational experience and even if the designer can provide appropriate rudder and roll control power, it is impossible to be sure that the larger crab or sideslip angles involved do not create serious handling hazards by themselves. One must not forget in this context that STOL aircraft are expected to approach much more steeply than present aircraft and that this will make the flare a more demanding manoeuvre to which cross-wind control difficulties make a cumulative contribution. If one ignores the additional flare problem, then it would appear safe to expect STOL aircraft to be able to accept at least the present cross-wind angles and from Fig. 19 we observe that this would permit less than 20 knots cross-wind of 80 knots air speed. It would seem wise to accept such a figure as a provisional limitation unless and until practical flight experience shows it to be too conservative. Alternatively undercarriages designed to accept large drift angles can also provide a solution.

In a rational approach to the analysis of cross-wind control one could visualise the required control power as being simply that demanded for control of steady cross-wind plus an allowance for control of gusts. The former is proportional to the cross-wind component V_c of wind speed, the latter, however, to absolute wind speed V_w. The total control demand would then be defined by an equation of the form

$$\Sigma \text{ control} = K_1 V_w + K_2 V_c \tag{15}$$

where the factors K_1 and K_2 reflect the aerodynamic characteristics of the vehicle. If we substitute on the left hand side maximum available control power and divide equation (15) by this factor, we get an equation of the form

$$1 = F_1 V_W + F_2 V_W \sin \psi_W \tag{16}$$

where ψ_W is the wind azimuth angle so that $V_c = V_W \sin \psi_W$ (see Fig. 20). Equation (16) now defines a boundary $V_W = f(\psi_W)$ within which control is possible. It is readily seen that $F_1 = 1/V_{W_{\max}}$ is the inverse of the maximum mean wind speed in which the associated gusts can just be controlled if there is no mean cross-wind component and $F_2 = 1/V_{a_{\max}}$ the inverse of the maximum cross wind that can be controlled

in the absence of turbulence. The boundary defined by equation (16) has the form shown by the solid line in Fig. 21, it does not define a line of constant cross-wind. It would seem that the framing of approach limitation along such a boundary would be much more realistic than just limiting cross-wind as such.

Since landing runway requirements are essentially related to ground speed rather than airspeed, it would be perfectly appropriate in principle to increase airspeed to maintain ground speed in the presence of a headwind component. From the geometry of the speed polygon in Fig. 20, the adjusted approach speed V_a could be related to the 'scheduled' value V_{a0} by

$$\frac{V_a}{V_{a0}} = \sqrt{1+2\frac{V_W}{V_{a0}}\cos\psi_W+\left(\frac{V_W}{V_{a0}}\right)^2}. \tag{17}$$

If we assume that for a given aircraft the control requirements vary in inverse proportion to airspeed, equation (16) would then become

$$1 = V_W \frac{V_{a0}}{V_a}(F_1+F_2\sin\psi_W) \tag{18}$$

and as a consequence the controllability limit of Fig. 21 will widen in the manner indicated by the dashed line. A useful by-product of this approach technique would be that glideslope and vertical velocity retain their normal relationship irrespective of wind speed and direction. The lack of this was particularly criticised in Ref. 1.

There is perhaps another control aspect worth noting when considering cross-wind control of slow aircraft. The rate of change of heading associated with a given bank angle increases with decreasing airspeed as shown in Fig. 22. To maintain a given precision in heading control the slower aircraft needs more precise bank angle control and this may prove difficult with the inevitably more sluggish response of the STOL aircraft and when basically more sideslip, and hence bank angle, is required to hold a given cross-wind.

3.6. *Dynamic Longitudinal Response to Gusts.*

Although gust sensitivity in the sense discussed in the earlier chapters of this section is clearly an important parameter relevant to the behaviour of aircraft in turbulence, a more complete assessment must consider aircraft dynamic response as well. Recently, J. G. Jones has formulated an approach to this problem in which the atmosphere is modelled as an assembly of self-similar discrete ramp gusts (see Refs. 12–14). Jones' theory had been originally developed for predicting design gust loads and as a consequence particular emphasis was laid on faithful modelling of the less frequent large gusts. By contrast, the power spectral method implying a Gaussian amplitude distribution allows better representation of the general fluctuations, but tends to mismatch the rarer gust. For an assessment of safety aspects rather than the average of a given gust-induced problem, the self-similar discrete gust model appears to be more realistic and appropriate.

As the details of this relatively unfamiliar procedure require thorough discussions it was considered appropriate to present this in a separate paper[15] and give here only the results.

We have considered two response parameters to cover what are believed to be the most relevant features of interest. Normal acceleration response Δn has been calculated as a measure of discomfort relevant to both the pilot and the passengers, but as a more meaningful criterion for control work load, excursions in vertical velocity or of the equivalent excursions in glide path angle were calculated.

A major assumption which has to be made before any response method can be applied is the choice of the aircraft response mode. If one takes simply the aircraft transfer function with controls fixed, the answer one usually obtains from power spectral analysis is heavily loaded by contributions from the low frequency end, especially if the phugoid is poorly damped. This contribution will then have to be eliminated by truncation in a very arbitrary manner. This process is particularly dubious if the phugoid and the short period are close in frequency as is inevitably the case (*see* Section 5.1) at STOL speeds. A much more

satisfactory process is to assume an aircraft mode in which this response is suppressed by a suitable and of course plausible piloting constraint. We have in fact chosen a rather radical form of such control constraint, namely the assumption that pitch attitude is held constant. In Section 4.2 we shall consider this mode in detail as being of particular interest in low speed flight and the reader is referred to the discussion there for further detail.

Pitch attitude constraint is perhaps the most immediate aim of longitudinal control and hence an entirely plausible concept provided the short period dynamics of the aircraft are well enough behaved to allow this ideal to be approached. Deficiencies in this area would demand correction, if necessary by artificial aids, and it is therefore not unreasonable to assume this mode as a basis for analysis.

It can now be argued that an aircraft will be satisfactory if maintenance of pitch attitude—which requires a certain amount of pilot effort—results in a generally well controlled aircraft response. On the other hand if major excursions still occur, obliging the pilot to generate constraints in addition to that in pitch, he is likely to register this as an undesirable increase in workload. The relative magnitude of such excursions could then be seen as a measure of control difficulty and may be expected to correlate in some way with pilot rating.

Results have been obtained for a number of hypothetical STOL designs defined below and compared with an aircraft typical of the present generation of jet transports (A) as a datum for comparison.

(A) Current large transport aircraft
$W/S = 488$ kg/m^2 (100 lb/ft) $V = 140$ knots
(B) Conventional aircraft semi-STOL performance by reduced wing loading
$W/S = 244$ kg/m^2 (50 lb/ft) $V = 100$ knots
(C) Semi-STOL performance achieved by major increase in non-powered $C_{L_{max}}$
$W/S = 488$ kg/m^2 (100 lb/ft^2) $V = 100$ knots
(D) Partly jet-borne STOL (59 per cent lift from jets)
$W/S = 390$ kg/m^2 (80 lb/ft) $V = 80$ knots $V_{00} = 125$ knots.
(E) Jet flaps STOL
$W/S = 390$ kg/m^2 (80 lb/ft) $V = 80$ knots $V_{00} = 125$ knots
(F) Slipstream STOL
$W/S = 390$ kg/m^2 (80 lb/ft) $V = 80$ knots $V_{00} = 125$ knots
All aircraft are assumed to have fairly high aspect ratio wings with $a = 6{\cdot}0$.

For a number of reasons which will be discussed in Ref. 15 only the response to horizontal gusts was considered. The numerical results presented apply to an atmosphere with turbulence of rms intensity 5 ft/sec at 250 ft altitude where the scale length is approximately 1000 ft. It is suggested that more notice should be taken of the differences between the results for the various aircraft considered than of the actual numerical results as such.

The results are presented as probabilities of exceeding given levels of the various response parameters considered and are presented in Figs. 23–24b. Since the discrete gust method used and its assumption of an exponential amplitude distribution becomes invalid for the smaller and more frequent gust fluctuations, the curves given in these figures are discontinued (indicated by transition to the dashed portion) at a level approximately equivalent to two standard deviations of the response parameter considered.

Fig. 23 gives the results for acceleration response. The results generally agree with Fig. 13 and indicate that in dynamic response, apart from the two configurations using power augmented wing lift, all the others are significantly worse than the datum aircraft (A) and even (D) and (E) are only marginally better than (A).

In Fig. 24a excursions in vertical velocity are considered and now we find that in this respect all STOL aircraft with the single exception of (C) are substantially better than the datum aircraft. Since we suggested this parameter as a criterion for handling difficulty, this is a reassuring result. As with Δn, the power-augmented wing lift designs show up best.

However, if we consider the same response in terms of flight path angle disturbance $\Delta\gamma$ rather than vertical velocity $w = \Delta\gamma V$, the STOL configurations are now all worse than the datum aircraft with the exception of the jet flap.

We observe therefore that the answer depends very much on the quantity one considers most relevant to the problem of flight path control. Until we have a clear understanding of the significance to the pilot of the various response parameters, no final judgement is possible. However, there is less difficulty in establishing an order of merit between the various STOL types, ignoring the datum case (A). We note that in every case the semi-STOL design using high wing loading but drastically increased C_L (Case (C)) is worst, followed by (B). At the other end of the scale the jet flap figures best in every case.

The presentation of the results of an investigation of a handling feature in statistical terms raises an interesting question that is not evident if one were merely presented with some measure of the average magnitude of the disturbance as for instance by the rms of say Δn, or w etc. The rms tells us what proportion of time the aircraft is displaced by a certain amount from the datum condition, but nothing about the frequency of such exceedances. This may be a meaningful result to judge the performance of a fully automated process but may have little relevance as a criterion for a handling problem. Here we are more interested in how often a certain exceedance occurs, or how big a disturbance we can expect with a given frequency, say every 10 minutes. We note especially from Fig. 23 that the answer to these last questions may depend on the level of upset considered.

We must conclude with the admission that this analysis has raised perhaps as many questions as it has answered, but it has highlighted areas of ignorance that urgently need further research.

4. *Stability in Flight under Partial Pilot Constraint.*

Since Neumark[10] drew attention to the practical importance of stability in flight under partial constraint, especially of flight path constraint, the idea of partially constrained flight has become accepted as a meaningful concept and has been successfully extended in Ref. 11. We are considering here two such conditions. First we examine the familiar case of speed stability under glide path constraint. Another equally plausible piloting constraint is that of pitch attitude, reflecting perhaps the most basic control instinct. It has not previously attracted much attention and the present analysis suggests that for the conventional aircraft it leads to the most innocuous highly stable flight condition. However, we will show that in the STOL speed regime, pitch attitude constraint may leave the aircraft with a much less acceptable oscillatory mode, which could constitute a significant handling deficiency.

4.1. *Speed Stability in Flight under Glide Path Constraint.*

In a STOL aircraft the pilot is generally presented with alternative means of controlling the longitudinal motion. In addition to the elevator he may be able to control thrust, both in magnitude and direction, and flap angle. These will be used generally by the pilot wishing to change airspeed. In the context of stability we are, however, mainly concerned about the maintenance of a trimmed state and in this case the elevator is still the most convenient and likely control and Neumark's concept of speed stability applies, i.e. glide path controlled by elevator. We are restricting the analysis therefore mainly to this case but shall consider the alternative of height control by use of vertical thrust for the partially jet-borne design.

Details of the analysis are presented in Appendix III. For aircraft which are fully supported by wing lift as with the jet flap and slipstream designs, the drag-versus-speed characteristics can be generally reduced to the familiar form illustrated in Fig. 25. If they are normalised as a function of the ratio of airspeed V to minimum drag speed $V_{D_{\min}}$ and of the maximum lift drag ratio $(L/D)_{\max}$ at $V_{D_{\min}}$, they uniquely define the time constant $\tau_S = \dfrac{1}{\lambda_S}$ of the speed stability mode as plotted in Fig. 26. Any design which utilises unconventionally powerful high lift defices will operate well below minimum drag speed and may experience a degrée of speed instability far greater than met in current practice. We note that at 50 per cent of $V_{D_{\min}}$, not too extreme a condition for some STOL aircraft, speed divergence time constants will be of the order of 3 to 6 seconds. This calls for drastic throttle activity and a very responsive power plant.

The results of Fig. 26 are computed under the assumption that only drag changes with airspeed, whereas thrust is constant. This will be adequate as an assumption for jet powered designs. With propeller driven aircraft, however, we must consider variations of thrust with speed. The most plausible assumption is $T \propto 1/V$. This relationship stabilizes the speed mode of the aircraft as shown in Fig. 27. It is interesting to note that now speed is neutrally stable at about 77 per cent of minimum drag speed. (Precisely at

$\sqrt[4]{\frac{1}{3}V_{D_{\min}}}$.) This result is of course especially relevant to the slipstream design.

Finally Appendix III treats partly jet-borne configurations, and in this case airframe drag, momentum drag, and the fore and aft component of vertical thrust have been taken into account. As the results of Fig. 28a indicate, the destabilizing contributions dominate the situation and the aircraft will be extremely unstable in the STOL regime.

Control of height by vertical thrust is an alternative technique in the partly jet-borne aircraft. The results for this control mode are shown in Fig. 28b and we note that now there will be speed stability except at speeds very close to V_{00}. But there the pilot is unlikely to use this form of control. The position of the thrust vector also has some influence on the result. Fig. 28c shows that speed stability is reduced in steep approaches when ε_E has to be positive and large.

4.2. *Stability in Flight under Attitude Constraint.*

Close control of pitch attitude is perhaps the most obvious piloting technique and is well achieved except in configurations prone to pilot induced oscillations. Pilots know from experience that by firm control of pitch the longitudinal motion of the aircraft as a whole is also well controlled. The most apparent result will be the effective suppression of the phugoid.

We shall now examine whether these observations are generally valid and in particular if they also apply at STOL speeds.

The analysis in Appendix IV shows that suppression of the pitch freedom leaves the aircraft with a second order response mode, which resembles the classical phugoid at very low speed but becomes rapidly heavily damped as speed increases towards the conventional range.

In Appendix IV the 'undamped' period of this mode is given as

$$P_n = 2\pi \frac{V_0}{g} \tag{19}$$

It increases with airspeed but for STOL aircraft using power augmented lift it remains constant below V_{00} as illustrated in Fig. 29. As a very crude approximation the damping ratio ζ of this mode can be expressed as

$$\zeta = \frac{a_{00}}{\sqrt{8}} \frac{\rho/2\, V_0^2}{W/S} \frac{F_\alpha}{\sqrt{F_A}} \tag{20}$$

and is seen to increase with the square of airspeed. This general trend is still evident in the correct solution shown for the case where $a_{00} = 6$ and $F_A = F_\alpha = 1$ in Fig. 30. It can be shown that the value of a_{00} assumed does not materially alter this picture, except that according to equation 20 ζ will be scaled by a_{00}. Fig. 30 applies, however, only to aircraft in which $F_A = F_\alpha = 1$ over the speed range and hence not to STOL designs employing power augmented lift. For convenience the results previously derived for these two factors are summarised in Fig. 31 for the principal STOL systems. For the partly jet-borne aircraft, $F_\alpha = 1$, but $F_A = (V/V_{00})^2$ below V_{00}. This has the result of reducing the rate at which damping drops with reducing speed, but there is still a downward trend as shown in Fig. 32a. To get a broad picture for the jet flap and slipstream aircraft, we have approximated the functions shown for F_α and F_A in Fig. 31 by the simple mathematical relationships indicated by dashed lines and this leads to the result given in Fig. 32b. Now damping ζ is virtually constant at all speeds below V_{00} and equal to that obtained for V_{00} from Fig. 30. Therefore STOL aircraft using engine augmented wing lift can be expected to be no worse than present aircraft in this respect at approach speeds.

As an illustration of the significance of the damping of this mode to practical flight, the response of the aircraft under pitch attitude constraint to a ramp gust has been computed for various levels of ζ with the results shown in Fig. 33. We note that the amplitude of the disturbance to the aircraft in response to a given gust increases rapidly as ζ decreases. It will be noted that these are examples of the responses that have been considered in the discrete gust theory in Section 3.6.

Finally we may observe that the damping of this mode is provided essentially by the (dimensional) lift slope and that therefore stability augmentation of the form in use today will not significantly alter it.

5. *Dynamic Stability.*

Finally we now consider stability in the conventional sense with controls assumed fixed. Dynamic stability depends on the interaction of a great number of aerodynamic derivatives and many of these may be profoundly affected in the STOL regime by the action of the lift mechanism employed. This will be particularly true where the flow through the power plant interferes with the aerodynamics of the airframe. Detailed considerations of such effects as in Ref. 4 go well beyond the scope of the present general study where we have to restrict ourselves to the most general trends.

One particular effect, relevant to all STOL aircraft may, however, be mentioned. Air entering the engine intakes has to be given momentum normal to the flight direction in the presence of incidence or sideslip and if the intake is ahead of the aircraft centre of gravity the reaction on the aircraft will be a destabilising moment.

If m_E is the mass flow through the engines, x_I the distance of the intakes from the CG, (x_I being positive for forward intakes) and l a reference length we get

$$-\Delta n_v = +\Delta m_w = m_E 2 \frac{x_I/l}{\rho S V}. \tag{21}$$

The change in static directional and longitudinal stability attributable to this effect is already noticeable with some conventional aircraft but it is apparent that the greater power requirements for the STOL aircraft, where the engines may have to work hard in the approach, together with the reduced speed, will tend to bring this phenomenon into prominence. It should be noted that an equivalent effect occurs with propeller driven designs and is associated with a term normally defined as propeller sideforce.

With conventional aircraft, coupling between the lateral and longitudinal motion can normally be ignored except in the special case of fast rolling of fighter aircraft.

Ref. 8 indicates, however, that the rotary mass of engines and propeller may induce gyroscopic coupling between these aircraft freedoms and destabilise one of the oscillatory short period modes if the coupling parameter

$$K' = \frac{(h/\omega)^2}{BC}$$

is sufficiently large. Here h is the total angular momentum of the engines, ω the frequency in rad/sec of the relevant aircraft mode, B and C are aircraft inertias in pitch and yaw. Since $\omega^2 \propto V$this factor will become more powerful at low speed, especially if an exceptional amount of engine power has to be installed. It can of course be made zero if engines are installed in handed pairs. This phenomenon needs careful consideration in a STOL design.

In the following analysis, however, we shall ignore all these aspects, consider lateral and longitudinal stability separately and also make simple assumptions for the aerodynamic derivatives. Two areas cause particular concern. As speed decreases the frequency of the longitudinal short period oscillation and that of the phugoid, approach one another since the phugoid frequency is inversely proportional to speed and that of the short period mode is directly proportional to speed. This trend is illustrated in Fig. 34. When these two normally widely separated modes combine, the stability of one is likely to suffer.

It is generally true that the damping of the dutch roll deteriorates as C_L increases and we shall be inter-

ested to find out if this is also true if part of the lift is supplied by the engines in some way or other.

As stated above, longitudinal and lateral stability will now be treated separately.

5.1. *Longitudinal Stability.*

Details of the assumptions made and of the unconventional procedure used for the analysis are given in Appendix V, Section V.1. Basically it is assumed that below V_{00} the aircraft is trimmed at constant incidence, the lift deficiency being made up by engine augmentation. We further make the rather sweeping assumption that the aerodynamic derivatives are constant, i.e. that they are defined by incidence and unaffected by the engine induced flow. This assumption permits one to reduce the speed dependence of the equations of motion into a single term, namely the gravity term $m\theta$ in the X force equation, after suitably normalising the equations. This term can be isolated from the basic differential equations and reintroduced as a feedback term. Now the system can be visualised as the servo loop illustrated in Fig. 35 where the gravity term appears as the factor (g/V_0^2), i.e. as a feedback gain. Root locus analysis is then used to calculate the change in stability as (g/V_0^2) varies from $0 \rightarrow \infty$, i.e. as speed varies from $\infty \rightarrow 0$. A typical root locus plot is shown in Fig. 36. According to the particular form in which the equations are normalized, the damping constants σ' and the frequencies ω' are distance constants rather than time constants as is more usually found in this type of analysis. The poles (X) define a degenerate form of the aircraft dynamic uncoupled modes, that for the short period is virtually correct, but the phugoid is replaced by a zero root and a slightly damped real root. (In Fig. 36 they are so close that they could not be pictorially separated.) The solution is only strictly valid for $V < V_{00}$ since above V_{00}, C_L reduces and the derivatives may vary. We note that as speed reduces the damping of the short period mode improves whereas the phugoid becomes rapidly unstable. The major portion of the complete root locus plot allowing $V \rightarrow 0$ applies to very small airspeeds and is therefore irrelevant to STOL. It must be noted that the normalisation procedure used has the consequence that the roots are defined as distance constants rather than as time constants. This does not affect nondimensional criteria such as damping ratios and observations about stability boundaries, but for better appreciation of the result they must be transported into the time domain. Fig. 39 gives the result for two of the cases considered in familiar form as periods and times to damp. Apart from the fact that the phugoid becomes unstable in the STOL range we also note that as expected from Fig. 34, periods of the two longitudinal modes become very close to each other although they appear to cross only at a speed below those of interest for STOL operations.

To illustrate the effect of variations in one important derivative, namely lift slope, Fig. 37 is presented comparing root loci for the datum case of Fig. 36 with corresponding results where its value is doubled and trebled. This is particularly relevant for power augmented wing lift devices where the lift slope increases as speed is decreased. The principal effect is a shift of the basic pole representing the uncoupled SPO, further into the stable quadrant, but the effect of speed itself is essentially unchanged.

The only parameter which according to Appendix V, Section V.1 could drastically change the pole-zero configuration is M_u and the effect of gross changes in this derivative is shown in the four root locus plots in Fig. 38. Although at first sight the picture appears to alter drastically, closer inspection reveals that the initial paths of the loci near the poles are not greatly different and we have already noted that we are only interested in this region. So the conclusion from Fig. 36 applies generally, namely, that when speed is reduced and the SPO frequency approaches that of the phugoid, damping tends to be transferred from the phugoid to the SPO, leading to instability of the former. From Fig. 39 we also note that once mode coupling occurs the derivative M_u has a strong effect on the period of the SPO, contrary to normal expectation.

5.2. *Lateral Stability.*

Lateral stability has been treated in Appendix V, Section V.2 in an analogous manner, again the gravity term—now in the Y equation—being isolated and treated as a feedback gain in the manner formally indicated in Fig. 40.

A typical root locus plot is shown in Fig. 41. The poles represent again a degenerate form of the lateral modes with the gravity effect removed, or more precisely a solution appropriate to $V = \infty$ where gravity effects vanish by comparison to aerodynamics. We note that as speed reduces, the dutch roll mode loses damping and becomes unstable in the STOL regime. The main beneficiary from the transfer of damping

is the roll subsidence. In this particular case the spiral mode becomes also progressively more unstable as speed is reduced.

To test if the trends revealed by Fig. 41 are to be expected, generally, various combinations of the derivatives which control the zero have been tried with the results shown in Fig. 42. We find no significant departures from the general trends already discussed, the principal observation being in every case the destabilisation of the Dutch roll with reducing speed. An interesting condition is met in case (*D*), where a large negative value of N_p is assumed. In an intermediate speed range the so called second oscillation replaces the roll and spiral subsidence, but as the presentation of this result in Fig. 43 indicates, this mode has very low frequency and should not be particularly noticeable to the pilot. By observing the rules of root locus geometry we can state that a second lateral oscillation can only exist if the zero lies to the left of the two real poles, i.e. if roll damping is poor and $(-N_p)$ is large.

5.3. *General Observations.*

In Ref. 9 Thorpe had earlier considered dynamic stability of the particular case of a partly jet-borne STOL aircraft, making the same assumption as we have done here. His results are in complete agreement with those of the present analysis. The treatment of the subject by root locus technique permits us, however, to observe that these trends are generally valid and do not depend on particular values of aircraft characteristics. The reader familiar with root-locus manipulation will readily see that the trends depicted in Figs. 38 and 42 for the longitudinal and the lateral motion respectively are inevitable and that they cannot be significantly altered by any conceivable combination of basic aerodynamic characteristics, i.e. for any conceivable root-zero configuration. Hence we can generally expect that in the STOL regime, the phugoid will become unstable and approach in frequency that of the short-period oscillation, which will gain in damping. The dutch roll will become unstable, the damping being mainly transferred to the roll subsidence mode, so that this mode will be more stable than one would normally expect at the low speeds involved.

6. *Conclusions.*

An attempt has been made to consider very broadly those areas in which the handling of STOL aircraft may differ from that of conventional aircraft. Since there are many distinct design approaches towards the realisation of STOL capability, we had first to identify those design features which lead to a natural classification into aerodynamically distinguishable major types. These were first what we describe as 'conventional' solutions, i.e. those in which power is not used to supplement airfoil lift. Then we considered three forms in which engine power can be utilised to augment natural wing lift, namely either directly as vertical thrust, or indirectly by blowing over the flaps or by immersing the wing in a propeller slipstream.

When considering longitudinal response to gusts, it was found that in the STOL regime fore and aft gusts are at least as important as vertical gusts and cannot, therefore, be ignored when assessing the behaviour of this class of aircraft in turbulence. Basic gust sensitivity was first examined, i.e. the instantaneous normal acceleration response to a step gust. In this respect, STOL aircraft would seem to be generally less sensitive than current aircraft, except that reductions in wing loading will have an adverse effect. However, STOL aircraft require increased incidence margins to protect them against stalling in the approach. When one takes into account aircraft dynamics as well, it is then shown that STOL aircraft are unlikely to be better than current aircraft, with the possible exception of slipstream and jet flap configurations. If STOL is achieved by drastic reductions in wing loading, very poor characteristics will result.

Response to lateral turbulence should not necessarily present great problems but rudder and roll control power must be adequately increased to combat the natural loss in effectiveness with decreased airspeeds.

Cross-wind control was then examined in some detail. It was noted that our understanding of the piloting aspects of cross-wind control is too imperfect at present to permit firm predictions. In view of this, it is suggested that it would be prudent not to expect greater cross-wind angles to be acceptable than are tolerated with present aircraft, unless and until flight experience can demonstrate this view to be too conservative. This would imply a reduction in cross-wind tolerance to less than 20 knots for typical STOL approach speeds. A general reappraisal of limiting wind conditions—rather than cross-wind alone—is recommended and in this context much could be gained by scheduling for constant ground speed rather

than airspeed when there is a significant headwind component.

Speed stability in flight under glide-path constraint was then considered. The use of high aerodynamic lift is likely to lead to quite substantial degrees of speed instability but, in propeller-driven designs (slip-stream aircraft), the speed dependence of thrust will have a stabilising influence. Aircraft using direct vertical thrust are likely to be very speed-unstable, when the elvator is used but stable when thrust is used to control the glide path.

It is suggested that another important flight case is that where the pilot maintains tight control of pitch attitude. In the speed regime covered by conventional aircraft, this constraint leads to a highly stable situation and this is suggested as the reason why this mode had not previously received any attention. It is shown that, with some STOL designs, attitude-constrained flight leaves the aircraft with a phugoid-type oscillation of relatively short period and that this might be less than satisfactory to the pilot.

Finally, classical dynamic stability (with controls fixed) is investigated with particular attention to designs in which part of the lift is provided by the engines. It is shown by generalised root-locus analysis that the STOL aircraft must be expected to develop an unstable phugoid of a frequency close to that of the so-called short-period oscillation and that this phenomenon is not greatly affected by the type of lifting mechanism employed.

In the lateral field, there is a strong tendency for the dutch roll to become unstable at STOL speeds but the roll subsidence mode will benefit from the damping transferred from the lateral oscillation. At the same time, the period of the dutch roll is likely to become rather long so that the lateral motion of the STOL aircraft is likely to be sluggish and indecisive.

It must be emphasised that in this report only broad trends are examined and that design details can influence many of the aerodynamic characteristics that were assumed to be unaltered here. In particular effects such as engine-induced aerodynamic interference with the airframe, must be determined in the wind tunnel and could not be allowed for in the present generalised study.

LIST OF SYMBOLS

a	Lift slope
a_{00}	Lift slope at V_{00}
A	Inertia in roll
a_i	Coefficients in the longitudinal stability polynomial
AR	Aspect ratio
A_P	Propeller disc area
A_∞	Cross-sectional area of slipstream
b	Wing span
b_i	Coefficients in the lateral stability polynomial
B	Inertia in pitch
C	Chord
C_L	Lift coefficient
$C_{L_e} = \frac{W/S}{\rho/2\, V_0^2}$	Equivalent lift coefficient
C_D	Drag coefficient
C_f	Flap chord
C_l	Rolling moment coefficient
C_n	Yawing moment coefficient
C	Inertia in yaw
C_μ	Jet momentum coefficient
D	Drag
$D_{\min}$	Minimum drag
E	Product of inertia
$F_\alpha = \frac{a}{a_{00}}$	Lift slope ratio
$F_A = \frac{L_A}{\Sigma L}$	Aerodynamic lift ratio

F_j	(*See* equation (A.7))
g	Earth gravity
G	Variable used in Appendix E, Section E.1
H	Variable used in Appendix E, Section E.2
$\dot{h}$	Vertical velocity
$i_A = \frac{A}{ml^2}$	Inertia coefficient in roll
$i_B = \frac{B}{ml^2}$	Inertia coefficient in pitch
$i_C = \frac{C}{ml^2}$	Inertia coefficient in yaw
k_x, k_y, k_z	Inertia radius in roll, pitch and yaw
K	Gain factor in root locus transfer function
L	Lift or rolling moment
L_A	Aerodynamic lift, portion of total lift varying with V^2
$L_\alpha = \frac{\partial L}{\partial \alpha}$	Dimensional lift slope
$L_\beta = \frac{\partial L}{\partial \beta}$	Rolling moment due to sideslip
$L_p = \frac{\partial L}{\partial_p}$	Rolling moment due to rate of roll
$L_r = \frac{\partial L}{\partial r}$	Rolling moment due to rate of yaw
l	Aircraft reference length (typically wing chord)

$l_v = \frac{\partial C_l}{\partial \beta}$ $l_p = \frac{\partial C_l}{\partial\left(\frac{pl}{V_0}\right)}$ $l_r = \frac{\partial C_l}{\partial\left(\frac{rl}{V_0}\right)}$	Nondimensional rolling moment derivatives
m	Mass
m_E	Engine mass flow per second
M	Pitching moment
$M_\alpha = \frac{\partial M}{\partial \alpha}$	Pitching moment due to incidence
$M_{\dot{\alpha}} = \frac{\partial M}{\partial \dot{\alpha}}$	Pitching moment due to rate of change of incidence
$M_q = \frac{\partial M}{\partial q}$	Pitching moment due to pitch rate
$m_w = \frac{\partial C_m}{\partial \alpha}$ $m_{\dot{w}} = \frac{\partial C_m}{\partial\left(\frac{\dot{\alpha} l}{V_0}\right)}$ $m_q = \frac{\partial C_m}{\partial\left(\frac{ql}{V_0}\right)}$	Nondimensional pitching moment derivatives
n	Normal acceleration load factor
N	Yawing moment
$N_\beta = \frac{\partial N}{\partial \beta}$	Yawing moment due to sideslip
$N_p = \frac{\partial N}{\partial p}$	Yawing moment due to roll rate

$N_r = \frac{\partial N}{\partial r}$	Yawing moment due to yaw rate
$n_v = \frac{\partial C_n}{\partial \beta}$	Nondimensional yawing moment derivatives
$n_p = \frac{\partial C_n}{\partial \left(\frac{pl}{V_0}\right)}$	
$n_r = \frac{\partial C_n}{\partial \left(\frac{rl}{V_0}\right)}$	
P	Period of oscillation
p	Rate of roll
q	Rate of pitch
r	Rate of yaw
S	Wing area
S_s	Wing area submersed in propeller slipstream
s	Laplace operator
$s' = \frac{s}{V_0}$	Laplace operator
T	Thrust
t	Time
T_V	Vertical thrust component
$u = V - V_0$	Velocity increment
u_g	Horizontal gust velocity
V	Airspeed
V_a	Approach speed
V_e	Equivalent airspeed
V_0	Datum airspeed

V_{oo}	Lowest airspeed for level flight without powered lift assistance
v_g	Lateral gust velocity
$W = mg$	Weight
w	Vertical velocity
x_i	Distance from CG of engine intake
X	Longitudinal force
$X_\alpha = \frac{\partial X}{\partial \alpha}$	
$X_u = \frac{\partial X}{\partial \left(\frac{u}{V_0}\right)}$	
Y	Sideforce
$Y_\beta = \frac{\partial Y}{\partial \beta}$	
Z	Vertical force
$Z_\alpha = \frac{\partial Z}{\partial \alpha}$	
$Z_u = \frac{\partial Z}{\partial \left(\frac{u}{V_0}\right)}$	
α	Angle of attack
β	Angle of sideslip
γ	Glide path angle
τ	Time constant
σ	Real part of root
ω	Angular frequency
θ	Pitch attitude
θ_j	Jet flap angle

λ	Stability root
ρ	Air density
ρ_{SL}	Air density at sea level

REFERENCES

No.	*Author(s)*	*Title, etc.*
1	Anon.	Tentative airworthiness standards for powered lift transport category aircraft. Flight Standards Service Department of Transportation, FAA Washington, USA (August 1970).
2	R. C. Innis, C. A. Holzhauser and H. C. Quigley	Airworthiness considerations for STOL aircraft. NASA TN D-5594 (1970).
3	H. W. Chinn, D. Lean and W. Pinsker ..	Some basic capabilities and limitations of STOL aircraft. Unpublished MAS material.
4	J. Williams and M. N. Wood	Aerodynamic interference effects with jet-lift V/STOL aircraft under static and forward-speed conditions. R.A.E. Technical Report 66403 (A.R.C. 28795) (1966).
5	J. Williams, S. F. J. Butler and M. N. Wood	The aerodynamics of jet flaps. A.R.C. R. & M. 3304 (1961).
6	R. Smelt and H. Davies ..	Estimation of increase in lift due to slipstream. A.R.C. R. & M. 1788 (1936).
7	B. Thwaites (Editor)	*Incompressible Aerodynamics. Section XII*, 21, Oxford, Clarendon Press (1960).
8	W. J. Pinsker	The effect of gyroscopic engine coupling on the longitudinal and lateral motion of aircraft. R.A.E. Technical Report 70113 (1970) A.R.C. 32530.
9	A. W. Thorpe	The stability and control of an aircraft supported partly by deflected jet thrust. R.A.E. Technical Note Aero 2207 (1952) A.R.C. 15856.
10	S. Neumark	Problems of longitudinal stability below minimum drag speed and theory of stability under constraint. A.R.C. R. & M. 2983 (1953).
11	W. Pinsker	Directional stability in flight with bank angle constraint as a condition defining a minimum value for n_v. A.R.C. R. & M. 3556 (1967).
12	J. G. Jones	A theory for extreme gust loads in an aircraft based on the representation of the atmosphere as a self similar intermittent random process. R.A.E. Technical Report 68030 (1968) A.R.C. 30592.
13	J. G. Jones	Similarity theory of gust loads on aircraft. Development of Gaussian patch representation. R.A.E. Technical Report 69094 (1969) A.R.C. 31392.

14 J. G. Jones . . . . . Similarity theory of gust loads on aircraft. Development of discrete gust theory and introduction of empirical functions. R.A.E. Technical Report 69171 (1969) A.R.C. 31983.

15 J. G. Jones and W. J. G. Pinsker . . . . The application of discrete gust theory to the prediction of the gust response of STOL aircraft in the landing approach. R.A.E. Technical Report (to be published).

16 A. Jameson . . . . . Analysis of wing slipstream flow interaction. NASA CR-1632 (August 1970).

APPENDIX I

Lifting Properties of the Jet Flap Wing

Ref. 5 suggests that the lift on a jet flap wing of infinite aspect ratio can be expressed as the sum of the two contributions:

$$C_L = \theta \frac{\partial C_L}{\partial \theta} + \alpha \frac{\partial C_L}{\partial \alpha} \tag{A.1}$$

where α is the wing incidence and θ the angle of the jet sheet in relation to the wing chord. This expression is strictly only valid in two-dimensional flow, but we shall apply it more generally to wings of finite span. This is justified for mainly two reasons. To apply the jet flap principle efficiently large aspect ratio wings are required in which case corrections for finite span will not be very large. Secondly the analysis here is aimed at expressions defining ratios of lifts and in these the errors introduced by ignoring three-dimensional flow will largely cancel.

The two lift slopes in equation (A.1) are functions of the jet momentum coefficient

$$C_\mu = \frac{M_j V_j}{\frac{\rho}{2} V^2 S} \tag{A.2}$$

and $\partial C_L/\partial\theta$ in addition depends on the ratio of the flap chord C_f to the wing chord C. Fig. 5 gives results from Ref. 5 as applicable to a jet flap operating uniformly over the full span. The values given for $C_f/C = 1$ define the wing lift slope $\partial C_L/\partial\alpha$. Ignoring designs with very small relative flap chords and the range of small momentum coefficients we can approximate these curves by the linear expression:

$$\frac{\partial C_L}{\partial \theta} = 7\left\{1 - 0{\cdot}6\left(1 - \frac{C_f}{C}\right)^2\right\} + 1{\cdot}6 C_\mu \tag{A.3}$$

and therefore

$$\frac{\partial C_L}{\partial \alpha} = 7 + 1{\cdot}6 C_\mu. \tag{A.4}$$

Equation (A.4) or its more accurate equivalent given in Fig. 5 defines the lift slope relevant to aircraft stability and response to vertical gusts.

We also need the change of lift with respect to increments in airspeed ΔV at fixed incidence and throttle or thrust as relevant to phugoid stability and response to horizontal gusts. If V_0 is a datum speed and $C_{\mu 0}$ the associated trimmed momentum coefficient, we note from equation (A.2) that

$$C_\mu = C_{\mu 0}\left(\frac{V_0}{V_0 + \Delta V}\right)^2. \tag{A.5}$$

From

$$L = \frac{\rho}{2} S(V_0 + \Delta V)^2 C_L \tag{A.6}$$

we get with equations (A.3) and (A.5) the total lift

$$\Sigma L = \frac{\rho}{2} S\{7(F_j\theta+\alpha)(V_0+\Delta V)^2 + 1{\cdot}6C_{\mu 0} V_0^2 (\theta+\alpha)\} \tag{A.7}$$

where F_j is a flap chord factor.

$$F_j = 1-0{\cdot}6\left(1-\frac{C_f}{C}\right)^2.$$

Only the first term in the bracket varies with $(V_0+\Delta V)$ and if we define this contribution as 'aerodynamic lift' L_A we obtain the ratio of $L_A/\Sigma L$ as

$$\frac{L_A}{\Sigma L} = \frac{1}{1+C_{\mu 0}\dfrac{1{\cdot}6}{7}\dfrac{\theta+\alpha}{F_j\theta+\alpha}}. \tag{A.8}$$

If we exclude improbable combinations of α, θ, and flap chord C_f/C, this ratio depends practically only on $C_{\mu 0}$ (Fig. 6).

In order to obtain results in a form usable for stability work, we must find a relationship between $C_{\mu 0}$ and V_0.

For this we assume that over the STOL speed range the aircraft is flown with constant flap angle θ_0 and incidence α_0. If V_{00} is the lowest speed at which the aircraft can support itself fully in this configuration without power assistance, i.e. $C_{\mu 0} = 0$ then from (A.7)

$$W = L = \frac{\rho}{2} V_{00}^2 S7 (F_j\theta_0+\alpha_0)$$

and for $V < V_{00}$

$$W = \Sigma L = \frac{\rho}{2} V^2 S\{7(F_j\theta_0+\alpha_0)+1{\cdot}6C_\mu(\theta_0+\alpha_0)\}.$$

By equating these two expressions we get

$$C_\mu = \frac{'7}{1{\cdot}6}\frac{F_j\theta_0+\alpha_0}{\theta_0+\alpha_0}\left\{\left(\frac{V_{00}}{V}\right)^2-1\right\},$$

which reduces to

$$C_\mu = \frac{7}{1{\cdot}6}F_j\left\{\left(\frac{V_{00}}{V}\right)^2-1\right\}$$

if we assume that $\alpha_0 \ll \theta_0$. For a flap chord of 10 per cent C, Fig. 7 gives F_j as 0·51 and

$$C_\mu = 2{\cdot}2\left\{\left(\frac{V_{00}}{V}\right)^2-1\right\}. \tag{A.9}$$

We note that within the practical range of chord ratios, F_j does not vary too much and so we take the expression (A.9) as a general approximation. This allows us to calculate $\partial C_L/\partial\alpha(V)$ and $L_A/\Sigma L(V)$ using Figs. 5 and 6 with the results shown in Fig. 8 where the lift slope is expressed as the ratio of the value at a given speed to that at V_{00}

$$F = \frac{(\partial C_L/\partial \alpha)_V}{(\partial C_L/\partial \alpha)_{V_{00}}}. \tag{A.10}$$

APPENDIX II

Lifting Properties of the Wing Immersed in a Propeller Slipstream

A rigorous treatment of the slipstream effect is a complex subject not attempted here; we refer to the first attempted method of estimation by R. Smelt and H. Davies[6] and to the account given by Thwaites[7]. A thorough analysis of the wing in slipstream has more recently been presented in Ref. 16. We shall restrict ourselves to an elementary approach based on momentum theory. Also, we ignore cases such as the tilt-wing aircraft where the propeller axis is greatly inclined to the flight direction. The general configuration and definitions are illustrated in Figs. 9 and 10. Of the total wing area S only S_s is immersed in the slipstream which is assumed to be fully contracted and homogeneous within its boundaries. We also ignore lift losses due to uneven spanwise distribution of circulation.

Propellers located forward of the wing affect lift in three ways. First the velocity of the flow over the wing is increased by the slipstream (Fig. 9). Secondly, the slipstream, if inclined with respect to the flight direction will change the effective incidence of the wing. Thirdly, the component of the thrust normal to the direction of flight also makes a significant contribution.

The increase in flow velocity due to the slipstream velocity increment u_s modifies the basic wing lift to

$$L = \frac{\rho}{2} C_L \{V^2(S - S_s) + (V + u_s)^2 S_s\}^*, \tag{B.1}$$

where V is freestream velocity and C_L the lift coefficient of the airfoil in freestream.

If we assume that the slipstream velocity increment is imparted exactly in the direction of the propeller axis, i.e. at an angle α_P that part of the wing immersed in the slipstream is subject to an induced incidence:

$$\alpha_i = -\alpha_P \frac{u_s}{V + u_s} \tag{B.2}$$

so that:

$$\Delta_1 L = \frac{\rho}{2} (V + u_s) S_s a \alpha_P u_s \tag{B.3}$$

where a is the lift slope of the wing in freestream conditions**.

The third contribution derives from the direct component of the thrust (otherwise termed propeller side force) normal to the flight direction. The assumption made earlier with respect to the direction of the slipstream implies that thrust acts along the propeller axis and the associated lifting component is then

$$\Delta_2 L = T\alpha_P \tag{B.4}$$

for small values of α_P.

---

* Strictly according to Ref. 1, this increase in lift results from an increase in the effective geometric incidence by a factor $(1 + 2u_s/V)$ with, however, the same result.

** This increment will be less if the wing is close to the propeller, where the final slipstream velocity has not yet been reached; and the final result would also be affected by the number of propellers and their positions along the span. To obtain an accurate answer would, therefore, require a more detailed investigation and experimental verification. For the present purpose, the simple relation (B.3) is thought to be adequate.

Adding (B.1), (B.3) and (B.4) we get the total effective lift as

$$\Sigma L = \frac{\rho}{2}[C_L\{V^2(S-S_s)+(V+u_s)^2S_s\}-(V+u_s)S_s a\alpha_P u_s]+T\alpha_P. \tag{B.5}$$

When analysing the lifting behaviour of the other types of STOL aircraft it was possible and plausible to make the assumption that at all speeds below V_{00} they are trimmed at the same incidence or C_L. This assumption is not permissible with the slipstream aircraft as here the pilot is not free to select engine power just to control lift. Rather, thrust must be chosen to balance drag and the incidence then adjusted so that the resultant lift equals weight. In other words the required C_L must be determined from equation (B.5), putting $\Sigma L = W$.

Our main interest is to find derivatives of lift with respect to changes in airspeed and incidence from a given trimmed equilibrium condition at V_0.

Basic momentum considerations define a relationship between u_s, V and T as

$$T(V, u_s) = \rho A_\infty (V+u_s)u_s\,. \tag{B.6}$$

If A_P is the propeller disc area and A_∞ the cross-sectional area of the fully contracted slipstream, continuity demands that

$$\frac{A_\infty}{A_P} = \frac{1+\frac{1}{2}\frac{u_s}{V}}{1+\frac{u_s}{V}} \tag{B.7}$$

since classical propeller theory states that the value of the velocity increment at the disc is half that at infinity downstream. Equations (B.6) and (B.7) combined give

$$T = \rho A_P V u_s\left(1+\frac{1}{2}\frac{u_s}{V}\right). \tag{B.8}$$

This equation can be solved for (u_s/V):

$$\frac{u_s}{V} = -1 \pm \sqrt{1+\frac{2T}{\rho A_P V^2}} \tag{B.9}$$

where only the solution with the positive square root has physical significance.

We also require a relationship between thrust and airspeed for fixed throttle, in other words an expression defining the change in thrust T from the datum value T_0 required for flight equilibrium at V_0. We use the common assumption that thrust is inversely proportional to airspeed

$$T = T_0\frac{V_0}{V} \tag{B.10}$$

but remember that this simple law only applies approximately in the principal operational regime for the propeller and becomes invalid at very low speeds where thrust tends to be constant. With (B.10) we can express equation (B.9) as

$$\left(\frac{u_s}{V}\right) = -1+\sqrt{1+\frac{\tau_0 V_0}{V^3}} \tag{B.11}$$

where

$$\tau_0 = \frac{2T_0}{\rho A_P}. \tag{B.12}$$

Finally we need to know the equilibrium thrust T_0 required for a given datum speed V_0.

Restricting the analysis to level flight we can equate thrust to drag and as a crude approximation we may assume that in the high lift range in STOL flight the induced drag contribution predominates, hence

$$D_0 = T_0 \simeq \frac{W}{S}\frac{W}{\frac{\rho}{2}\pi AR}\frac{1}{V_0^2}. \tag{B.13}$$

For more accurate calculations we can of course readily obtain the correct drag from WT measurements or more detailed drag estimates.

Having thus stated the assumptions we can now proceed to calculate the change of lift with incidence $\Delta\alpha$ and with respect to velocity increments ΔV, i.e. we can calculate the effective lift slope $\partial C_L/\partial\alpha$ and the lift ratio $L_A/\Sigma L$. To derive the effective lift slope we first nondimensionalise equation (B.5), and with $V = V_0$ get

$$C_L = \frac{\Sigma L}{\frac{\rho}{2}V_0^2 S} = C_L\left\{\left(1-\frac{S_s}{S}\right)+\left(1+\frac{u_s}{V_0}\right)\frac{S_s}{S}\right\}-\left(1+\frac{u_s}{V_0}\right)\frac{S_s}{S}a\alpha_P\frac{u_s}{V_0}+\frac{T_0}{\frac{\rho}{2}V_0^2 S}\alpha_P. \tag{B.14}$$

To differentiate with respect to α we write the basic lift coefficient C_L in the usual linearised form

$$C_L = C_{L_{(\alpha=0)}}+a\alpha \tag{B.15}$$

where α is wing incidence and we further observe that

$$\frac{d\alpha_P}{d\alpha} = 1. \tag{B.16}$$

This leads to

$$\frac{\partial C_L}{\partial\alpha} = a\left[1-\frac{S_s}{S}+\left(1+\frac{u_s}{V_0}\right)^2\frac{S_s}{S}-\left(1+\frac{u_s}{V_0}\right)\frac{u_s}{V_0}\frac{S_s}{S}\right]+\frac{T_0}{\frac{\rho}{2}V_0^2 S}. \tag{B.17}$$

The ratio of this lift slope to the basic lift slope a then gives the lift slope amplification factor

$$F = \frac{\partial C_L/\partial\alpha}{a} = 1-\frac{S_s}{S}+\left(1+\frac{u_s}{V_0}\right)^2\frac{S_s}{S}-\left(1+\frac{u_s}{V_0}\right)\frac{u_s}{V_0}\frac{S_s}{S}+\frac{T_0}{\frac{\rho}{2}V_0^2 Sa} \tag{B.18}$$

To obtain a numerical solution we must first calculate T_0 from (B.13) or its more accurate equivalent and then obtain (u_s/V_0) from (B.11) for the range of V_0 of interest.

To obtain the rate of change of lift with ΔV it is necessary to substitute the analytical expression for (u_s/V_0), i.e. equation (B.11) into (B.5) since (u_s/V_0) is itself a function of V. This leads to fairly tedious algebra and we give only the final answer which reads

$$\frac{L}{\frac{\rho}{2}S} = C_L V^2 \left\{ 1+\frac{\tau_0 V_0}{V^2}\frac{S_s}{S} \right\} - \frac{S_s}{S} V^2 \left(1+\frac{\tau_0 V_0}{V^3} - \sqrt{1+\frac{\tau_0 V_0}{V^3}} \right) a\alpha_P + \frac{T_0}{\frac{\rho}{2}S}\frac{V_0}{V}\alpha_P. \tag{B.19}$$

We can calculate from this equation the value of C_L appropriate to a given equilibrium flight condition by putting $V = V_0$ and $L = W$,

$$\text{i.e. } C_{LO} = \frac{\frac{W}{\frac{\rho}{2}SV_0^2} + \frac{S_s}{S}\left(1+\frac{\tau_0}{V_0^2} - \sqrt{1+\frac{\tau_0}{V_0^2}} \right) a\alpha_P - \frac{T_0\alpha_P}{\frac{\rho}{2}V_0^2 S}}{1+\frac{\tau_0}{V_0^2}\frac{S_s}{S}} \tag{B.20}$$

On the other hand differentiating equation (B.19) gives

$$\frac{d}{dV}\left(\frac{L}{\frac{\rho}{2}S}\right) = V_0 \left\{ C_{LO}\left(2-\frac{\tau_0}{V_0^2}\frac{S_s}{S}\right) - 2a\alpha_P\frac{S_s}{S}\left(1-\frac{1}{2}\frac{\tau_0}{V_0^2} - \frac{1+\frac{1}{4}\frac{\tau_0}{V_0^2}}{\sqrt{1+\frac{\tau_0}{V_0^2}}} \right) - \frac{T_0}{\frac{\rho}{2}S}\frac{\alpha_P}{V_0^2} \right\}. \tag{B.21}$$

In this differentiation we have taken S_s to be constant with speed as this only introduces negligible errors.

The corresponding result for an aircraft flying entirely on aerodynamic lift is

$$\frac{\partial}{\partial V}\frac{L}{\frac{\rho}{2}S} = 2\frac{W/S}{\frac{\rho}{2}}\frac{1}{V_0}. \tag{B.22}$$

Dividing (B.21) by (B.22) gives the ratio $L_A/\Sigma L$. To illustrate the characteristics of a typical slipstream STOL aircraft, numerical calculations were made assuming the following aircraft

$$W = 100{,}000 \text{ lb.} \qquad W/S = 75 \text{ lb/ft} \qquad a = 6$$

$$AR = 8{\cdot}0 \qquad A_p/S = 1{\cdot}28 \qquad V_{00} = 120 \text{ knots.}$$

This gives the following thrust and slipstream data:

V(knots)	T_0 (lb)	u_s/V_0	S_s/S	τ	C_{LO}
50	40000	0·94	0·870	19660	2·86
75	26700	0·40	0·935	13100	2·21
100	20000	0·16	0·962	9780	1·64
125	16000	0·08	0·970	7860	1·205
150	13000	0·05	0·990	6380	0·894

The lift slope amplification factor F obtained from equation (B.18) and $L_A/\Sigma L$as calculated from equations (B.21) and (B.22) are plotted against V_0/V_{00} in Fig. 11. Since dL/dVclearly depends on α_P the calculations were made for two values of $\alpha_P = 0°$ and $+10°$.

APPENDIX III

Speed Stability in Flight with Height Constraint

The induced drag acting on an aircraft is determined by the amount of lift carried by the wing and in this context it is irrelevant whether this lift is natural airfoil lift or lift amplified by engine power. On the other hand if part of the aircraft weight is supported by direct vertical thrust only the wing lift will contribute to induced drag. For the study of speed stability under glide path constraint where drag is a dominant factor, these two classes of STOL aircraft will be treated separately.

III.1. *All Lift Carried on the Wing.*

We assume that C_{DO} is unaffected by the wing lifting mechanism and also that $\partial C_D/\partial C_L^2$ is identical to that for the wing without powered lift. If both C_{DO} and $\partial C_D/\partial C_L^2$ are constant over the range of C_L and speed of interest here, we can express drag in the usual form

$$D = \frac{\rho}{2} V^2 S \left(C_{DO} + \frac{\partial C_D}{\partial C_L^2} C_L^2 \right) \tag{C.1}$$

and with

$$C_L = \frac{W}{\frac{\rho}{2} V^2 S}$$

this leads to

$$D = C_{DO} \frac{\rho}{2} V^2 S + \frac{\partial C_D}{\partial C_L^2} \frac{W^2}{\frac{\rho}{2} S V^2}. \tag{C.2}$$

It can be readily shown that this expression can be written in the form

$$D = \tfrac{1}{2} D_{\min} \left\{ \left(\frac{V}{V_{D_{\min}}} \right)^2 + \left(\frac{V_{D_{\min}}}{V} \right)^2 \right\} \tag{C.3}$$

where $D_{\min}$ is the minimum value which drag assumes at the minimum drag speed $V_{D_{\min}}$ (Fig. 25).

The stability root λ_S defining speed stability in rectilinear flight constrained by elevator control is given as:

$$\lambda_S = \frac{1}{m} \frac{d}{dV} \{ D(V) - T(V) \}. \tag{C.4}$$

For jet powered aircraft we can assume $T(V) = \text{const.}$ and in this case equation (C.4) is fully determined by considering only variations in drag with speed, i.e. equation (C.3).

Differentiating this expression leads to

$$\lambda_S = \frac{dD/dV}{m} = \frac{g}{W} \frac{D_{\min}}{V_{D_{\min}}} \left\{ \left(\frac{V_{D_{\min}}}{V} \right)^3 - \frac{V}{V_{D_{\min}}} \right\} \tag{C.5}$$

or with $W/D_{\min} = (L/D)_{\max}$

$$\lambda_S = \frac{^L g}{(L/D)_{\max}} \frac{1}{V_{D_{\min}}} \left\{ \left(\frac{V_{D_{\min}}}{V} \right)^3 - \frac{V}{V_{D_{\min}}} \right\} . \tag{C.6}$$

This expression has been evaluated and plotted in Fig. 26.

It is of course conceivable that, in STOL aircraft, throttle might be used instead of elevator for height control and the implied increase in thrust as speed reduces would be stabilizing.

If one considers propeller driven designs such as the slipstream vehicle, thrust can no longer be assumed to be invariant with speed and we must introduce in equation (C.4) an appropriate relationship for $T(V)$. The most plausible general assumption is that thrust varies in inverse proportion to speed. From equation (C.3) we obtain the equilibrium thrust at V_0 for level flight as

$$T_0 = \tfrac{1}{2} D_{\min} \left\{ \left(\frac{V_0}{V_{D_{\min}}} \right)^2 + \left(\frac{V_{D_{\min}}}{V_0} \right)^2 \right\} \tag{C.7}$$

and therefore for throttle fixed by this condition

$$T = T_0 \frac{V_0}{V} = \frac{1}{2} \frac{V_0}{V} D_{\min} \left\{ \left(\frac{V_0}{V_{D_{\min}}} \right)^2 + \left(\frac{V_{D_{\min}}}{V_0} \right)^2 \right\} . \tag{C.8}$$

Differentiation with respect to speed gives

$$\frac{\partial T}{\partial V} = -\tfrac{1}{2} D_{\min} \left\{ \left(\frac{V_0}{V_{D_{\min}}} \right)^2 + \left(\frac{V_{D_{\min}}}{V_0} \right)^2 \right\} . \tag{C.9}$$

Substitutions of (C.9) and (C.6) into (C.5) leads to an expression for the speed stability of the propeller aircraft

$$\lambda_S = \frac{g}{(L/D)_{\max}} \frac{1}{2V_{D_{\min}}} \left\{ \left(\frac{V_{D_{\min}}}{V_0} \right)^3 - 3 \frac{V_0}{V_{D_{\min}}} \right\} . \tag{C.10}$$

The expression is plotted in Fig. 27 and by comparison with Fig. 26 we note that this type of aircraft will be speed stable down to 77 per cent of minimum drag speed and that it generally has more favourable characteristics. If power is used instead of elevator to control height, speed stability is further improved as it would be with jet powered designs.

III.2. *Partly Jet-Borne Flight.*

If part of the aircraft weight is supported by direct vertical thrust T_V there are three contributions to the fore and aft force X we must consider to establish speed stability. Instead of equation (C.4) we write

$$\lambda_S = \frac{1}{m} \frac{d}{dV}(X) = \frac{1}{m} \frac{d}{dV} \{ -D(V) - T_V \Delta\alpha - D_m(V) \} \tag{C.11}$$

when $D(V)$ is the airframe drag, $T_V\Delta\alpha$ the change in the fore and aft component of the vertical thrust with change in incidence and $D_m(V)$ the intake momentum drag. The latter is made up of two components, one associated with propulsive thrust and one with vertical thrust. We ignore the first, as being relatively insignificant in the STOL regime.

To establish airframe drag $D(V)$ we observe that

$$C_L = \frac{W - T_V}{\frac{\rho}{2} V^2 S} \tag{C.12}$$

so that instead of equation (C.2) we get

$$D = C_{DO}\frac{\rho}{2}V^2S + \frac{\partial C_D}{\partial C_L^2}\frac{(W-T_V)^2}{\frac{\rho}{2}S}\frac{1}{V^2}. \tag{C.13}$$

In trimmed flight at V_0:

$$W - T_{VO} = \frac{\rho}{2}V_0^2 S C_{LO}$$

and we are assuming that below V_{00} the aircraft is trimmed at constant incidence, i.e. that

$$C_{LO} = \frac{W}{\frac{\rho}{2}V_{00}^2 S}.$$

From these relationships we can calculate the change in drag with airspeed V when $T_V = T_{VO}$ is set for a given trimmed datum airspeed V_0 and elevator is used to maintain height as

$$D = C_{DO}\frac{\rho}{2}SV^2 + \frac{\partial C_D}{\partial C_L^2}\frac{2W^2}{\rho S}\left(\frac{V_0}{V_{00}}\right)^2\frac{1}{V^2}. \tag{C.14}$$

This expression is identical to (C.2) except that the second term has a factor $(V_0/V_{00})^2$. Hence in analogy with (C.3) we can write

$$D(V) = \tfrac{1}{2}D_{\min}\left\{\left(\frac{V}{V_{D_{\min}}}\right)^2 + \left(\frac{V_0}{V_{00}}\right)^2\left(\frac{V_{D_{\min}}}{V}\right)^2\right\}. \tag{C.15}$$

Differentiation with respect to V gives a contribution to the speed stability root (C.11)

$$\Delta_1\lambda_S = \frac{g}{(L/D)_{\max}}\frac{1}{V_{D_{\min}}}\left\{\left(\frac{V_0}{V_{00}}\right)^2\left(\frac{V_{D_{\min}}}{V_0}\right)^3 - \frac{V_0}{V_{D_{\min}}}\right\}. \tag{C.16}$$

To obtain the second term for equation (C.11) we take T_V to be constant T_{VO} and selected to be appropriate for the equilibrium speed V_0. Hence

$$\frac{d}{dV}(T_{VO}\Delta\alpha) = \frac{T_{VO}}{a}\frac{\partial C_L}{\partial V} = -2\frac{T_{VO}}{a}\frac{W - T_{VO}}{\frac{\rho}{2}S}\frac{1}{V_0^3} \tag{C.17}$$

and the associated contribution to λ_S is

$$\Delta_2 \lambda_S = 2g \frac{1-\frac{T_{VO}}{W}}{\frac{\rho}{2} S} \frac{T_{VO}}{a} \frac{1}{V_0^3},$$

with $\left(\frac{V_0}{V_{00}}\right)^2 = \left(1-\frac{T_{VO}}{W}\right)$ and $\frac{W/S}{\frac{\rho}{2}} = C_{LO} V_{00}^2$,

then

$$\Delta_2 \lambda_S = 2g \frac{C_{LO}}{aV_0} \left\{1-\left(\frac{V_0}{V_{00}}\right)^2\right\}. \tag{C.18}$$

To obtain the momentum drag contribution we use the relationships

$$T_{VO} = m_E V_j \quad \text{and} \quad D_m = m_E V,$$

where m_E is the engine mass flow, and V_j the jet efflux velocity. Hence

$$\frac{D_m}{V_{TO}} = \frac{V}{V_j} \quad \text{and} \quad \frac{d}{dV}(D_m) = \frac{T_{VO}}{V_j}.$$

This gives the third contribution to λ_S as

$$\Delta_3 \lambda_S = -\frac{g}{V_j}\left\{1-\left(\frac{V_0}{V_{00}}\right)^2\right\}. \tag{C.19}$$

Adding (C.16), (C.18) and (C.19) we get finally the speed stability root for the partly jet-borne aricraft as

$$\lambda_S = \frac{1}{(L/D)_{\min}} \frac{1}{V_{D_{\min}}} \left\{\left(\frac{V_0}{V_{00}}\right)^2 \left(\frac{V_{D_{\min}}}{V_0}\right)^3 - \frac{V_0}{V_{D_{\min}}}\right\} + g\left\{1-\left(\frac{V_0}{V_{00}}\right)^2\right\} \left\{2\frac{C_{LO}}{aV_0} - \frac{1}{V_j}\right\} \tag{C.20}$$

This expression is of course only valid for $V_0 \leqslant V_{00}$ and if glide path is controlled by the elevator, throttle remaining constant.

Equation (C.20) is essentially made up of four contributions, the first two are due to airframe drag, this being composed of a destabilising induced drag term, which is reduced by the factor $(V_0/V_{00})^2$ and a stabilising parasitic drag term. The lift engines also make two contributions. That due to varying fore and aft component is destabilising and the last term $1/V_j$ is the stabilising effect of the intake momentum drag. We note that the latter is entirely dependent on the jet efflux velocity and hence on the type of lift propulsion used. If high velocity jets supply the lift thrust, this contribution will be small and one can expect the destabilising terms to dominate, but with lift fans having low exit velocity V_j, there will be substantial momentum drag and speed stability will be more favourable. This is evident from the numerical examples presented in Fig. 28a. For these we have assumed for convenience that $V_{00} = V_{D_{\min}} = 120$ knots and $V_j = 1500$ ft/sec for the case representing the high velocity jets and $V_j = 500$ ft/sec for the example more appropriate to a lift fan.

If the pilot maintains α constant, using vertical thrust to control height, incidence will remain constant so that airframe drag varies simply as

$$D(V) = D_{00}\left(\frac{V}{V_{00}}\right)^2$$

and differentiation with respect to V gives a stabilising contribution to the speed stability root:

$$\Delta\lambda_S = -\frac{dD/dV}{m} = 2\frac{D_{00}}{W}g\left(\frac{V_0}{V_{00}}\right)\frac{1}{V_{00}}. \tag{C.21}$$

In addition we must consider the contribution of the momentum drag:

$$D_m = m_E V \tag{C.22}$$

and from

$$m_E = \frac{T_V}{V_j} \quad \text{then} \quad D_m = \frac{T_V}{V_j}V.$$

Since for rectilinear flight

$$\frac{T_V}{W} = 1-\left(\frac{V}{V_{00}}\right)^2, \tag{C.23}$$

then

$$D_m = \left[1-\left(\frac{V}{V_{00}}\right)^2\right] W\frac{V}{V_{j_{max}}}\frac{V_{j_{max}}}{V_j}. \tag{C.24}$$

We now require a relationship between V_j and thrust or speed. For a range of current jet and fan engines this relationship was studied and it was found that with very good approximation we can write

$$\frac{V_j}{V_{j_{max}}} = \frac{m_E}{m_{E\,max}} = \sqrt{\frac{T}{T_{max}}}. \tag{C.25}$$

This relationship allows us to express the momentum drag as

$$\frac{D_m}{m} = \frac{g}{V_{j_{max}}}\sqrt{1-\left(\frac{V}{V_{00}}\right)^2}\,V\sqrt{\frac{T_{max}}{W}}$$

using equation (C.23) to relate thrust to speed. Differentiation with respect to speed gives a contribution to the speed stability root

$$\Delta\lambda_S = -\frac{d}{dV}\left(\frac{D_m}{m}\right) = -\frac{g}{V_{j_{max}}}\sqrt{\frac{T_{V_{max}}}{W}}\,\frac{1-2\left(\frac{V_0}{V_{00}}\right)^2}{\sqrt{1-\left(\frac{V_0}{V_{00}}\right)^2}}. \tag{C.26}$$

A third contribution derives from the fact that unless the vertical thrust acts precisely in a direction normal to the flight direction, a change in thrust will produce a change in fore and aft force

$$\Delta X = -\Delta\varepsilon_E\,\Delta T_V,$$

where ε_E is the angle by which the angle of the thrust vector differs from the normal to the flight path. Since we are considering here a condition in which incidence is held constant, ε_E = const. so that

$$\Delta X = -\varepsilon_E \Delta T_V .$$

Substituting for T_V in equation (C.23) we get

$$\frac{\Delta X}{m} = -g\varepsilon_E \left\{1-\left(\frac{V}{V_{00}}\right)^2\right\}$$

and differentiation with respect to speed gives

$$\Delta\lambda_S = \frac{d}{dV}\left(\frac{X}{m}\right) = 2\frac{g}{V_{00}}\varepsilon_E\left(\frac{V_0}{V_{00}}\right), \tag{C.27}$$

a destabilising contribution if ε_E is positive, i.e. if the lift engines or nozzles are tilted in the decelerating sense and vice versa.
Adding equations (C.21), (C.26) and (C.27) gives finally

$$\lambda_S = \left(\frac{V_0}{V_{00}}\right)\frac{2g}{V_{00}}\left\{-\frac{1}{(L/D)_{00}}+\varepsilon_E\right\} - \frac{g}{V_{j\max}}\frac{1-2\left(\frac{V_0}{V_{00}}\right)^2}{\sqrt{1-\left(\frac{V_0}{V_{00}}\right)^2}}. \tag{C.28}$$

Again this is only valid for $V \leqslant V_{00}$ and for the case where the pilot maintains height by vertical thrust control. It is interesting to observe that the momentum drag contribution, i.e. the last term in equation (C.28) leads theoretically to infinite speed instability at $V_0 = V_{00}$. This condition is, however, of no practical significance because it implies the use of very low values of vertical thrust which are below the idling power of the engines. Furthermore a pilot is unlikely—even if it were possible—to control flight path by thrust application at a speed where there is adequate aerodynamic lift available for this purpose. Numerical examples for the characteristics defined by equation (C.28) are given in Fig. 28c.

APPENDIX IV

Stability in Flight Under Pitch Attitude Constraint

When pitch is constrained, only variations in speed and vertical motion need be considered. Since $\theta = \text{const}$, $\alpha = -\dot{\gamma} = w/V$ where w is the incremental vertical velocity. In flight path axes we get then:

$$m\dot{u} = mg\frac{w}{V_0} - \frac{\partial D}{\partial u}u - \frac{\partial D}{\partial \alpha}\frac{w}{V_0} \tag{D.1}$$

and

$$-m\dot{w} = \frac{\partial L}{\partial u}u + \frac{\partial L}{\partial \alpha}\frac{w}{V_0}.$$

In STOL flight only part of the lift is 'aerodynamic', i.e. varying with the square of speed and this must be appropriately considered in evaluating $\partial L/\partial u$ and $\partial D/\partial u$.

Expressing the aerodynamic derivatives in the form

$$\mathscr{L}_u = \frac{\partial L}{\partial u}\frac{1}{m},\quad \mathscr{L}_\alpha = \frac{\partial L}{\partial \alpha}\frac{1}{V_0}\frac{1}{m},\quad \mathscr{D}_u = \frac{\partial D}{\partial u}\frac{1}{m} \quad \text{and} \quad \mathscr{D}_\alpha = \frac{\partial D}{\partial \alpha}\frac{1}{V_0}\frac{1}{m} \tag{D.2}$$

equation (D.1) have as a solution the stability quadratic*

$$s = -\tfrac{1}{2}(\mathscr{D}_u + \mathscr{L}_\alpha) \pm \sqrt{\left(\frac{\mathscr{D}_u + \mathscr{L}_\alpha}{2}\right)^2 - \mathscr{L}_\alpha \mathscr{D}_u - \mathscr{L}_u\left(\frac{g}{V_0} - \mathscr{D}_\alpha\right)}. \tag{D.3}$$

We note that the damping of this mode is provided by $\mathscr{D}_u$ and $\mathscr{L}_\alpha$ and that the induced drag contribution $\mathscr{D}_\alpha$ only affects the frequency. To simplify numerical analysis we ignore here this last term, being of only minor significance. Hence

$$s \approx \frac{\mathscr{D}_u + \mathscr{L}_\alpha}{2} \pm \sqrt{\left(\frac{\mathscr{D}_u + \mathscr{L}_\alpha}{2}\right)^2 - \mathscr{L}_\alpha \mathscr{D}_u - \mathscr{L}_u \frac{g}{V_0}}. \tag{D.4}$$

In any equilibrium flight condition

$$W = L_A + T_V = \frac{\rho}{2}V_0^2 S C_{L0} + T_V, \tag{D.5}$$

$$C_{L0} = \frac{W - T_V}{\frac{\rho}{2}V_0^2 S}. \tag{D.6}$$

---

* It may be noted that the corresponding solutions for the phugoid mode with fixed controls and assuming $\alpha = 0$ is

$$S = -\frac{\mathscr{D}_u}{2} \pm \sqrt{\left(\frac{\mathscr{D}_u}{2}\right)^2 - \frac{g}{V_0}\mathscr{L}_u}.$$

If speed varies at constant $C_L = C_{L0}$,

$$L = \frac{\rho}{2} S V^2 \frac{W - T_V}{\frac{\rho}{2} V_0^2 S} + T_V. \tag{D.7}$$

Differentiation with respect to V, assuming T_V to be invariant with speed, gives

$$\frac{\partial L}{\partial u} = 2 \frac{W - T_V}{V_0},$$

or in the form defined in (D.2)

$$\mathscr{L}_u = \frac{\partial L / \partial u}{m} = 2 \frac{g}{V_0} F_A. \tag{D.8}$$

The dimensional lift slope is

$$\frac{\partial L}{\partial \alpha} = \frac{\rho}{2} V_0^2 S F_\alpha a_\infty \tag{D.9}$$

where a_{00} is the unaugmented lift slope at $V \geqslant V_{00}$ and F_α the lift amplification factor equation (A.10). From equation (D.2)

$$\mathscr{L}_\alpha = \frac{\partial L / \partial \alpha}{m V_0} = a_{00} F_\alpha \frac{\rho g V_0}{2(W/S)}. \tag{D.10}$$

From equation (D.4) we see that when subcritically damped, the pitch constrained aircraft motion is an oscillation with the undamped frequency

$$w_n = \sqrt{\mathscr{L}_u \frac{g}{V_0} + \mathscr{L}_\alpha \mathscr{D}_u}.$$

From $D = \dfrac{L}{L/D}$ we can write $\mathscr{D}_u = \dfrac{\mathscr{L}_u}{L/D}$ (D.11)

and therefore with (D.8) and (D.10)

$$\omega_n = \sqrt{\mathscr{L}_u \frac{g}{V_0} + \mathscr{L}_\alpha \frac{\mathscr{L}_u}{L/D}} = \frac{g}{V_0} \sqrt{2F_A + a_{00} \frac{F_\alpha \rho V_0^2}{2(W/S)(L/D)}} \tag{D.12}$$

For conventional aircraft where $F_A = F_\alpha = 1$ this reduces to

$$\omega_n = \frac{g}{V_0} \sqrt{2 + a_{00} \frac{\rho V_0^2}{2(W/S)(L/D)}} \tag{D.13}$$

Assuming $a_{00} = 6$ and sea level flight values for ρ this expression has been evaluated with the result shown in Fig. 29a. We note that even at the lowest STOL speeds of practical interest the period never falls below

15 secs. This is even more true for partially jet borne designs as seen from Fig. 29b. This result has been obtained by substituting $F_A = (V_0/V_{00})^2$ in equation (D.12). Below V_{00}, the period remains virtually constant at the value appropriate to V_{00}, the lowest conventional flying speed. Calculations have also been made for jet flap and slipstream type designs, but the results did hardly differ from those obtained for the partially jet borne aircraft, so that the trend depicted in Fig. 29b can be taken as representative of all power-augmented designs.

It has been thus established that the frequency of the mode under study is low enough for effective pilots control at this frequency to be plausible and we can be reasonably assured that the mathematical assumption of close pitch altitude control is justified and meaningful.

Our main interest, however, lies in the damping of this mode. From (D.4) we get the damping ratio ζ as:

$$\zeta^2 = \frac{\left\{\frac{1}{2}\left(\frac{\mathscr{L}_u}{L/D} + \mathscr{L}_\alpha\right)\right\}^2}{\mathscr{L}_u \frac{g}{V_0} + \mathscr{L}_\alpha \frac{\mathscr{L}_u}{L/D}} \tag{D.14}$$

which can be expressed in the form:

$$\zeta^2 = \tfrac{1}{2} \frac{1 + \frac{1}{2}\frac{\mathscr{L}_u}{\mathscr{L}_\alpha L/D} + \frac{1}{2}\frac{\mathscr{L}_\alpha L/D}{\mathscr{L}_u}}{1 + \frac{g}{V_0}\frac{L/D}{\mathscr{L}_\alpha}}, \tag{D.15}$$

where with equations (D.8) and (D.10)

$$\frac{\mathscr{L}_u}{\mathscr{L}_\alpha}\frac{1}{L/D} = 2\frac{F_A}{F_\alpha}\frac{C_{L_e}}{a_{00}\, L/D} \tag{D.16}$$

and

$$\frac{g}{V_0}\frac{L/D}{\mathscr{L}_\alpha} = \frac{C_{L_e}\, L/D}{a_{00}\, F_\alpha}.$$

If we define C_{L_e} as the equivalent lift coefficient

$$C_{L_e} = \frac{W/S}{\rho/2\, V_0^2}. \tag{D.17}$$

For the specific case where $a_{00} = 6$ and $F_A = F_\alpha = 1$ equation (D.15) has been evaluated with the result shown in Fig. 30. It may be noted that although changes in a_{00} will not alter the basic trends shown in Fig. 30, the numerical results are of course altered. We observe that the damping of the attitude-constrained mode attains very high values at high speeds and this is why this form of flight control is so successful in conventional aircraft. However, when speeds fall into the STOL range, the normally supercritically damped mode becomes oscillatory and damping gets less the lower the speed. It should be noted that in traversing the speed range, L/D will normally change, so that an appropriate interpolation must be used.

Fig. 30 applies directly to the type of aircraft we had defined as conventional STOL where F_A and F_α are equal to unity over the whole speed range.

Let us now consider broadly how engine lift augmentation will affect this picture. From Fig. 31 we see that for the jet lift design $F_\alpha = 1$ but $F_A = \left(\frac{V_0}{V_{00}}\right)^2$.

After substitution of this expression into (D.16) and (D.15) we get below V_{00} a change to the trend in damping as illustrated for some examples with $a_{00} = 6$ and $L/D = 5$ in Fig. 32a. Above V_{00} the solution shown in Fig. 30 applies but below V_{00}, damping is now less strongly attenuated, although there is still a steady loss of damping as speed is reduced.

Finally for the jet flap and the slipstream aircraft we can from Fig. 31 very roughly approximate: $F_\alpha = V_{00}/V$, F_A again equal to $(V_0/V_{00})^2$ and if these relationships are used in (D.16), the loss in damping ratio with reducing speed is now halted and as Fig. 32b shows there is even a tendency for damping to improve in the STOL regime.

APPENDIX V

Controls-Fixed Dynamic Stability

We make the usual assumption that the longitudinal and lateral freedoms of the STOL aircraft can be considered separately. However, it must be realised that cross-coupling between these modes may become significant with the unusual aerodynamic characteristics of some possible STOL configurations. An effect that requires particular attention is that generated by the rotary momentum of the engines which according to Ref. 8 can become dominating at very low speed, unless the engines are installed in handed pairs.

V.1. *Longitudinal Stability.*

The standard form of the equations of motion apply, and we get, in body axis notation:

$$\begin{aligned} M_\alpha \alpha + M_q q + M_{\dot{w}} \dot{\alpha} + M_u \hat{u} &= B\ddot{\theta}, \\ Z_\alpha \alpha + Z_u \hat{u} &= mV_0 (\dot{\alpha} - \dot{\theta}), \\ X_\alpha \alpha + X_u \hat{u} - mg\theta &= mV_0 \dot{\hat{u}}, \\ \text{and } q &= \dot{\theta}. \end{aligned} \tag{E.1}$$

where $\hat{u} = \dfrac{u}{V_0}$.

Although formally these equations have familiar appearance we must carefully re-examine the significance of the terms in these equations. As in all the other aspects treated in this report we assume for stability analysis that at all speeds below V_{00} the aircraft is trimmed at constant α. This suggests the broad assumption that the nondimensional aerodynamic derivatives are also constant in this regime. This assumption was also made by Thorpe in Ref. 9 where he treats aircraft partly supported by deflected jet thrust, with results virtually identical to those derived below. The gravity term in the X-equation is normally expressed in terms of C_L, but this is only valid if the aircraft weight is entirely supported by aerodynamic lift and not therefore normally with STOL. Hence we retain the form mg θ which is of course always correct. The Z_u term in the normal force equation expresses principally the rate of change in lift with speed at constant incidence. This term is therefore directly associated with what previously we had defined as 'aerodynamic lift', L_A. It is readily seen that if C_L is constant, then $L_A \propto V^2$ as is strictly true with the partly jet-borne configuration, and as a consequence $Z_u = -\partial L_A \Big/ \partial\left(\dfrac{u}{V_0}\right) \propto V_0$. We note from Fig. 31 that a very generous interpretation suggests that a similar relationship applies for the other STOL types as well but not of course to the 'conventional' design using merely wing loading and $C_{L_{max}}$ as a means of reducing approach speed. We propose therefore to use the assumption: C_L = const. as a fair approximation for all 'unconventional' STOL.

Another term needing some attention is Z_α which is associated with the lift slope. For the conventional aircraft and partially jet-borne designs $\partial C_L/\partial\alpha$ is constant at all speeds, but as indicated by Fig. 31 when power augmented wing lift is used F, i.e. the effective lift slope, increases below V_{00}. In the analysis to follow we have ignored this effect as its inclusion would have made it impossible to use the attractively simple root locus approach. Since the main function of Z_α is to damp the short period oscillation, we may expect that the analysis underestimates the damping of this mode for power augmented wing lift design in the STOL speed range unless an appropriate value for the lift slope is assumed. This error, however, will not be significant as this mode becomes highly damped as speed reduces even when this effect is ignored.

We propose to use root locus analysis in such a manner that speed—or more precisely $1/V^2$—appears as the feedback gain so that the root loci obtained trace out the change in longitudinal stability with reducing

airspeed. For this purpose we divide, in equations (E.1), the pitching moment equation by $B \times V^2$ and the force equations by $m \times V^2$. This gives:

$$(M'_\alpha + M'_{\dot\alpha} s')\alpha + (M'_q s' - s'^2)\theta + M'_u \hat{u} = 0, \tag{E.2}$$

$$(Z'_\alpha - s')\alpha + s'\theta + Z'_u \hat{u} = 0 \tag{E.3}$$

and

$$X'_\alpha \alpha + (X'_u - s)\hat{u} = \frac{g}{V_0^2}\theta. \tag{E.4}$$

The operator appears in the form

$$s' = \frac{s}{V_0} \tag{E.5}$$

and the corresponding roots define distance constants rather than time constants. The aerodynamic derivatives are defined as:

$$\begin{aligned} M'_\alpha &= \frac{\rho}{2}\frac{gm_w}{W/S\, i_B l}, & M'_{\dot\alpha} &= \frac{\rho}{2}\frac{gm_{\dot w}}{W/S\, i_B}, \\ M'_q &= \frac{\rho}{2}\frac{gm_q}{W/S\, i_B}, & M'_u &= \frac{\rho}{2}\frac{gm_u}{W/S\, i_B l}, \\ Z'_u &= \rho g \frac{C_L}{W/S}, & Z'_\alpha &= \frac{\rho}{2}\frac{gZ_\alpha}{W/S}, \\ X'_u &= -\frac{g\rho}{W/S} C_D, & X'_\alpha &= \frac{\rho}{2} g \frac{X_\alpha}{W/S}. \end{aligned} \tag{E.6}$$

Within the assumptions made above, these derivatives are constant for all speeds $V_0 \leqslant V_{00}$. This does not of course apply above V_{00} where obviously C_L would reduce as speed increases. We note that in the form equations (E.2) to (E.4) are written, the gravity term $\{\theta g/V_0^2\} = G$ appears as the only speed dependent contribution and is brought to the right hand side of equation (E.4). If we now find the transfer function $\theta(s')/G$ and close the loop with (g/V_0^2) as the feedback as indicated by the block diagram of Fig. 35, we have transformed the solution of equation (E.1) into the standard form required for servo control analysis with $g/V_0^2 = K$ as the gain factor and use the root locus method to obtain the solution. The transfer function is

$$\frac{\theta}{G}(s) = \frac{(s'-z)}{s'(s'-p_1)(s'+2\zeta\omega' s'+\omega'^2)}, \tag{E.7}$$

where the zero

$$z = -\frac{M'_\alpha - M'_u \dfrac{Z'_\alpha}{Z'_u}}{M'_{\dot\alpha} - \dfrac{M'_u}{Z'_u}}. \tag{E.8}$$

The poles p_1, ζ and ω are the roots of the cubic

$$s'^3+s'^2\,a_2+s'\,a_1+a_0=0\,,$$

with

$$\begin{aligned} a_2 &= -M'_q-M'_{\dot\alpha}-Z'_\alpha-X'_u\,,\\ a_1 &= -M'_\alpha+X'_u(M'_q+M'_{\dot\alpha}+Z'_\alpha)+M'_q\,Z'_\alpha-X'_\alpha\,Z'_u \qquad \text{(E.9)}\\ \text{and}\qquad a_0 &= X'_u(M'_\alpha-M'_q\,Z'_\alpha)+X'_\alpha(M'_q\,Z'_u-M'_u)\,. \end{aligned}$$

This cubic defines a degenerate form of the longitudinal motion with the gravity term missing from the X-equation. The real root p_1 has no simple physical meaning, but bears some relationship to the speed stability mode. The second order mode with damping ratio ζ and the undamped frequency ω', is practically identical to that of the normal short period solution.

The open loop transfer function of the system defined in Fig. 35 is then

$$\frac{g}{V_0^2}\,\frac{\theta}{G}(s')$$

and from this we can obtain the result of loop closure by root locus analysis.

For the aircraft with the characteristics defined in Table 1, such a solution has been obtained. A detailed root locus plot for the case where $M'_u=0$ is presented in Fig. 36. Following convention the poles are denoted by the symbol X and the zeroes by 0's. The poles correspond to the aircraft stability roots for $g/V_0^2=0$, i.e. to $V=\infty$ and the root loci show how these roots change as the gain $g/V_0^2\to\infty$. For the range of speeds of interest here these are indicated in the graph. We note that short period damping improves with reducing speed, but this effect only becomes significant at speeds below the practical STOL range. It should be noted that in the analysis, the increase in lift slope experienced by most STOL aircraft below V_{00} has been ignored. If this effect is also considered, short period damping would be seen to increase more rapidly in the STOL regime. The phugoid, however, becomes unstable in the STOL range and this trend continues as speed is further reduced. The effect of increasing L_α as relevant to aircraft with power-augmented wing lift is presented separately in Fig. 37, showing only the centre portion of the graph.

In Fig. 38 are shown further root locus graphs illustrating the influence of M'_u which is the only derivative capable of having a major effect on the general pole-zero configuration. At first sight the root loci appear to change dramatically as a result. However, inspection of Fig. 36 reveals that we are only concerned with the parts of the loci close to the poles and that the remaining portion applies to speeds far below those of practical interest here. Near the poles all the results given in Fig. 38 show similar trends and these can be taken as generally applicable in all cases. The stability roots defined in these graphs are given as distance constants rather than in the more familiar form of time constants. The results for two of the cases considered are presented in Fig. 39 in terms of period and damping time constants to be more immediately intelligible to the reader.

V.2. *Lateral Stability.*

Analysis of lateral stability can be performed in an analogous manner. The gravity term isolated and treated as a feedback term now appears as $\frac{g}{V_0^2}\phi$ in the sideforce equation. The appropriate block diagram is shown in Fig. 40. The equations of motion corresponding to equations (E.2) to (E.4) are:—

$$b_1 = \frac{1}{1-\frac{E^2}{AC}} \left\{ N'_\beta + L'_\beta \frac{E}{C} + Y'_\beta \left(N'_p \frac{E}{A} + L'_r \frac{E}{C} \right) + Y'_\beta (N'_r + L'_p) + N'_r L'_p - N'_p L'_r \right\}$$

and $$b_0 = \frac{1}{1-\frac{E^2}{AC}} \{ -N'_\beta L'_p + L'_\beta N'_p + Y'_\beta (N'_p L'_r - N'_r L'_p) \} .$$

This cubic has one real root p_R and a complex root defining an oscillation with damping ratio ζ_D and frequency ω'_D as a solution. The real root is a close approximation to the roll subsidence root, but the complex root gives a rather distorted approximation to the dutch roll, since the destabilising effect of (mg ϕ) is missing. It is convenient to combine the factor in equation (E.11) with the feedback gain g/V_0^2 to give an effective gain:

$$K = \frac{g}{V_0^2} \frac{L'_\beta + N'_\beta \frac{E}{A}}{1-\frac{E^2}{AC}} . \tag{E.15}$$

The open loop transfer function is therefore

$$G(s') = K \frac{s - Z_L}{s'(s' - p_R)(s'^2 + 2\zeta_D \omega'_D s' + \omega'^2_D)} \tag{E.16}$$

and the corresponding closed loop stability roots will again be obtained by root locus analysis.

For the numerical examples defined in Table 2 such solutions have been obtained, one particular plot given in detail in Fig. 41. We note that as speed is reduced, i.e. as the root loci move away from the poles ($V_0 = \infty$) roll damping (in terms of a distance constant) improves, whereas the spiral mode destabilises. The dutch roll becomes unstable at $V_0 = 110$ knots and becomes progressively more unstable with further speed reduction.

In Fig. 42 all the root locus plots obtained are shown and we note in every case the same trend as far as the dutch roll and the roll subsidence is concerned. The spiral root can, however, go either way, depending on the combination of derivatives. The last example is particularly interesting as it illustrates a case in which the so called second lateral oscillation occurs, resulting from a merger of the spiral and the roll mode. But we note that as speed is further reduced, i.e. K increased, the oscillation again splits up into two subsidences. From the rules of root locus geometry we can deduce a simple criterion for the condition required for the second oscillation to be possible, namely that the zero must lie to the left of the two real poles, i.e. in practice to the left of the roll subsidence root defined by equation (E.13).

The results of two of the cases presented in Fig. 42 have been replotted in the more familiar form giving periods and time constants in Fig. 43.

The most important trend revealed by this analysis is, however, the deterioration in dutch roll damping with decreasing speed, which is inevitable with any conceivable pole-zero configuration and must therefore be considered to be a major problem area with any STOL aircraft.

TABLE 1

Data Used in Longitudinal Stability Analysis of Appendix V, Section V.1

	Basic	2 × mg	3 × mg	$+m_u$	$-m_u$
M'	−40	−40	−40	−40	−40
M'_q	−2·0	−4·0	−6·0	−2·0	−2·0
$M'_{\dot{\alpha}}$	−1·0	−1·0	−1·0	−1·0	−1·0
M'_u	0	0	0	+5·0	−5·0
Z'_α	−3·3	−3·3	−3·3	−3·3	−3·3
Z'_u	−2·5	−2·5	−2·5	−2·5	−2·5
X'_u	−0·5	−0·5	−0·5	−0·5	−0·5
X'_α	−2·0	−2·0	−2·0	−2·0	−2·0

TABLE 2

Data Used in Lateral Stability Analysis of Appendix V, Section V.2

	Basic A	B	C	D
N'_β	20	20	20	20
N'_r	−1·0	−1·0	−1·0	−1·0
N'_p	−0·1	−0·1	+0·5	−0·5
L'_β	−60	−60	−60	−60
L'_p	−2·0	−2·0	−2·0	−2·0
L'_r	0	+4·0	+4·0	0
Y'_β	−0·5	−0·5	−0·5	−0·5
E	0	0	0	0

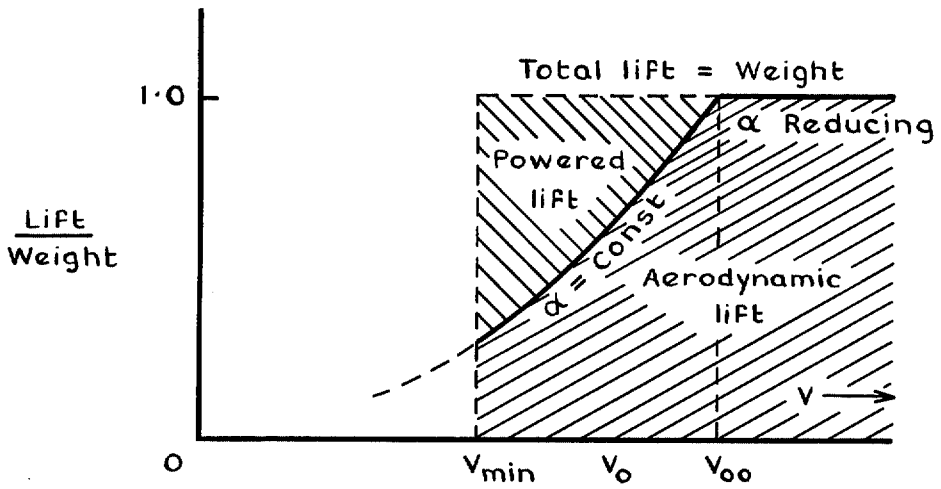

FIG. 1. Breakdown of lift for stabilized flight of STOL aircraft.

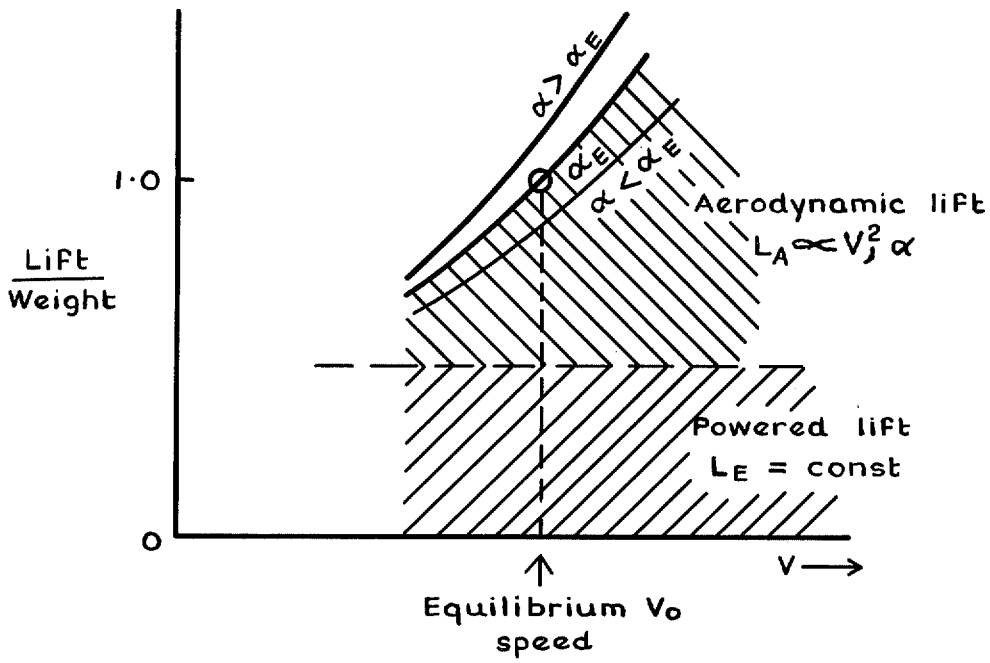

FIG. 2. Variation of lift with speed and incidence for a given power setting.

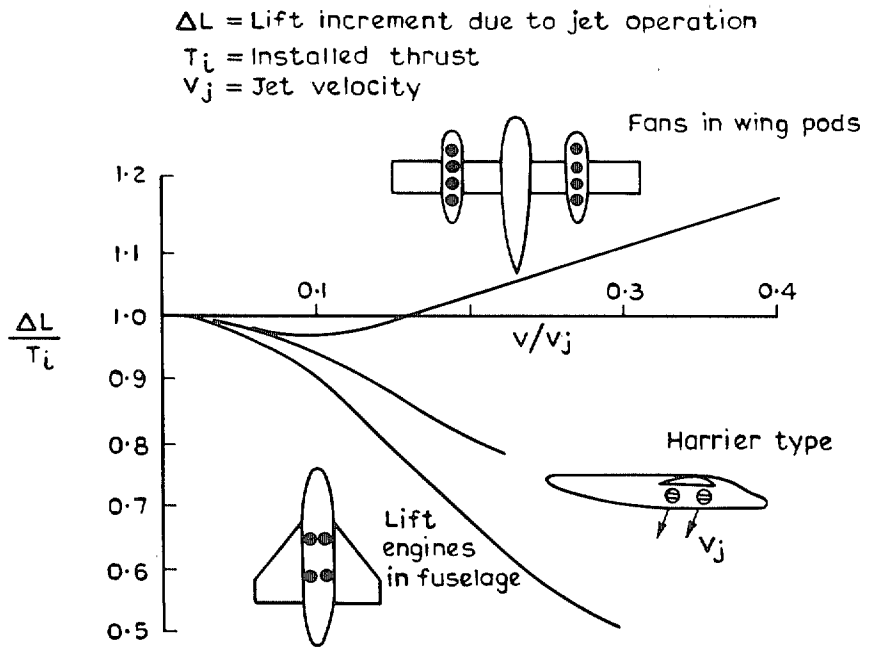

FIG. 3. Some examples of jet interference on lift from aircraft with various forms of lift engine installations (from Ref. 1).

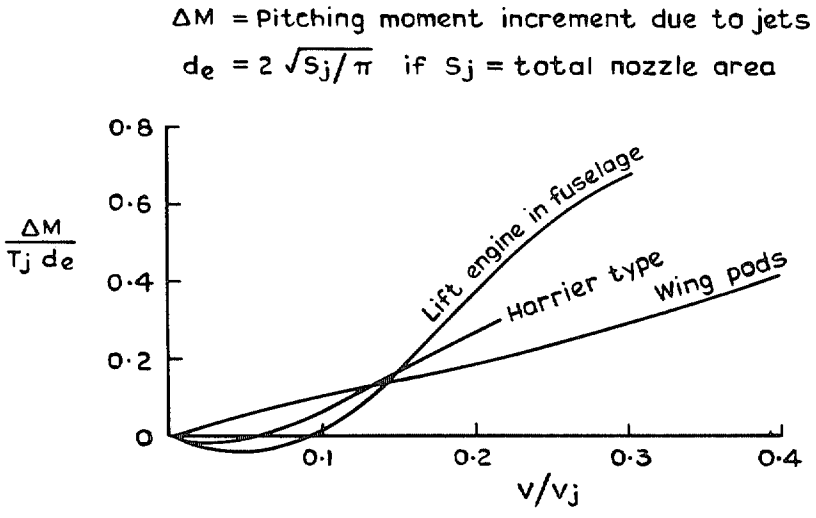

FIG. 4. Some examples of jet interference on pitching moments.

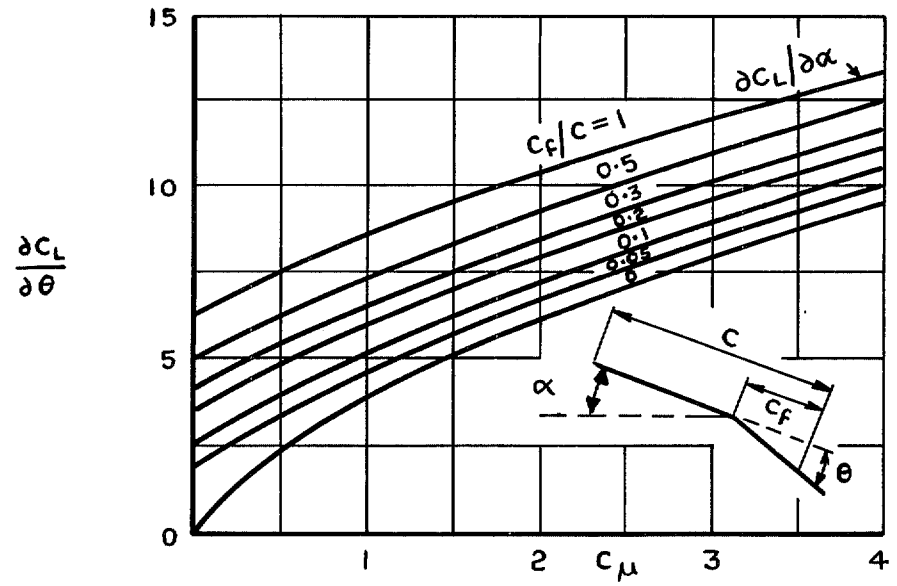

FIG. 5. From Ref. 4 theoretical estimates of jet flap lift efficiency for two dimensional flow.

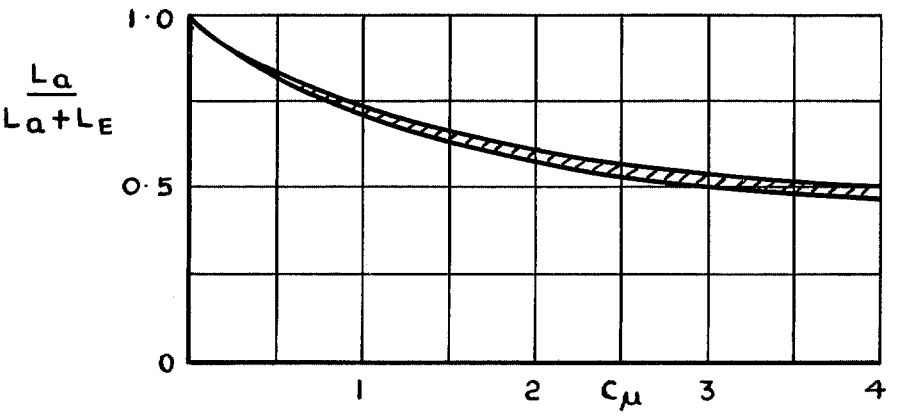

FIG. 6. Friction of V-dependant lift (L_a) of total lift for a jet flap aircraft (practically independant of θ and α).

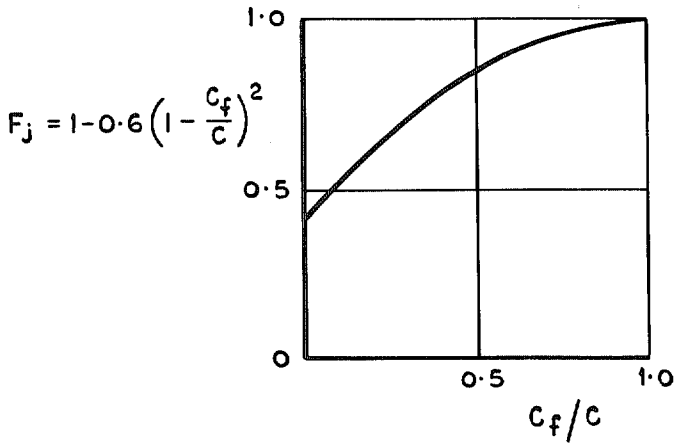

FIG. 7. Flap chord lift efficiency factor for jet flap.

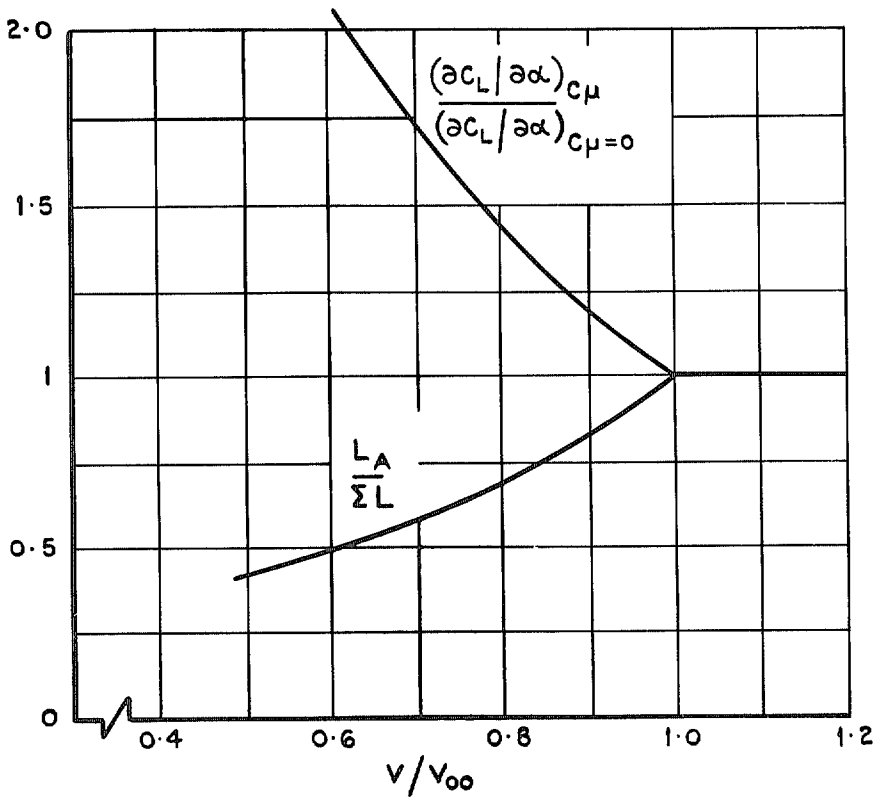

FIG. 8. Typical variation with speed of the lift characteristics of a jet flap aircraft (App I).

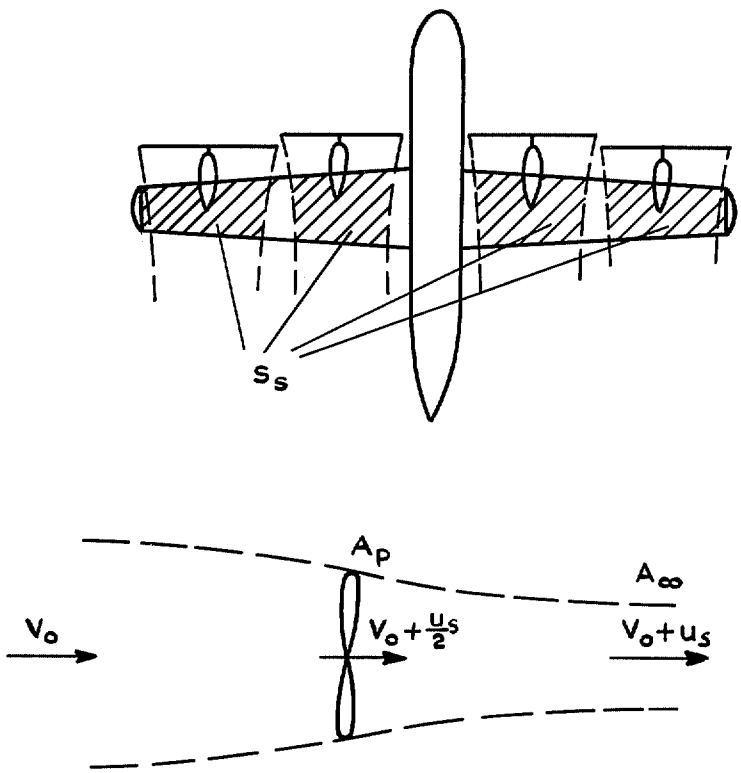

FIG. 9. Simple model of a slipstream aircraft.

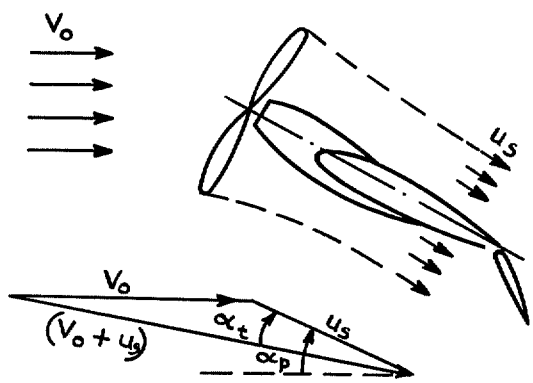

FIG. 10. Flow in the slipstream.

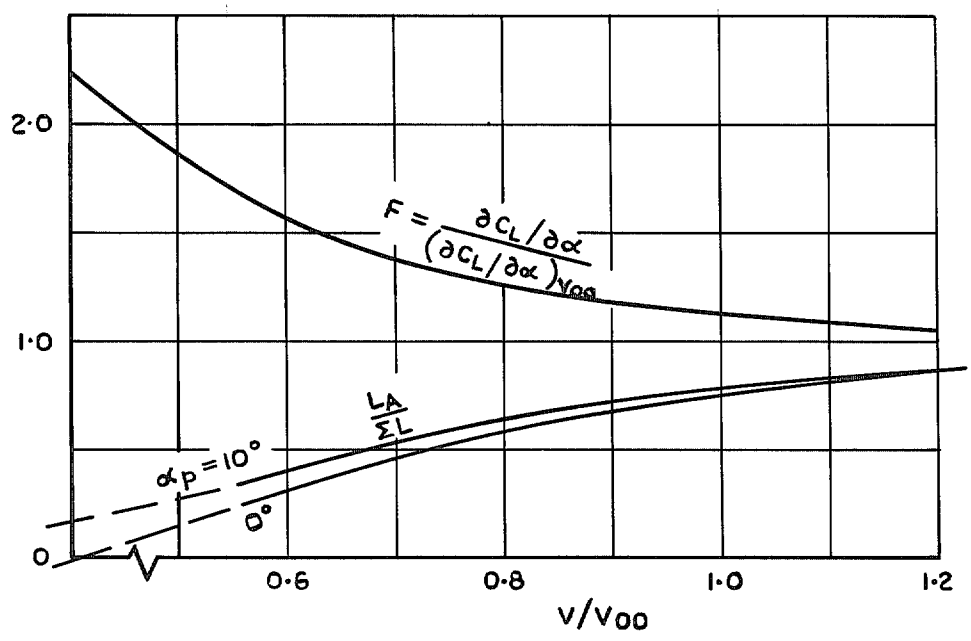

FIG. 11. Typical variation with speed of the lift characteristics of a slipstream aircraft (App II).

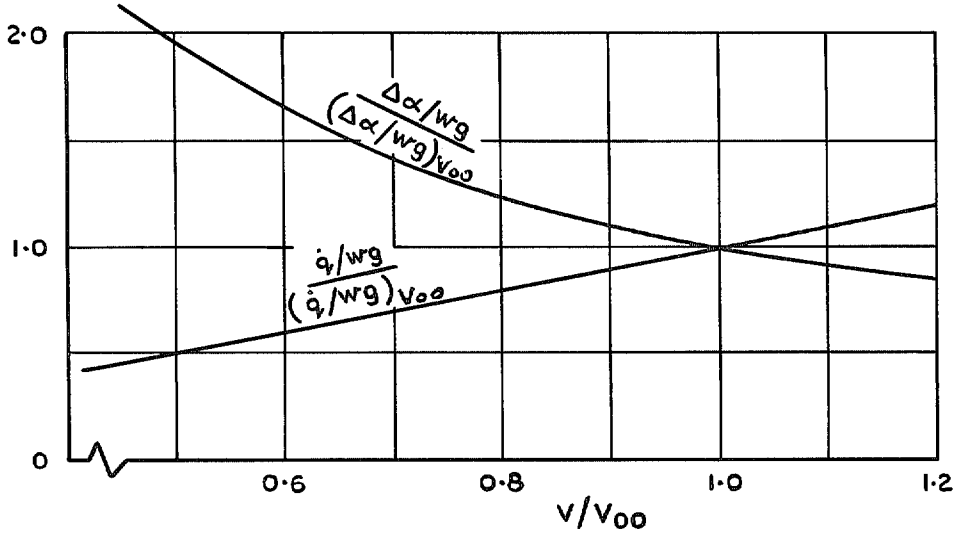

FIG. 12. Change with speed of the response in incidence and pitch acceleration to vertical gusts.

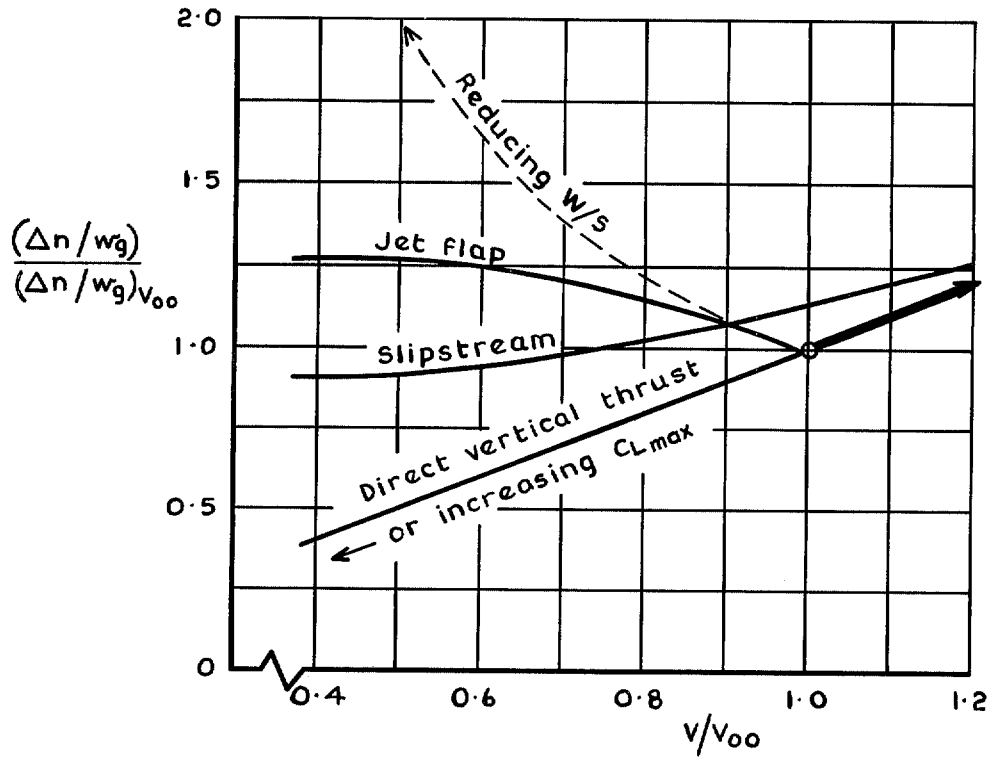

FIG. 13. Normal acceleration response to vertical gusts of various types of STOL aircraft.

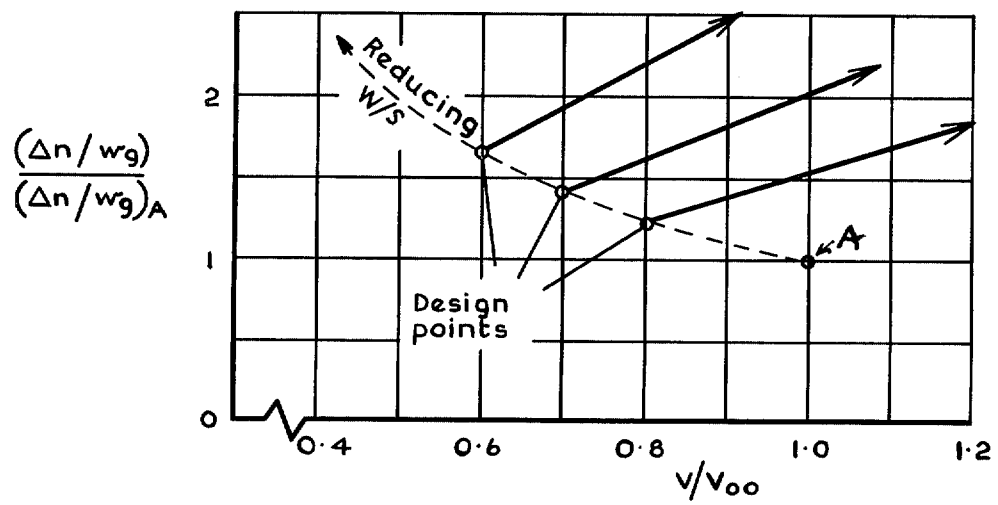

FIG. 14. Variation with speed in vertical gust response of STOL aircraft in which low speed capability is achieved by reducing W/S.

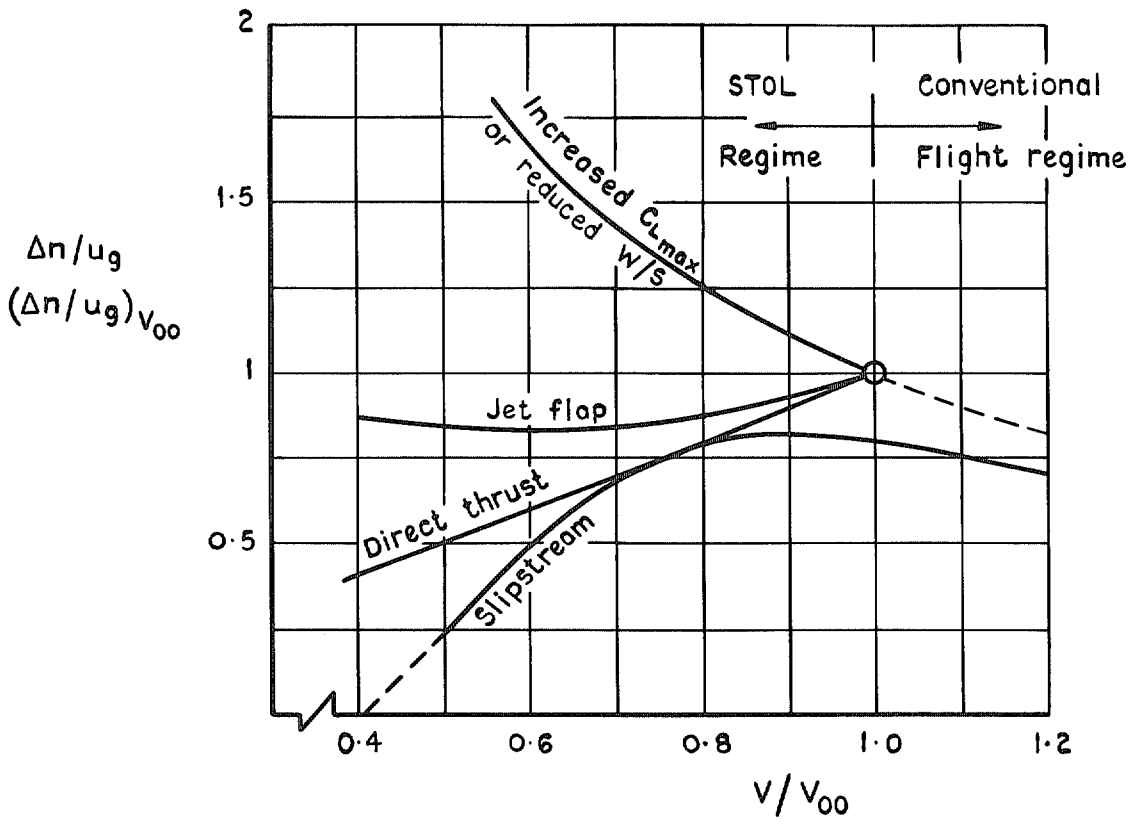

FIG. 15. Effect on normal acceleration sensitivity to horizontal gusts of various STOL techniques.

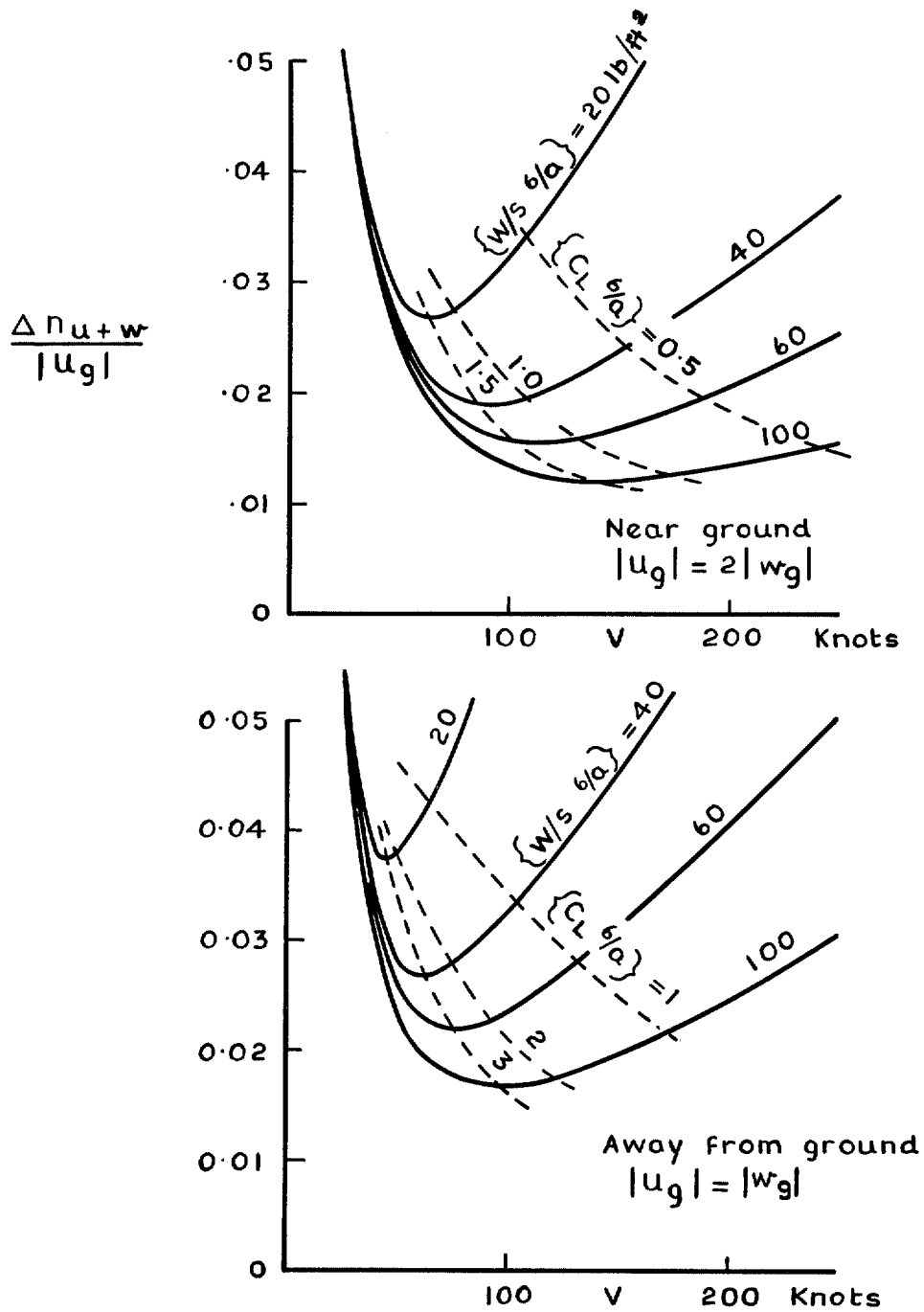

FIG. 16. Change in aircraft longitudinal general gust sensitivity with airspeed and wing loading.

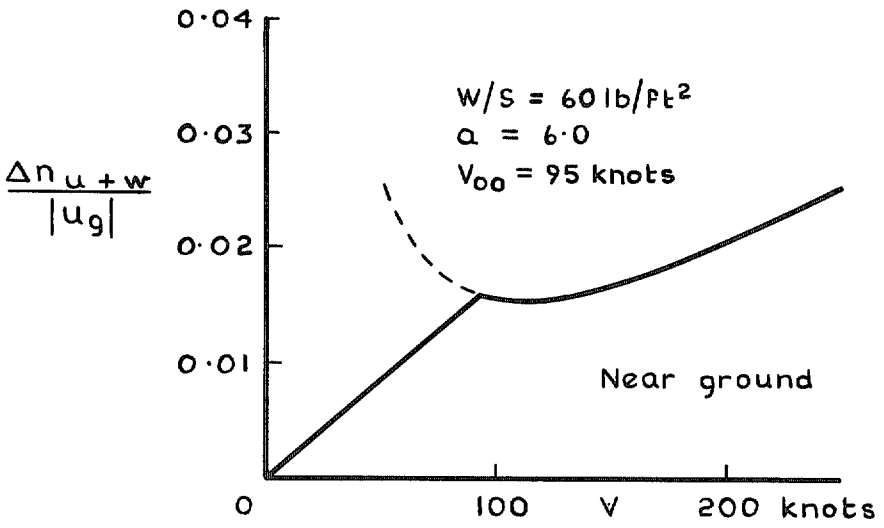

FIG. 17. Example of the change with speed of the general gust sensitivity of a partially jet borne STOL aircraft.

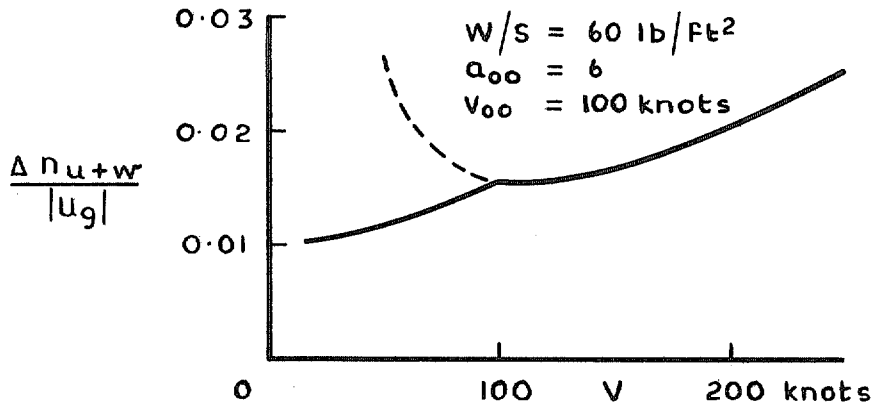

FIG. 18. Example illustrating the change with speed of the general longitudinal gust sensitivity of a jet flap or slipstream STOL aircraft.

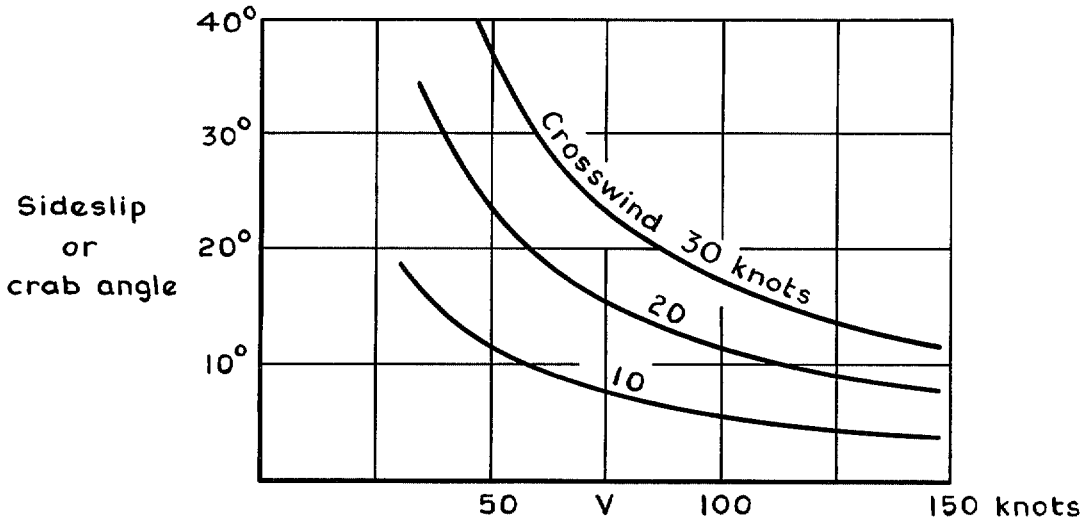

Fig. 19 Crosswind angle as a function of crosswind velocity and aircraft speed

FIG. 19. Crosswind angle as a function of crosswind velocity and aircraft speed.

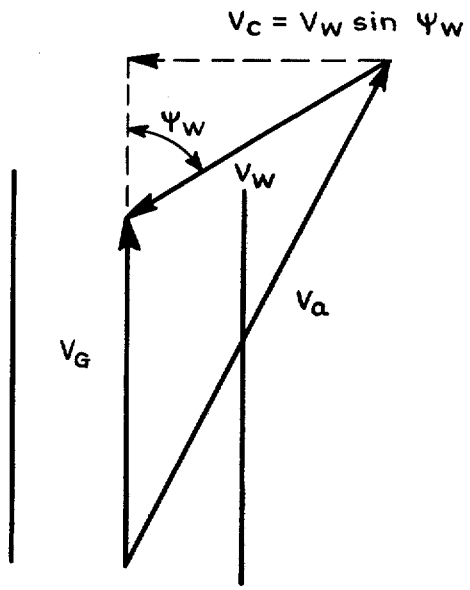

FIG. 20. Velocity polygon of airspeed V_{a_1} wind speed V_W and groundspeed V_G.

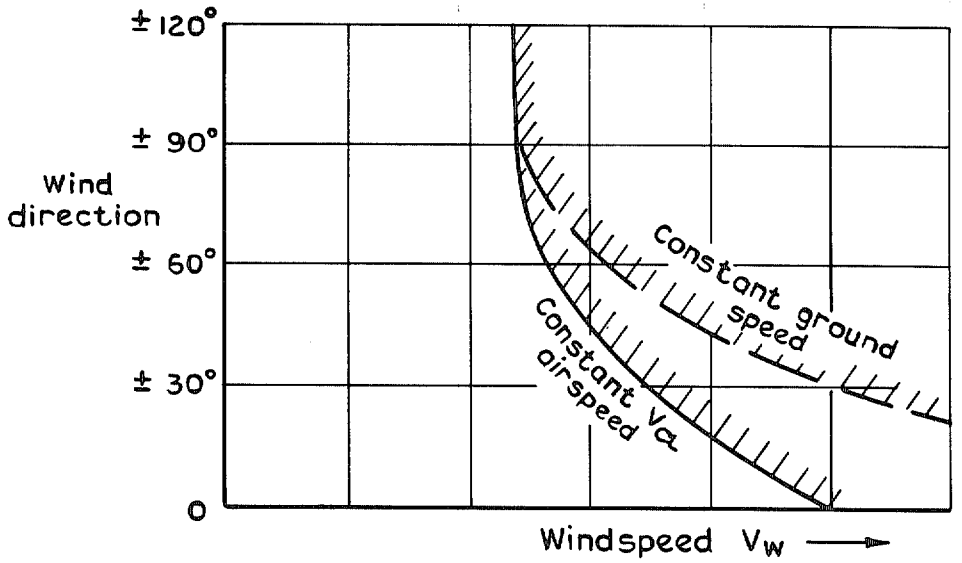

FIG. 21. Typical approach control boundary in terms of windspeed and direction.

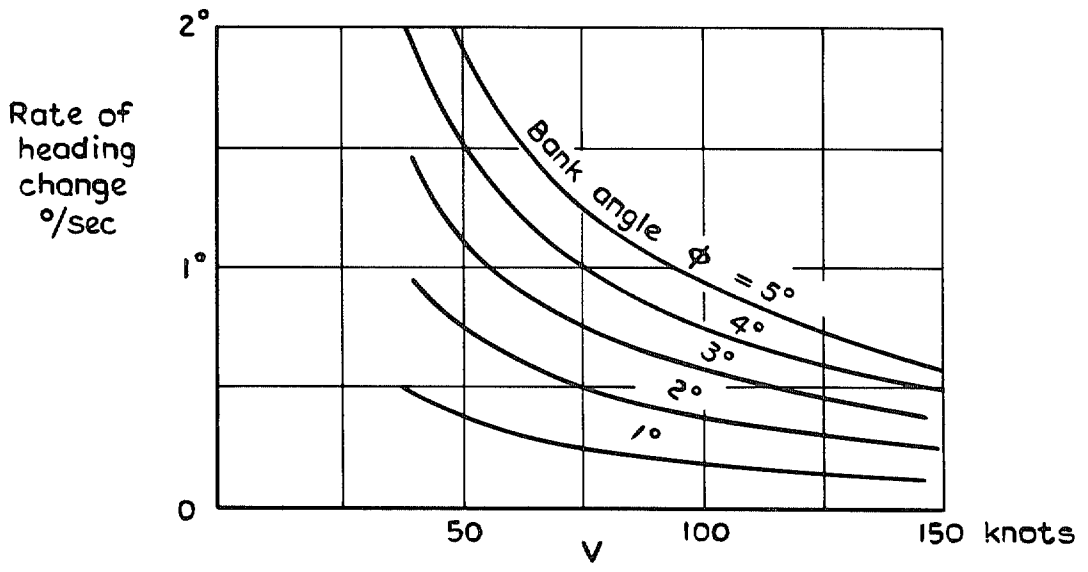

FIG. 22. Relationship between bank angle, airspeed and turn rate in the STOL range.

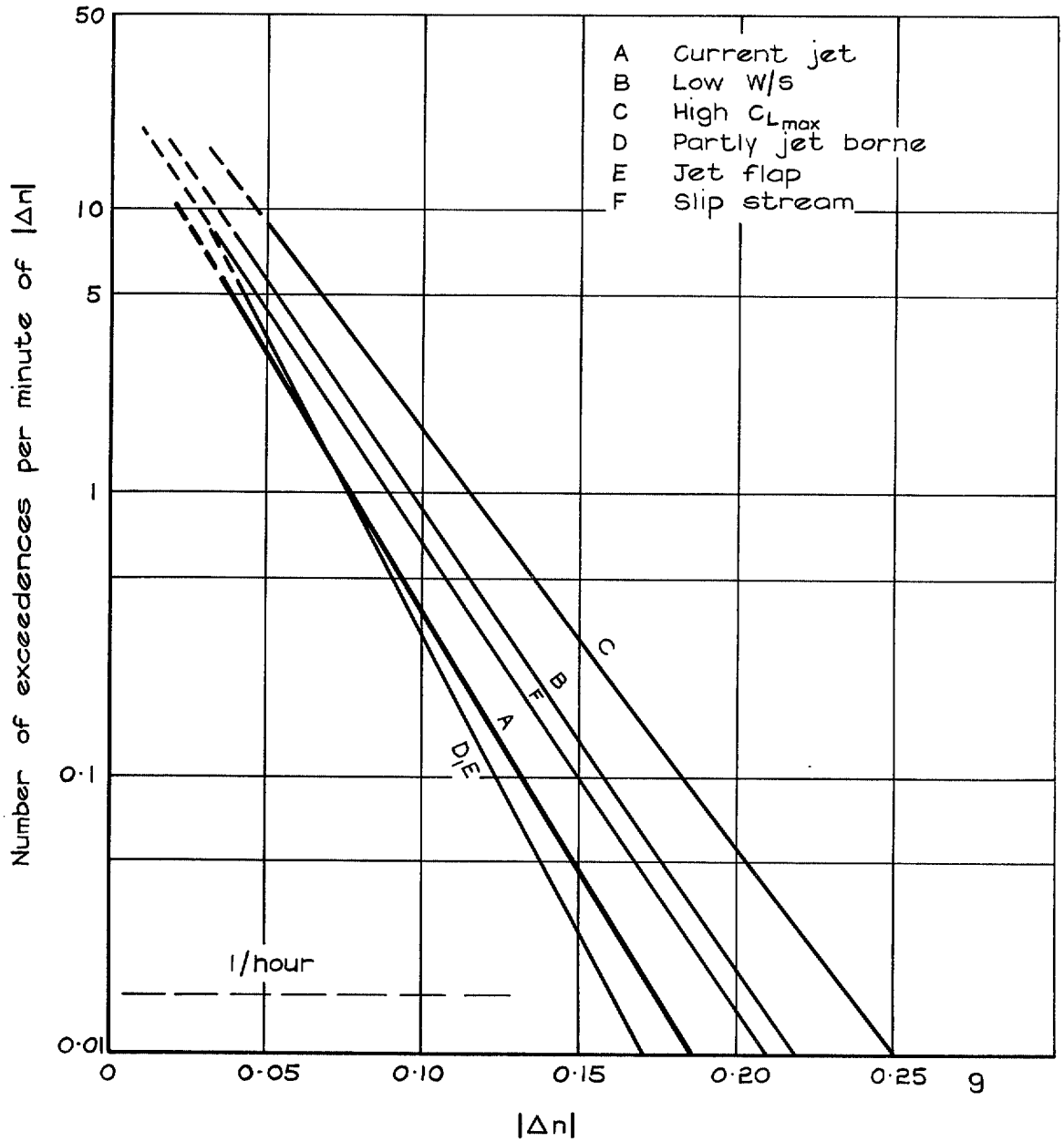

FIG. 23. Probability of exceeding normal acceleration increment $|\Delta n|$ in the approach in moderate turbulence (5 ft/sec rms) for a range of STOL aircraft.

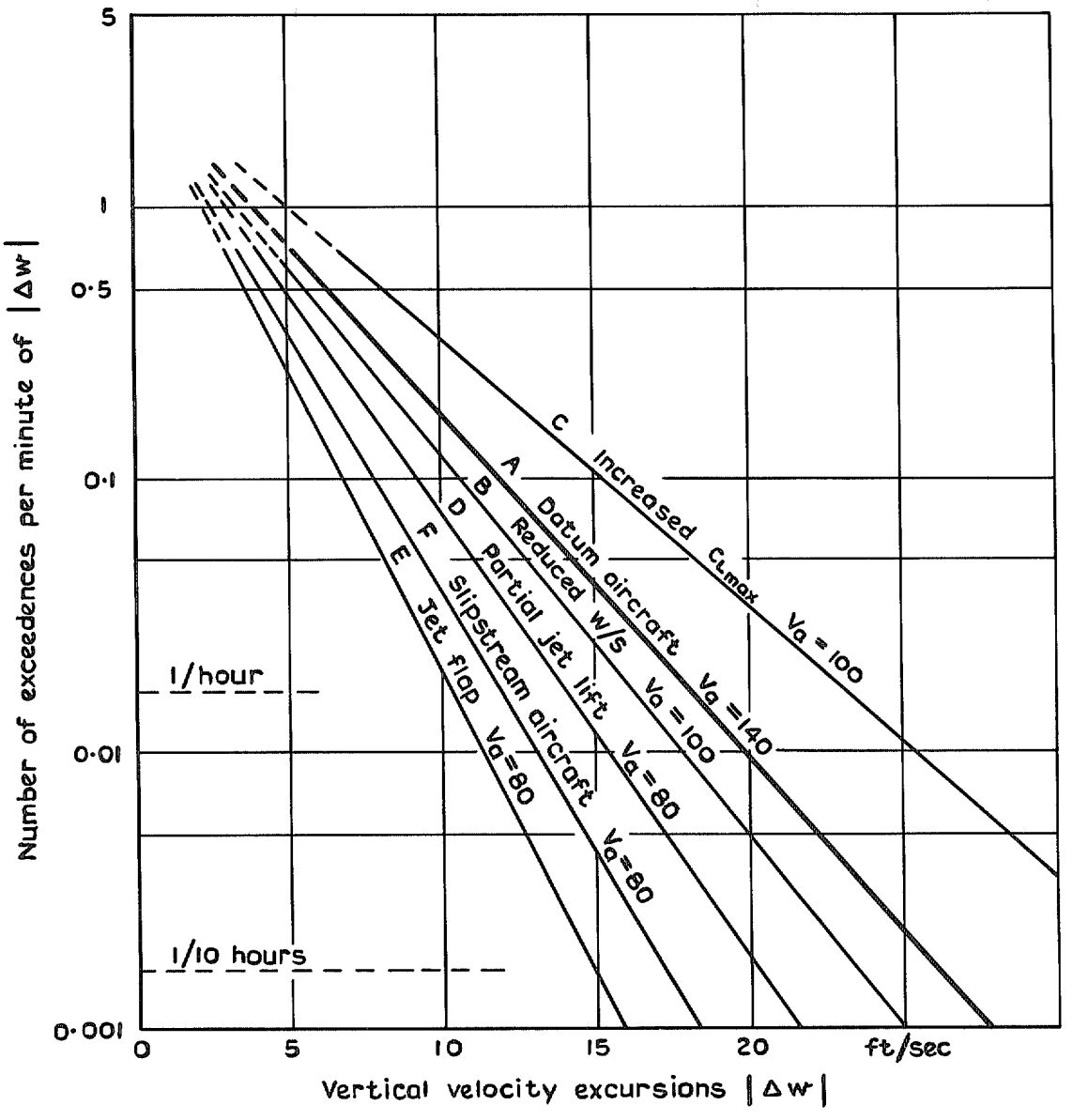

FIG. 24a. Probability of exceeding vertical velocity increment $|\Delta w|$.

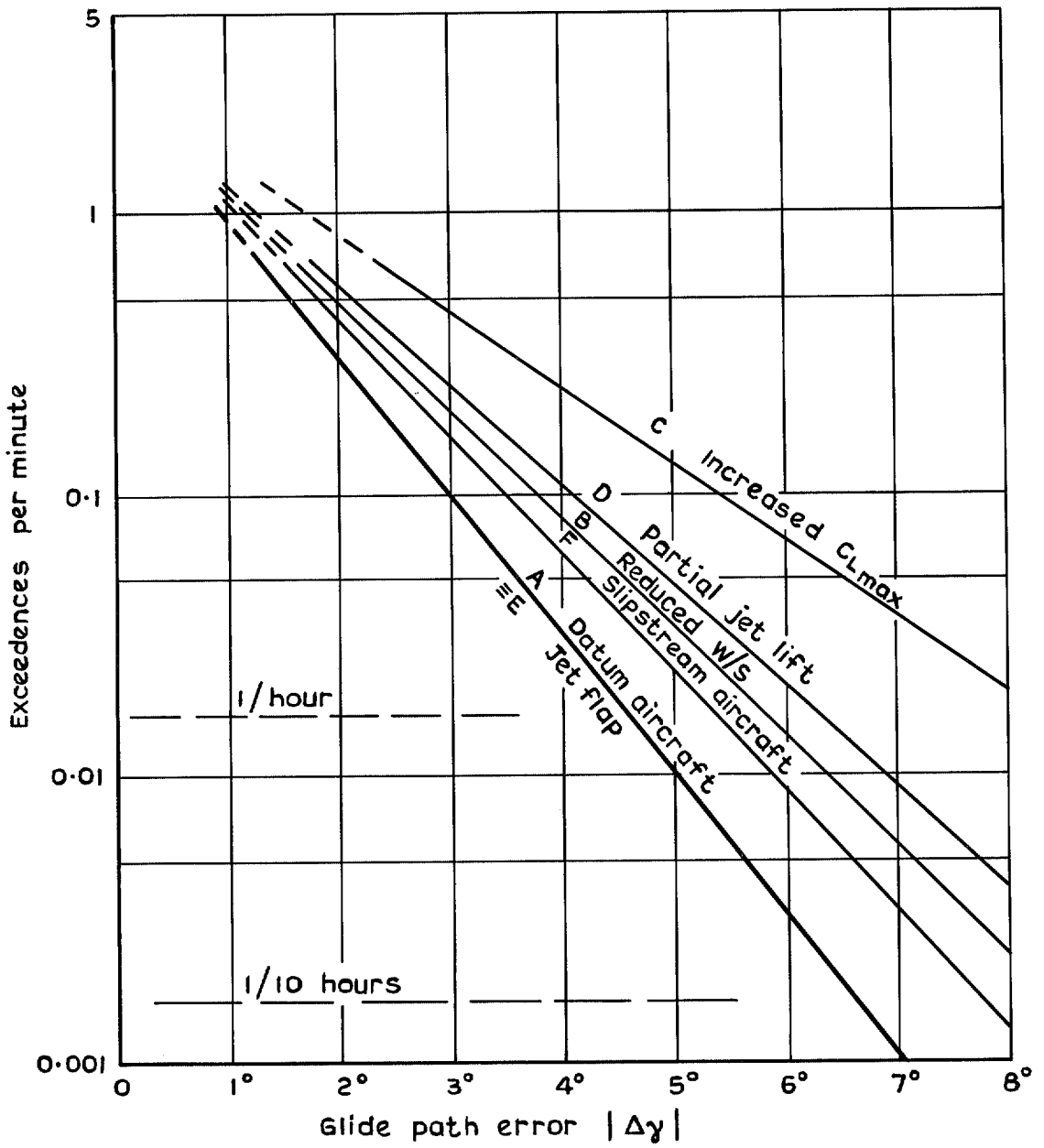

FIG. 24b. Probability of exceeding glide path error $|\Delta\gamma|$.

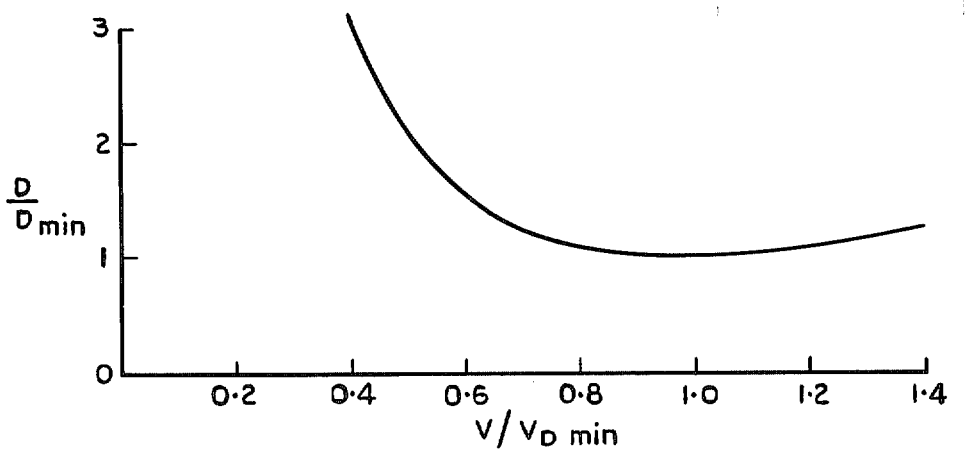

FIG. 25. Drag versus speed in trimmed rectilinear flight.

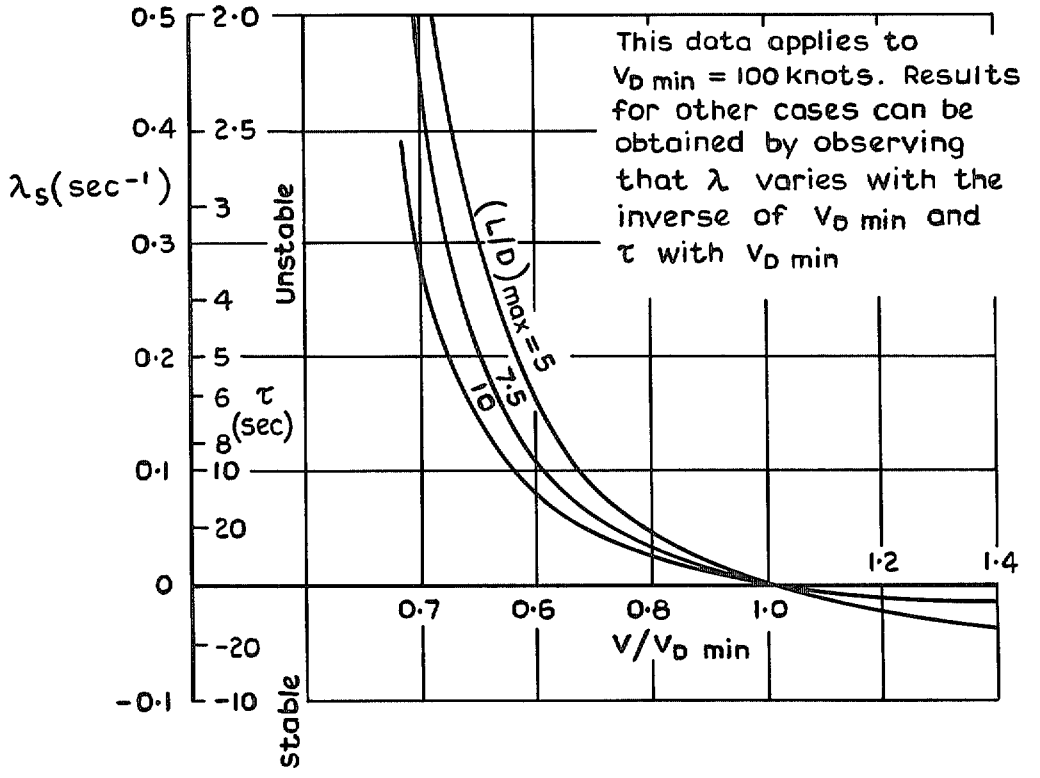

FIG. 26. Speed stability root λ_s or time constant τ for aircraft fully supported by wing lift relevant to conventional design and jet flap.

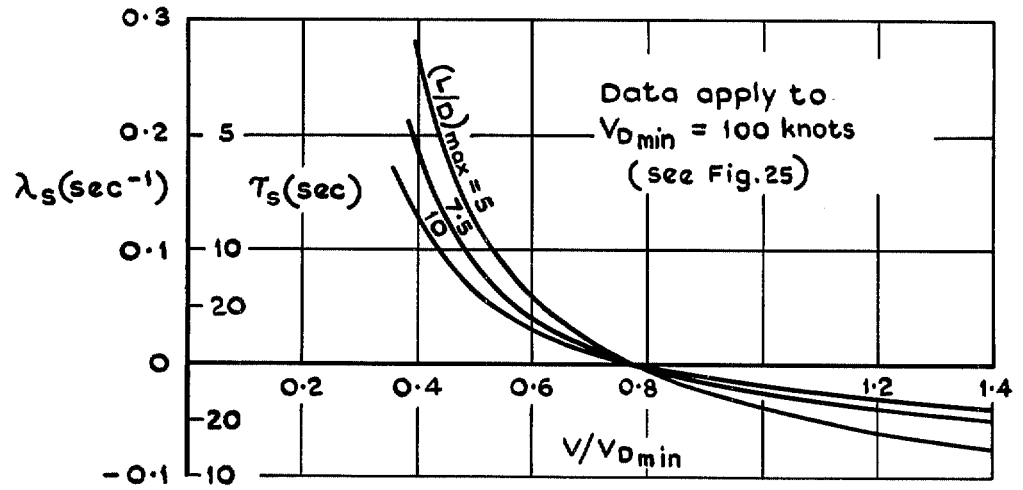

FIG. 27. Speed stability characteristics of propeller driven aircraft (assuming thrust $\propto 1/V$). Relevant to slipstream STOL.

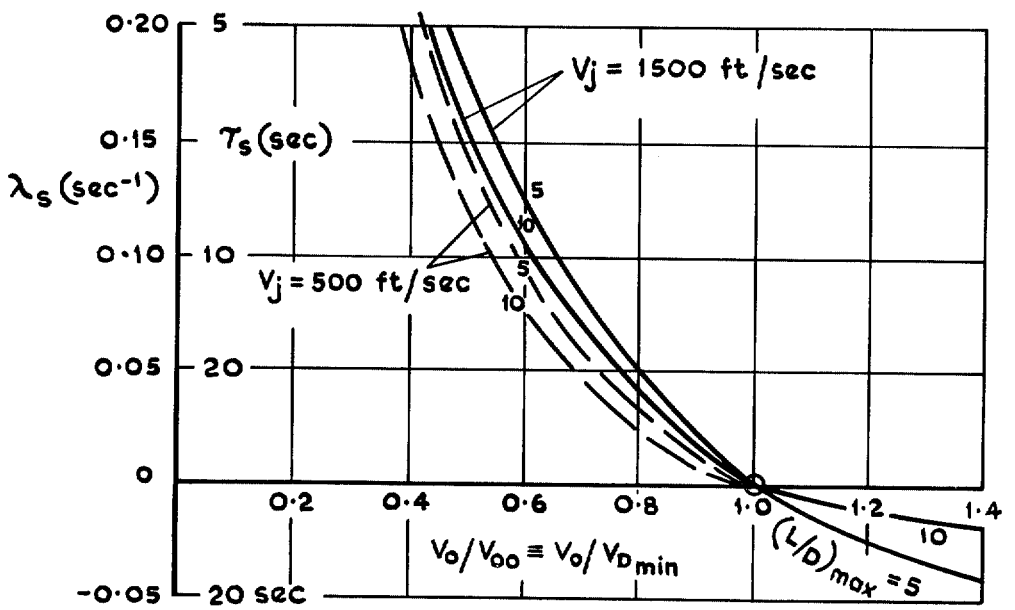

FIG. 28a. Speed stability characteristics of partly jet borne STOL under elevator control. $V_{00} = V_{D_{min}} = 120$ knots, $a = 5$, $C_{L0} = 1{\cdot}5$.

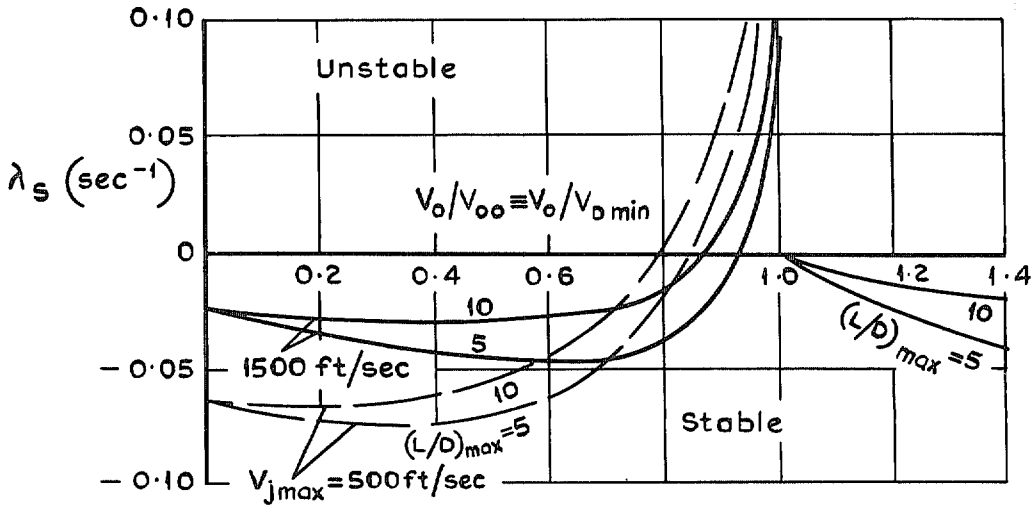

FIG. 28b. Speed stability of partly jet borne STOL under verti-thrust control.

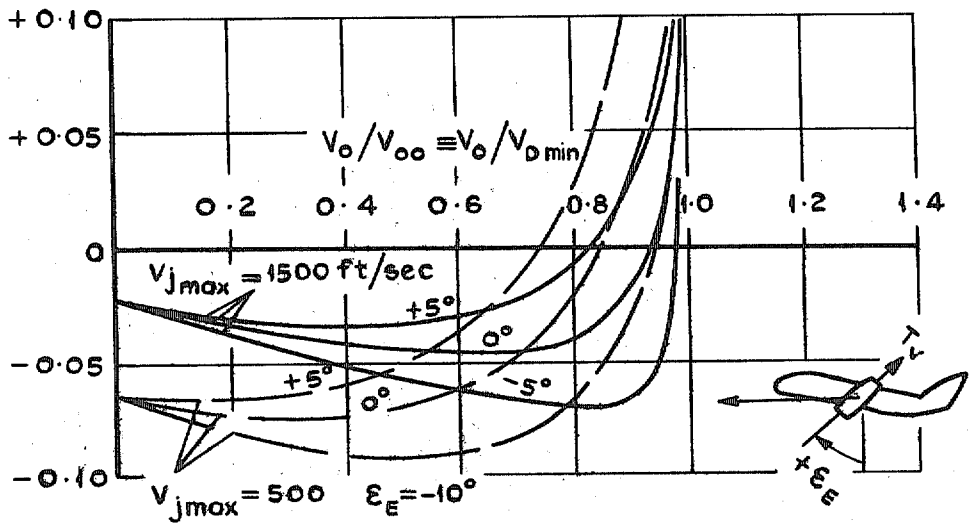

FIG. 28c. Illustrating effect of vertical thrust vector angle on speed stability under thrust control $(L/D)^{max}=5$.

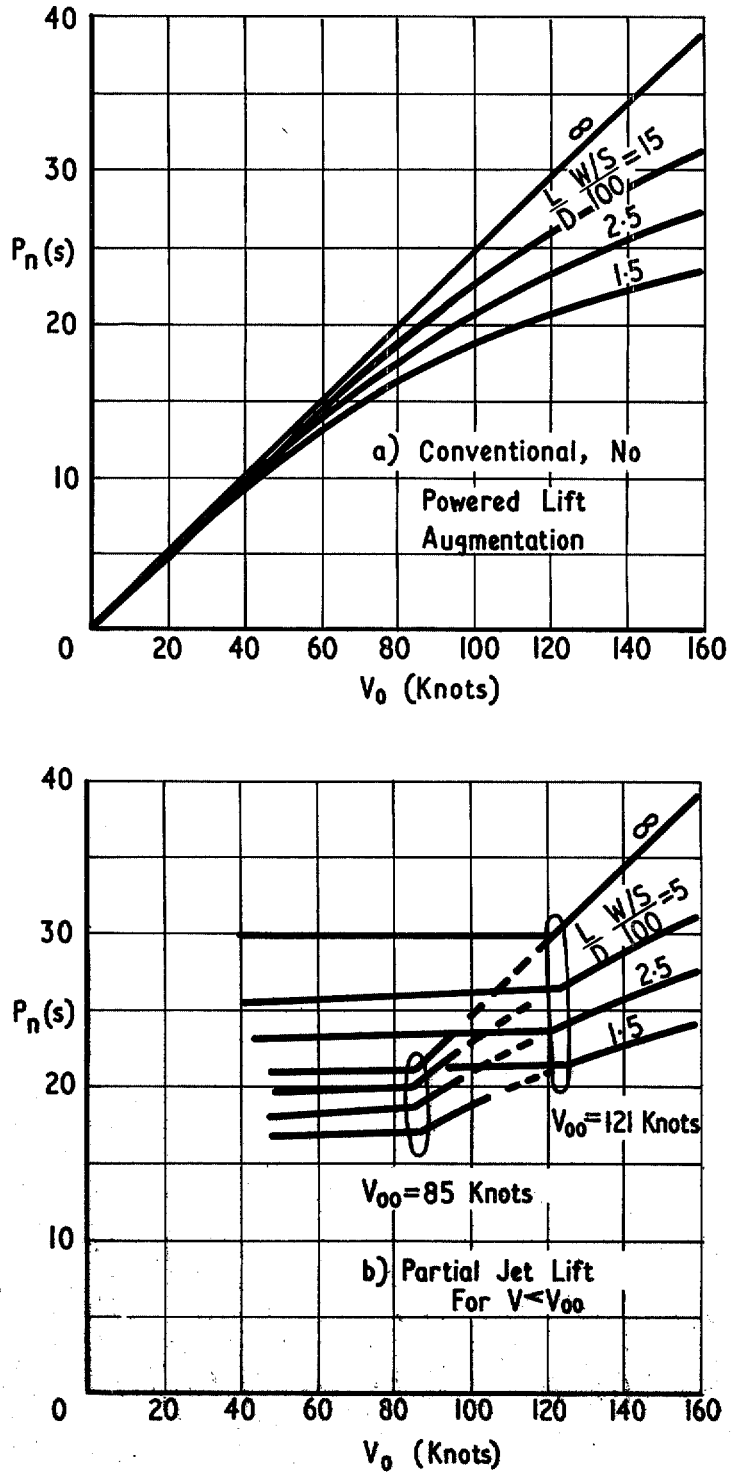

FIG. 29. Undamped period (P_0) of the Phugoid with or without attitude constraint as a function of true airspeed and aerodynamic lift ratio.

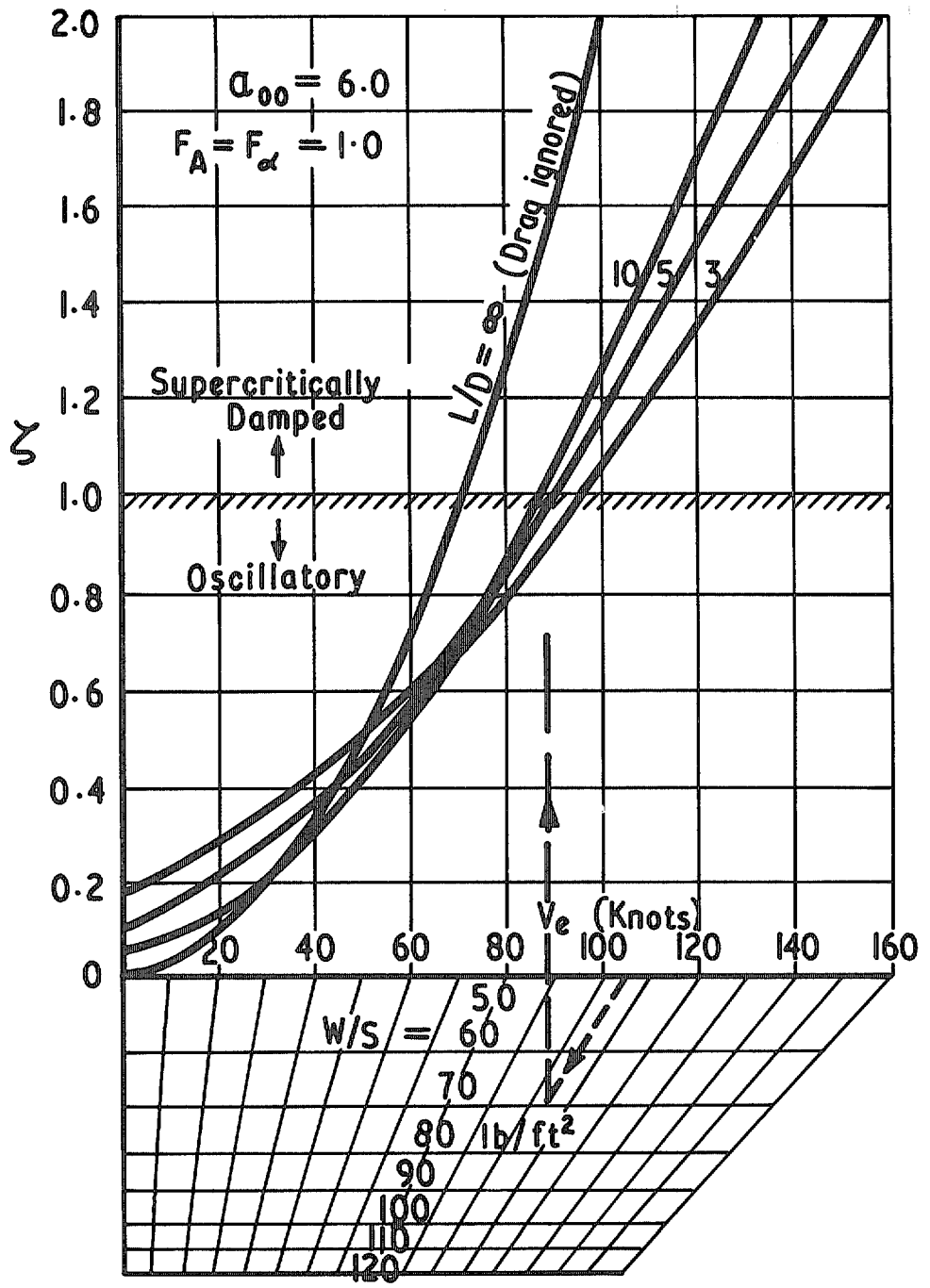

FIG. 30. Equivalent airspeed V_{ek} at which attitude constrained Phugoid becomes critically damped.

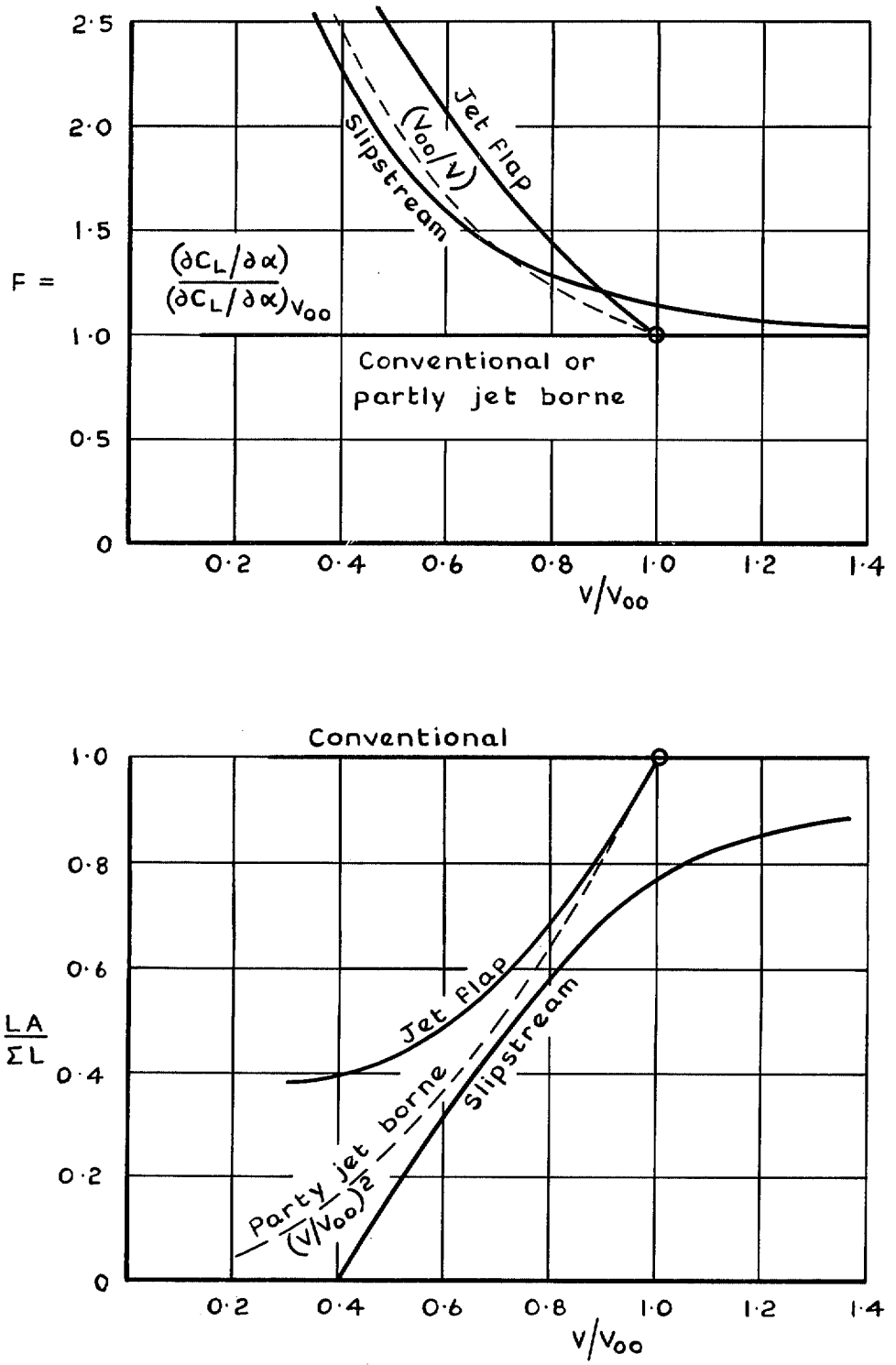

FIG. 31. Summary of the lifting characteristics for the main classes of STOL aircraft.

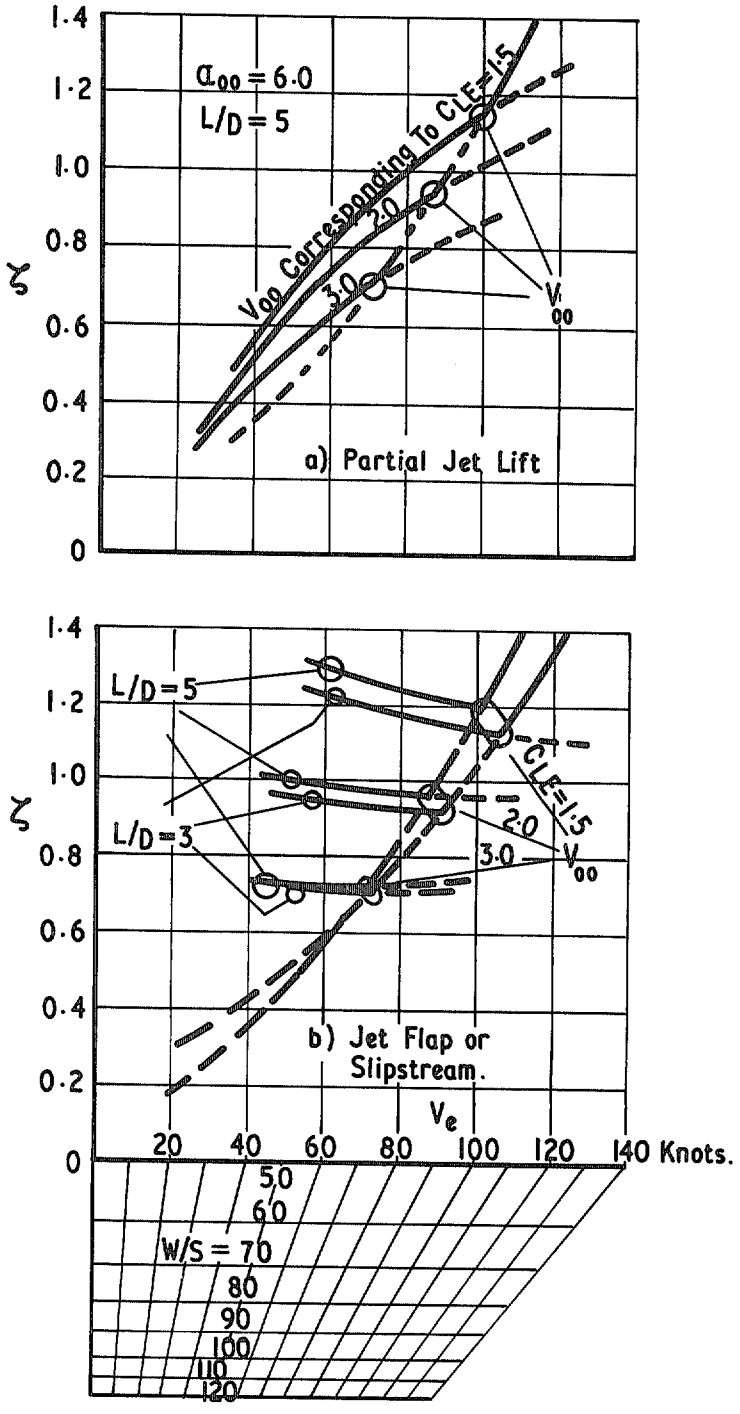

FIG. 32a–c. Variation of damping of attitude constrained motion for various STOL aircraft with W/S and speed.

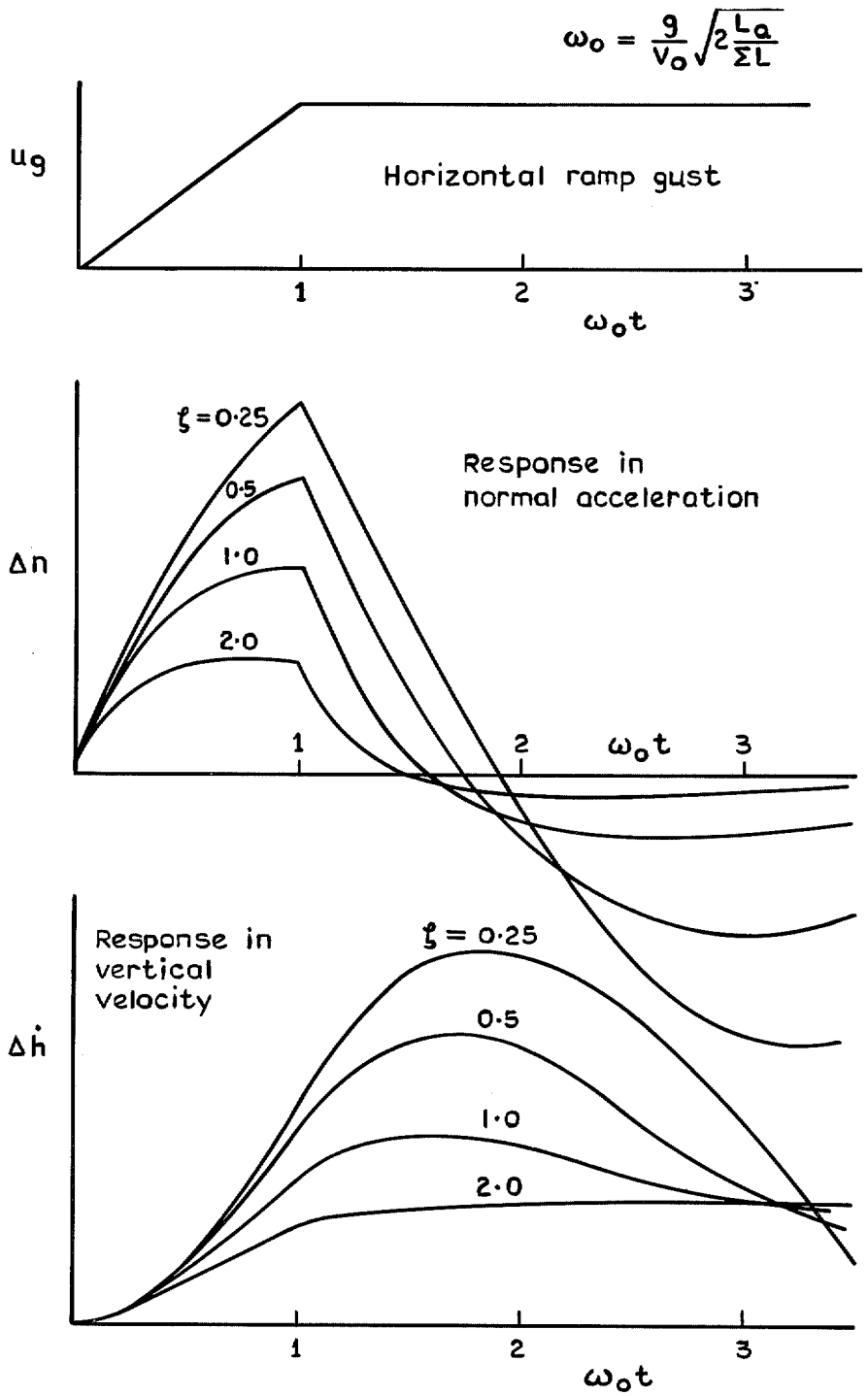

FIG. 33. Effect of relative damping ζ of attitude constrained 'phugoid' on aircraft response to horizontal gust.

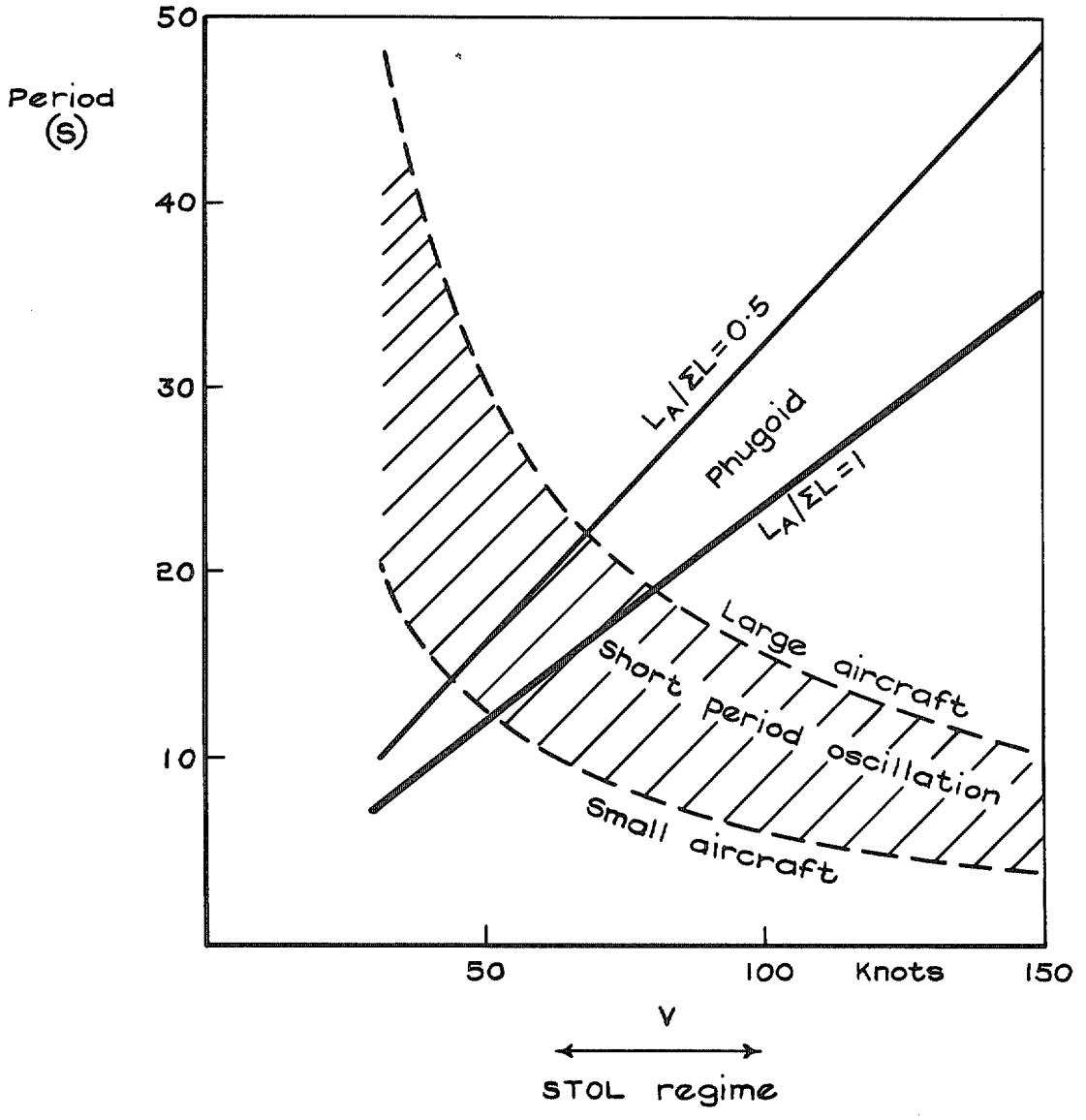

FIG. 34. General trend with speed in the period of the Phugoid and the longitudinal SPO ignoring possible coupling.

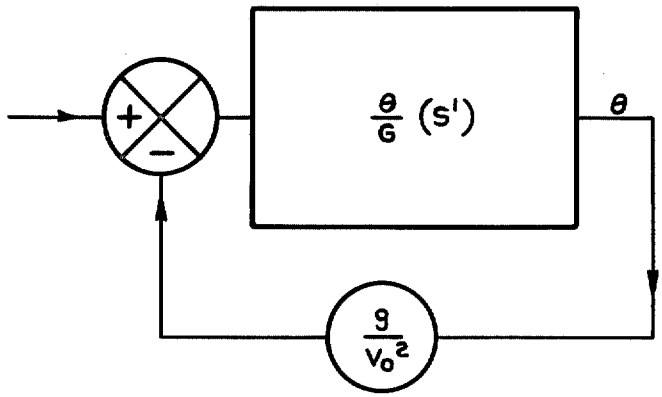

FIG. 35. Block diagram representation of the longitudinal stability analysis adopted in Appendix V.1.

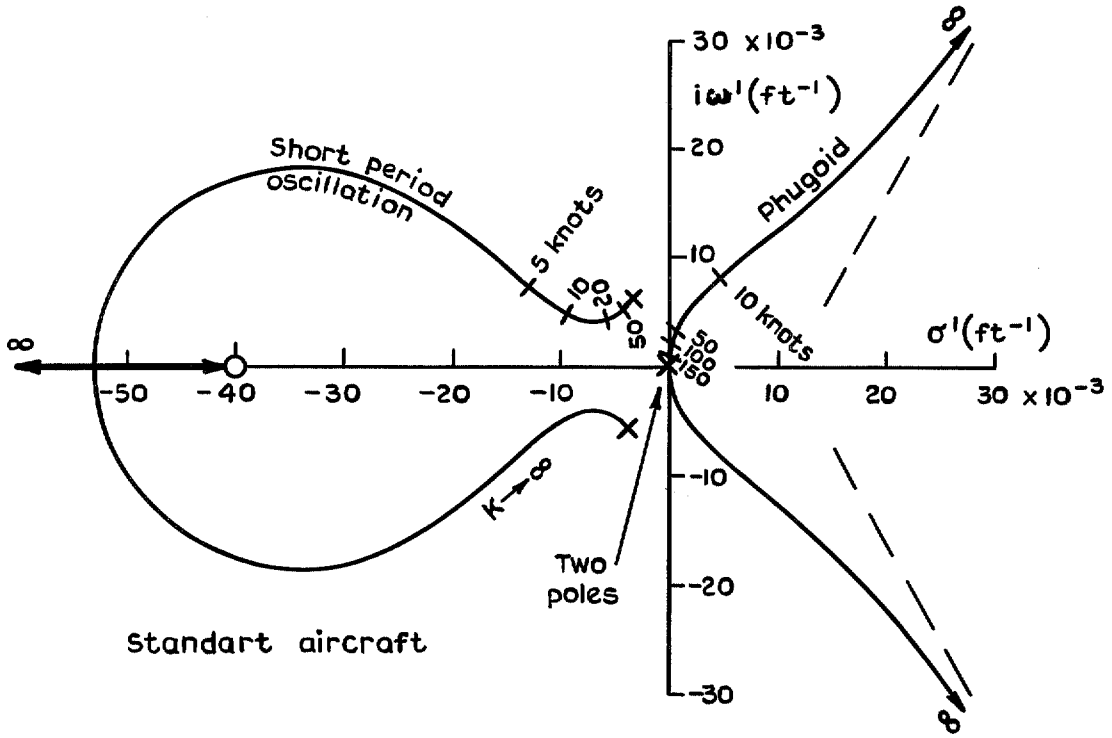

FIG. 36. Root locus plot showing change in dynamic longitudinal stability with airspeed for STOL aircraft (not valid for $V > V_{00}$).

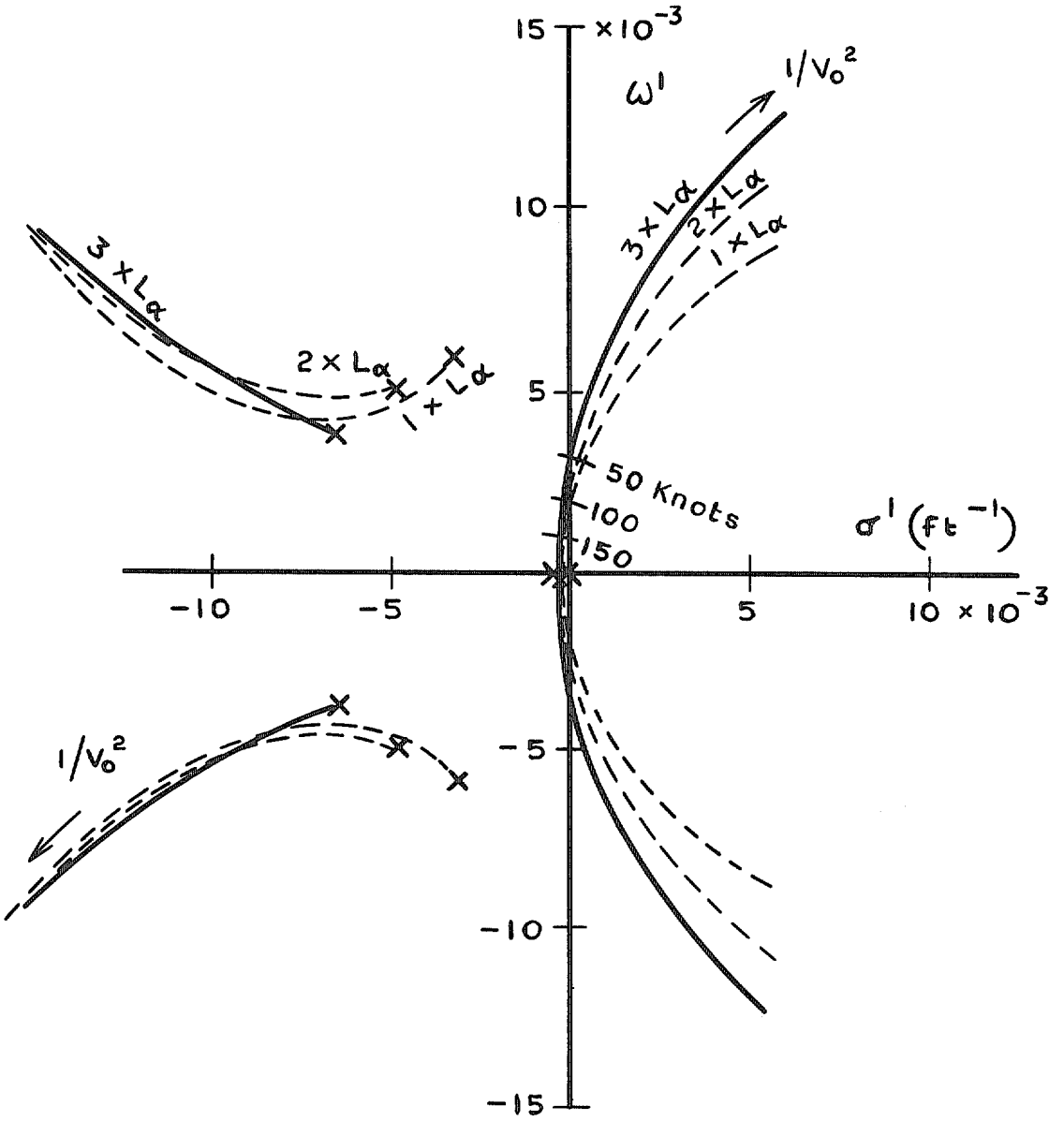

FIG. 37. Effect of increasing L_α on root locus of example shown in Fig. 35.

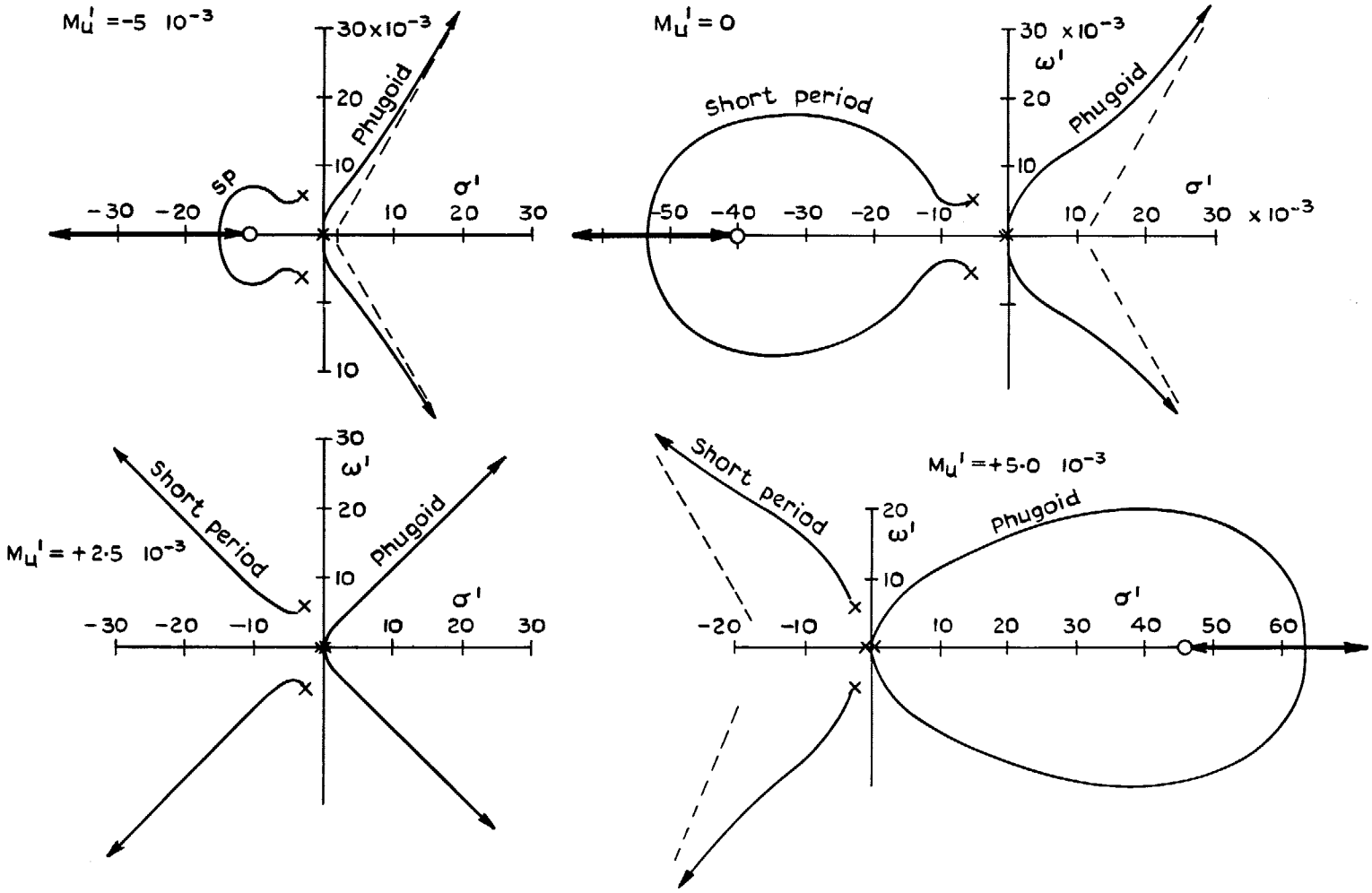

FIG. 38. Root locus plots of low speed longitudinal stability roots with various assumed values of M'_u.

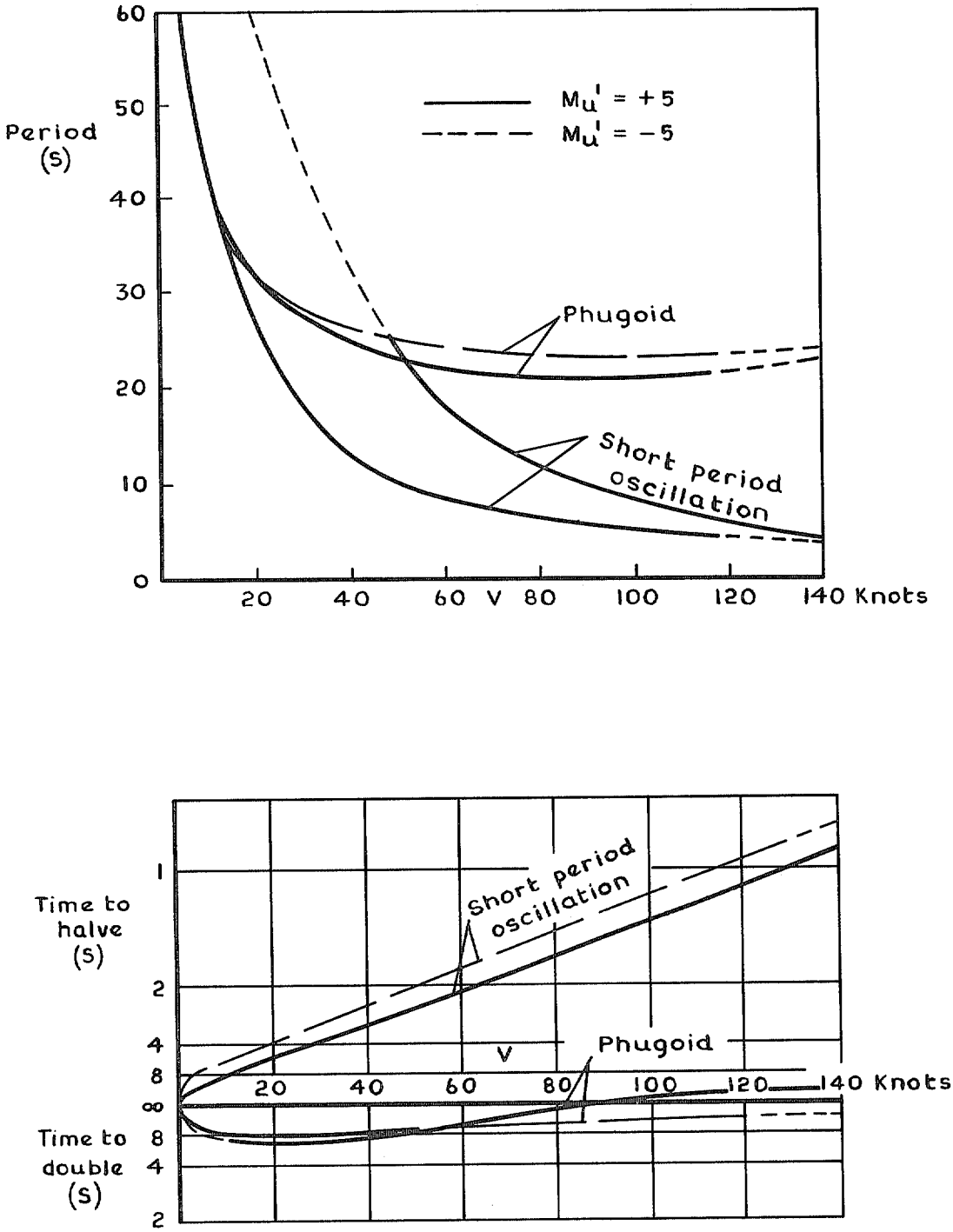

FIG. 39. Stability parameters of the longitudinal modes of a typical STOL aircraft.

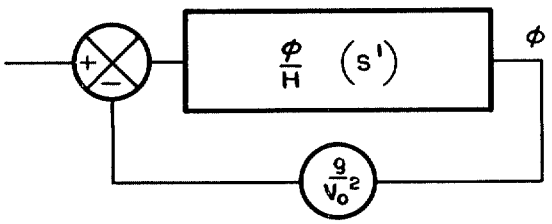

FIG. 40. Block diagram for lateral stability analysis of App. V.2.

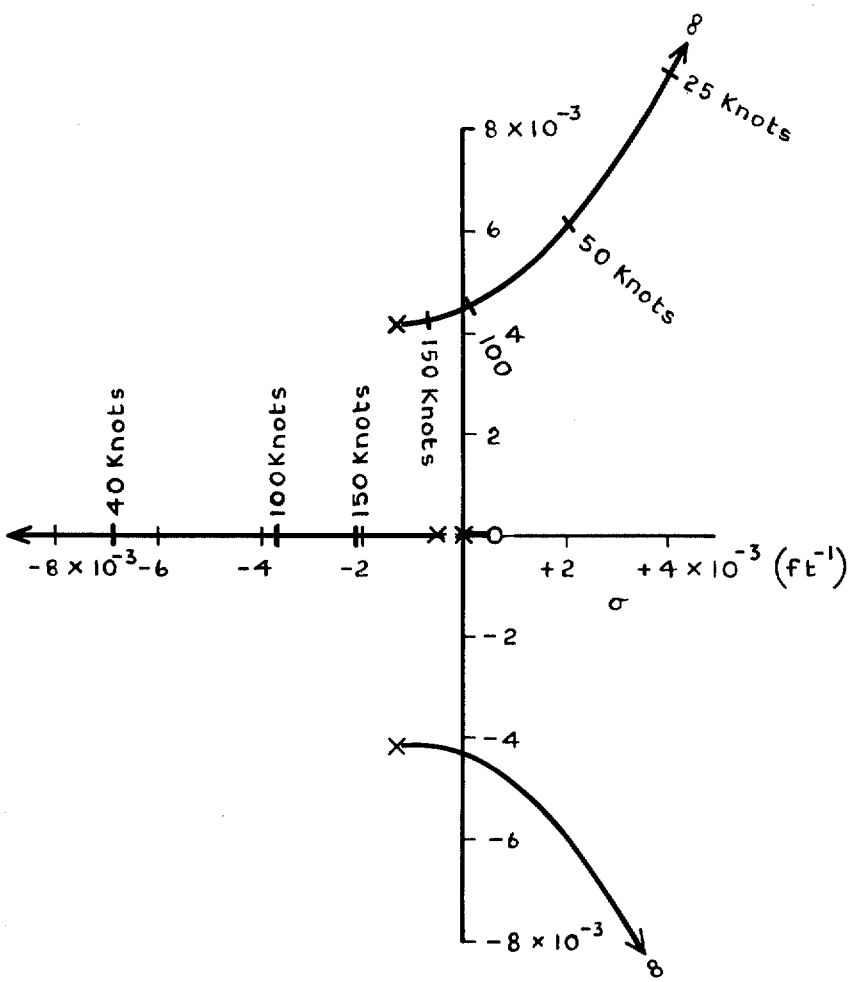

FIG. 41. Root locus plot showing change with airspeed of lateral stability roots for typical STOL aircraft.

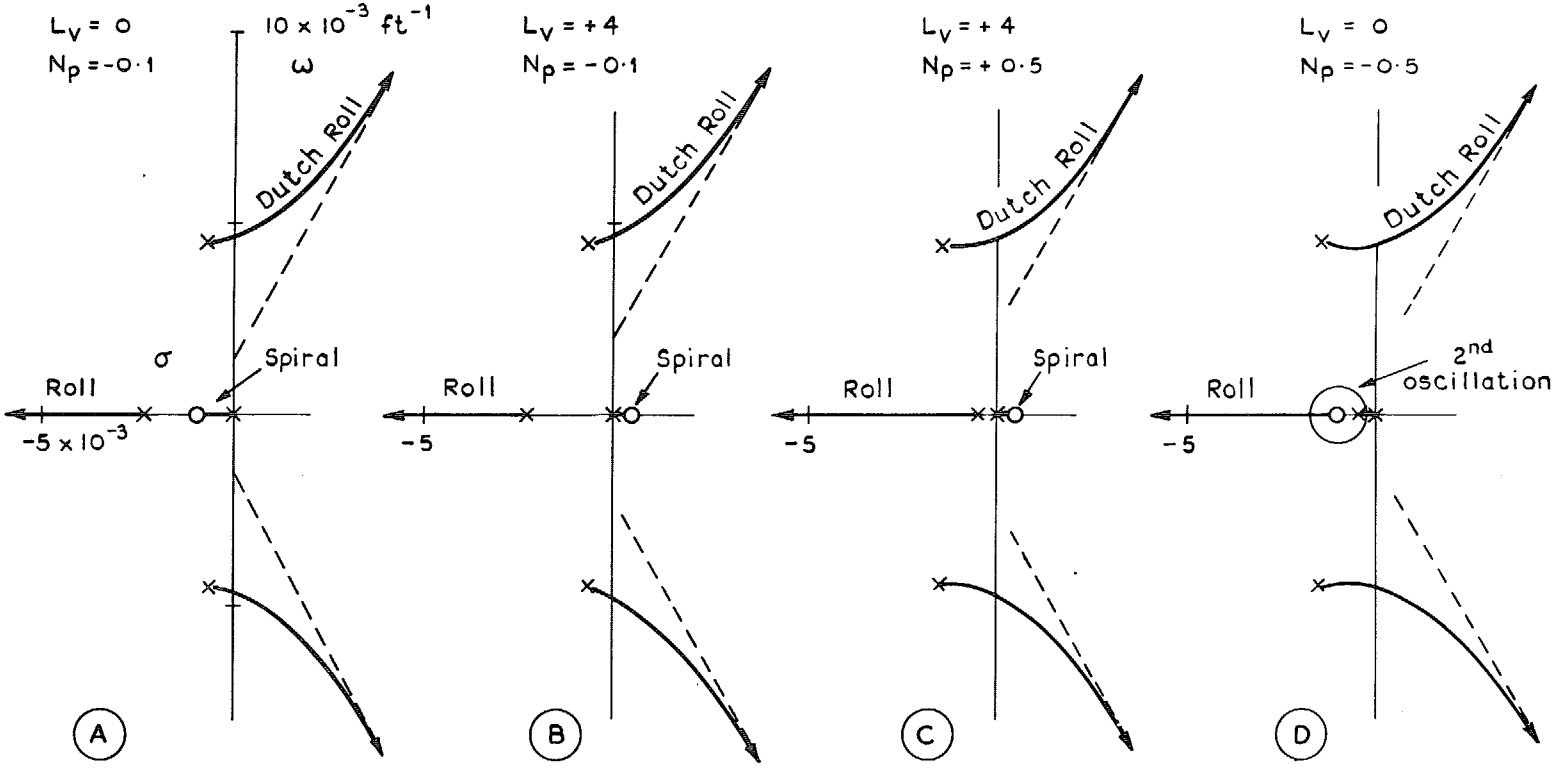

FIG. 42. Root locus plots for 4 variants of the example treated for lateral stability analysis.

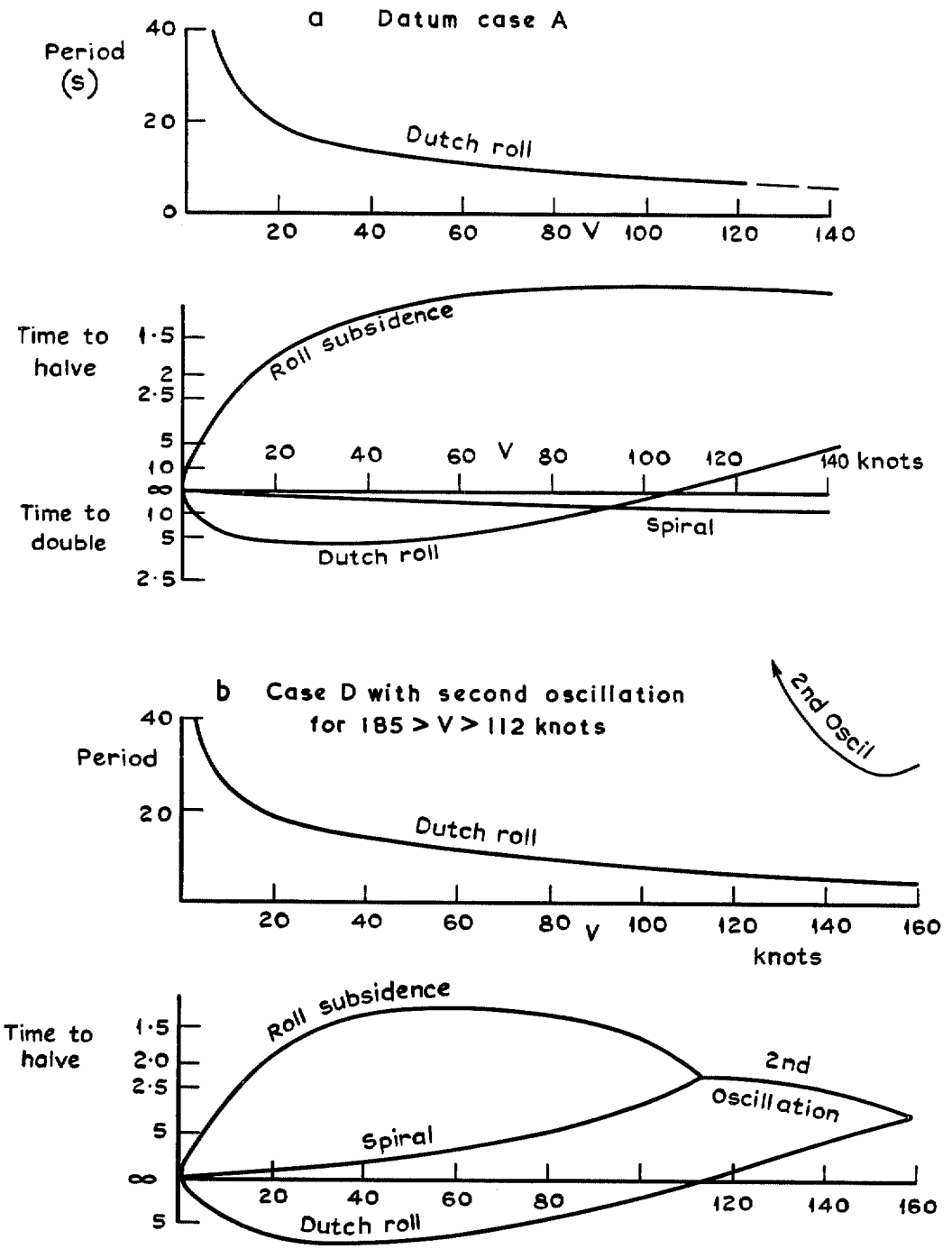

FIG. 43. Stability parameters for two of the cases shown in Fig. 41.

Printed in Wales for Her Majesty's Stationery Office by Allens Printers (Wales) Ltd.

Dd. 502110 K5

Published by
HER MAJESTY'S STATIONERY OFFICE

To be purchased from
49 High Holborn, London WC1V 6HB
13a Castle Street, Edinburgh EH2 3AR
109 St Mary Street, Cardiff CF1 1JW
Brazennose Street, Manchester M60 8AS
50 Fairfax Street, Bristol BS1 3DE
258 Broad Street, Birmingham B1 2HE
80 Chichester Street, Belfast BT1 4JY
or through booksellers

R. & M. No. 3686

SBN 11 470486 4